Modeling, Optimization and Environmental Assessment of Electrified Marine Vessels

by

Babak Manouchehrinia
B.Sc., Islamic Azad University, Iran, 2010
M.Sc., The University of Nottingham, England, 2012

A Dissertation Submitted in Partial Fulfillment
of the Requirements for the Degree of

DOCTOR OF PHILOSOPHY

in the Department of Electrical and Computer Engineering

Supervisory Committee

Modeling, Optimization and Environmental Assessment of Electrified Marine Vessels

by

Babak Manouchehrinia
B.Sc., Islamic Azad University, Iran, 2010
M.Sc., The University of Nottingham, England, 2012

Supervisory Committee

Dr. T. Aaron Gulliver, Department of Electrical and Computer Engineering
Co-Supervisor

Dr. Zuomin Dong, Department of Mechanical Engineering
Co-Supervisor

Dr. Panajotis Agathoklis, Department of Electrical and Computer Engineering
Departmental Member

Abstract

Supervisory Committee

Dr. T. Aaron Gulliver, Department of Electrical and Computer Engineering
Co-Supervisor

Dr. Zuomin Dong, Department of Mechanical Engineering
Co-Supervisor

Dr. Panajotis Agathoklis, Department of Electrical and Computer Engineering
Departmental Member

Electrified Vehicles (EVs), including Hybrid Electric Vehicles (HEVs) and Pure Electric Vehicles (PEVs), can provide substantial improvements in energy efficiency, emission reduction, and lifecycle cost over conventional vehicles solely powered by Internal Combustion Engines (ICE). Progress on electrification of marine vessels has been made, but the pace has been impacted by factors such as the different operational load profile of vessels, relatively small production levels and longer or varied lifetimes. In this dissertation, hybrid electric and pure electric propulsion system designs for fishing boats and passenger ferries are studied based on in-field acquired operational data. A new integrated marine propulsion system modeling and simulation method and a dedicated mobile data acquisition system have been introduced to analyze the energy efficiency, emission reduction, and lifecycle costs of new or retrofitted fishing boats and passenger ferries with hybrid electric and pure electric powertrains. Following the automotive industry Model Based Design (MBD) approach, modeling and simulation of electrified vessels using the acquired operation profile have been carried out using backward and forward-facing methods. Series hybrid electric and pure electric powertrain system designs with powertrain component models and rule-based system control, including a properly sized electric Energy Storage System (ESS) with a Supercapacitor (SC) or battery, have been studied. The total CO_2 equivalent (CO_{2e}) or Greenhouse Gas (GHG) emissions and lifecycle costs of various new, electrified vessel propulsion system designs have been evaluated. Clean propulsion system solutions for fishing boats and passenger ferries with

detailed powertrain system and control system designs are given which provide a foundation for further research and development.

This dissertation also addresses the environmental impact of Natural Gas (NG) as a transportation fuel, particularly for marine transportation use. A systematic evaluation of GHG emissions is provided for the upstream fuel supply chain of natural gas fuel in British Columbia (BC), Canada. The Liquefied Natural Gas (LNG) lifecycle GHG emissions produced in both the upstream supply chain and the downstream vessel propulsion are estimated quantitatively using manufacturer data and propulsion system models of marine vessels. Extensive data have been collected from oil and gas companies that have active operations in BC to determine the upstream supply chain GHG emissions of the NG fuel under three scenarios. The energy efficiency and emissions of natural gas engines are compared with traditional diesel fuel marine engines and generators. The results obtained indicate that LNG fuel can lower CO_{2e} by 10% to 28% with reduced local air pollutants such as sulfur oxides and particulates, compared to conventional diesel fuel. However, engine methane slip during combustion should be monitored as it can have a significant impact on the GHG emissions and so offset the environmental benefits of LNG.

Table of Contents

List of Tables

List of Figures

List of Abbreviations

AC	Alternating current		MBD	Model based design
BESS	Battery energy storage system		MOO	Multi objective optimization
BEV	Battery electric vehicle		Ni-MH	Nickel metal hydride
CO_{2e}	Carbon dioxide equivalent		n	Number of years
DC	Direct current		n_t	Time in seconds
DOD	Depth of discharge		OE	Total operation and investment cost
ESS	Energy storage system		PEV	Pure electric vehicle
e_a	Input voltage		P_{ESS}	Power generated by the energy storage system
e_b	Back electromotive force		P_{DG}	Power generated by the diesel generator
FC	Fuel consumption		P_{demand}	Vessel power demand
GDP	Gross domestic product		RPM	Revolutions per minute
GHG	Greenhouse gas		R_F	Diode resistance
HEV	Hybrid electric vehicle		R_a	Motor armature resistance
hp	Horsepower		$R_{ds\ ON}$	drain-to-source on-state resistance
ICE	Internal combustion engine		SC	Supercapacitor
IMO	International Maritime Organization		SOC	State of charge
I_F	Average diode current		$TC_{Hybrid\ series}$	Total cost of hybrid series architecture
I_m	Maximum switch current		t_f	Switch fall time
i_a	Armature current		t_r	Switch rise time
j	Motor's moment of inertia		V_F	Average diode voltage
K	Machine constant		V_m	Maximum voltage
K_b	EMF constant		tv	Applied voltage
K_t	Torque constant		B	Friction constant
kt	Knot		$\theta(t)$	Motor angular position
Li-ion	Lithium-ion		ΔT_j	Jth time interval
L_a	Armature inductance			

Acknowledgments

I would like to express my sincere gratitude to my supervisor Prof. Zuomin Dong for the continuous support of my Ph.D. I would like to thank you for encouraging my research and for allowing me to grow as a research scientist. Your advice on my research as well as my career has been invaluable.

I also would like to thank Prof. T. Aaron Gulliver for insightful comments and encouragement, but also for our long meetings and the hard questions which inspired me to widen my research for more general audiences.

I thank my fellow teammates in the UVic clean transportation group for the stimulating discussions and for all the fun we had in the last four years.

I would like to express my deepest gratitude to my family for their love and support. Special thanks to my parents who have always supported me and greatly inspired my motivation for pursuing a Ph.D. degree. I would like also to extend my sincerest thanks and appreciation to my lovely brother Ali for his unconditional support and advice throughout my Ph.D. journey.

Last but not least, I would like to thank my lovely wife Sara for her relentless patience and continuous support on the roller coaster of highs and lows of my Ph.D. degree. Her unconditional love and unwavering encouragement and support is the primary reason that I was able to complete this degree, for which I am eternally grateful.

Dedication

To my beautiful wife, Sara

for her patience, her effort, and her faith,

because she always understood.

1 Introduction

Maritime transport has a long history in human civilization. It has enabled humans to discover new territories and expand trade to other continents using vessels. Vessels have changed dramatically during the last 300 years from wind-powered sailing vessels to steamships to diesel engine powered vessels and recently to fully electric vessels. The main drivers of this transition in vessels are lower operational costs, increased reliability, safety, and faster transportation.

Maritime transport accounts for about 80% of world global trade by volume and 70% of global trade by value [1][2]. The shipping industry is continuously seeking new ways to increase its overall efficiency. A promising approach is introducing Integrated Power Systems (IPSs) and electric propulsion systems in commercial ships to replace conventional mechanical propulsion. The potential reduction in GHG emissions due to IPS architectures will help marine industry meet the strict and ever evolving environmental regulations enforced by regional and national governments as well as the International Maritime Organization (IMO) [3].

Despite the environmental friendliness of maritime transportation, ship emissions contribute 2.2% of global CO_2 emission [4][5] and also 15% of global NO_x and 13% of global SO_2 emissions [6]. To address these issues, IMO Tier I, II and III regulations have been introduced to limit the allowable NO_x, SO_x and Particulate Matter (PM). The NO_x emission regulation of MARPOL Annex VI apply to all engines installed on vessels with more than 130 kW power. The NO_x emissions depend on engine maximum operating speed. The NO_x regulation limits are presented in Table 1 where Tier I and Tier II are global limits and Tier III applies only to Emission Control Areas (ECA).

Table 1: MARPOL Annex VI NOx emission limits

Tier	**Ship construction date after**	**NO_x Limit, g/kWh**		
		n < 130	**130 ≤ n < 2000**	**n ≥ 2000**
Tier I	Jan 1, 2000	17.0	$45n^{-0.2}$	9.8
Tier II	Jan 1, 2011	14.4	$44n^{-0.23}$	7.7
Tier III	Jan 1, 2016	3.4	$9n^{-0.2}$	2.0

n is engine speed.

The Annex VI regulation also include a limit on the sulfur content of fuel which indirectly controls PM emissions. The sulfur limits and enforcement dates are presented in Table 3. The current sulfur limit is about 3.5% and 0.1% for global and ECA respectively. The new emission standards announced in 2018 by IMO will be enforced in 2020 and set a limit of 0.5% for global shipping which can be a challenging problem for the marine industry. These new emission standards have prompted new research focused on the reduction of SO_x and NO_x emissions. Moreover, many marine manufacturers are focused on the implementation of new technologies such as Exhaust Gas Recirculation (EGR) and Selective Catalytic Reduction (SCR) [7][8][9] to reduce emissions. To address the environmental restrictions, IPS architectures and different fuel pathways are examined in this dissertation.

Table 2: MARPOL Annex VI fuel sulfur limits

Date	**SO_x Limit in Fuel (% m/m)**	
	ECA	**Global**
July 1st, 2000	1.5%	4.5%
July 1st, 2010	1.0%	
Jan 1st, 2012		3.5%
Jan 1st, 2015	0.1%	
Jan 1st, 2020		0.5%

Electric propulsion for vessels is not a new concept and has been applied for more than 100 years in ship design (albeit in few vessels). The river tanker Vandal is an example of an electrically propelled ship. It was the first vessel to be powered by a diesel generator, whereas up to that point most vessels were powered by steam turbine generators [10]. In the 1980s, a revolution in solid-state and semiconductor switching devices occurred which made speed control of large electric motors possible and as a result, electric propulsion became more feasible for ship designers. Initially, speed control of DC motors was introduced and later replaced by precise control of AC motors using sophisticated control mechanisms such as vector control. Synchronous and asynchronous motors are the most common choices for propulsion and have dominated propulsion and thruster applications for a long time. In general, asynchronous motors are used for applications below 5 MW and synchronous motors are used for higher power applications along with Voltage Source Inverters (VSIs).

An electric propulsion system provides high dynamic maneuverability for vessels. This is particularly important for vessels such as icebreakers [11]. Because of the low-speed, high-torque characteristics and fast response, maneuverability can dramatically increase due to the capability of electric motors to respond rapidly to abrupt changes in power demand. Figure 1 illustrates the recent trend in the number of electric propulsion vessels worldwide.

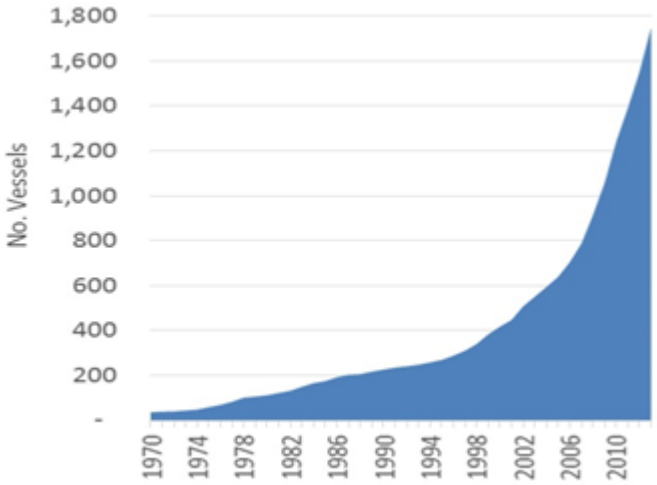

Figure 1: Development of the electric propulsion fleet [10]

The power for electric propulsion is usually provided by diesel generators on board the vessels. Diesel electric propulsion systems are used in many vessels due to advances in electric powertrain component technologies. The advantage of this system is the mechanical link decoupling of the diesel engine and propeller. This allows the diesel engine to operate at an efficient speed and torque range for both high and low speed propulsion torque, and allows more flexible engine space arrangements in vessels.

A high efficiency can only be obtained if an electric ESS is added as an energy reservoir. A hybrid electric system is particularly suitable for vessels with a dynamic load profile when the engine has to work at different speeds. Depending on the vessel load profile, a hybrid electric system can reduce the overall fuel consumption. The drawback of this configuration is the unavoidable energy conversion loss from mechanical to electrical and then from electrical to mechanical. It has been estimated that the losses are about 5% to 10% [12] of the total generated power. The approximate energy conversion losses for a diesel electric AC power system are shown in Figure 2.

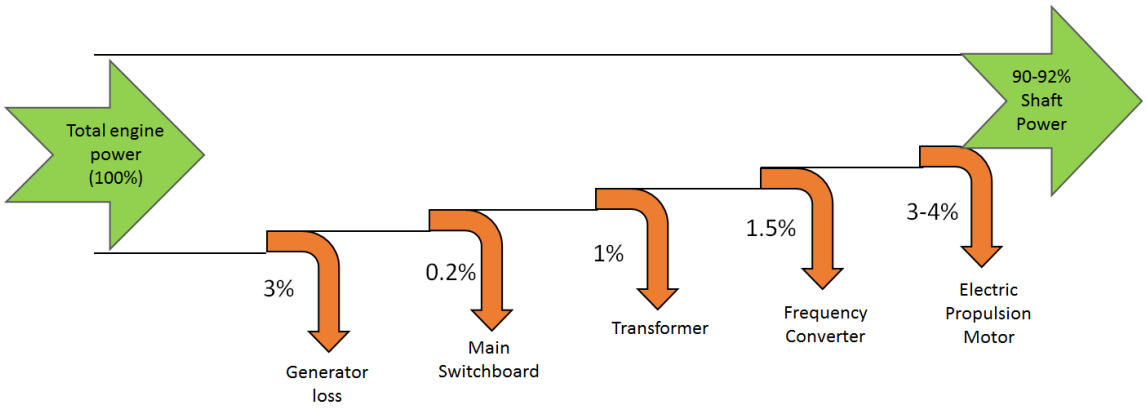

Figure 2: Approximate powertrain loss with an AC bus

The electrification of ship power has resulted in the concept of pure electric vessels. In a pure electric system, all ship loads, i.e. propulsion, steering, navigation and hotel loads are satisfied with electric power. All energy required for the vessel is provided by the ESS such as a battery system or supercapacitor. The advantage of a pure electric vessel is high efficiency at all speeds and power. Mechanical propulsion systems with diesel engines are designed to operate at a rated power and rated speed which makes them inefficient in off-design conditions. A pure electric propulsion system powered by an onboard ESS has lower acoustic noise compared to traditional mechanical propulsion systems which make them more environmentally friendly.

The power plants in electric vessels are similar to commercial land based power plants. It consists of fixed or variable AC or DC generators. For AC fixed frequency power generation the generators rotate at a constant speed and a 50 or 60 Hz voltage is created. In variable AC generation, an AC-DC-AC converter is employed to create a constant output voltage. In a variable DC power plant, a rectifier transfers the AC voltage to a constant DC voltage using a voltage regulator. In all cases, the combination of power plant and electric propulsion in vessels must satisfy many performance criteria such as fuel consumption, maneuverability, redundancy, GHG emissions, acoustic noise, and capital and maintenance costs.

1.1 Research Problem

Diesel engine propulsion has been a standard architecture for vessels over the last 50 years. However, new emission regulations by the IMO and other organizations have forced maritime industries to shift from purely mechanical or diesel electrical architectures to newer powertrain architectures with higher efficiencies. The maritime industry is now exploring opportunities such as the hybridization of mechanical and electric propulsion systems, pure electric system, and NG fuel along with powertrain hybridization to achieve lower GHG emissions.

With the addition of a Battery ESS (BESS), present diesel electric powertrain systems can easily be converted to hybrid electric propulsion systems using a series powertrain architecture similar to a series hybrid electric vehicles, as shown in Figure 3.

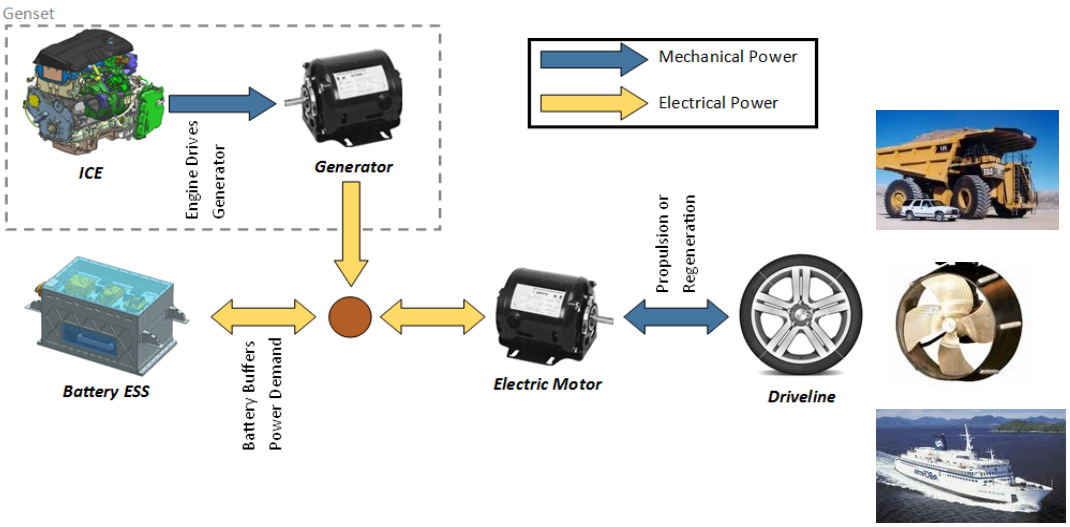

Figure 3: Series hybrid electric powertrain for a vehicle or ship

Conversion with an added energy reservoir makes the design and control of a hybrid electric propulsion system more challenging due to the added flexibility and possible variations in powertrain layout and component sizes. Moreover, advanced series or parallel hybrid electric propulsion systems will add other challenges. To address these issues, the model based design and optimization developed by the automotive industry is used. This dissertation is focused on the integrated modeling of hybrid electric marine propulsion systems and their environmental impacts.

At present, most vessels use an AC power distribution system to support electric propulsion. AC distribution remains popular mainly due to the proven AC technology and the availability of various AC electric drives and power electronics components. In recent years, DC distribution has received significant attention from ship manufacturers and the research community. DC distribution in vessels offers many advantages compared to AC distribution systems. DC systems have lower overall losses and fewer synchronization and harmonic distortion problems. A DC electric power distribution system also utilizes proven AC generators and motors and opens new opportunities for improved performance and fuel savings due to the fact that the diesel engine is no longer locked at s specific speed (for example 60 Hz), and variable speed generation is possible. This new freedom of controlling the diesel generator speed independent of other sources of power opens up numerous ways of optimizing engine operation and reducing fuel consumption. One focus of this dissertation is to explore and investigate different approaches for minimizing vessel fuel consumption using a DC distribution power system.

For the design of electric and hybrid electric marine propulsion systems, it is essential to have the speed and load profiles for the vessel, as well as accurate power and energy models to account for the ship drag and propeller thrust under different operating conditions. Unlike most passenger vehicles, there are no standardized drive cycle and vessel dynamic power loss models that can be applied. In addition, the marine drive cycle can vary significantly between vessels due to their applications. In this dissertation, actual ship power load profiles representing different classes of vessels are used as inputs to the model. At present no model exists that represents the interactions between all propulsion components with sufficient detail. This dissertation presents hybrid electric and pure electric powertrain models for marine vessels with sufficient details to evaluate their energy efficiencies, lifecycle cost, and environmental impact.

1.2 Background

1.2.1 Present Marine Propulsion Systems

The shipping industry is under pressure to reduce fuel consumption and the environmental impact of vessels. While this pressure has increased recently, the applicability of ships has also increased rapidly and ships have been designed for different roles such as cargo ships (for transportation of cargo), tankers (for transportation of liquids), passenger ships (ferries and cruise ships) and container ships, which carry most of the manufactured goods and products worldwide. Because of the diverse operating profiles, different propulsion and power architectures are employed. The architectures need to have high performance in areas such as

- Fuel consumption
- Emissions
- Noise
- Propulsion availability
- Maneuverability
- Comfort due to noise, vibrations, and smell
- Maintenance cost
- Purchase cost

The three popular architectures in maritime industries are mechanical, diesel electric and battery electric. The mechanical powertrain architecture is illustrated in Figure 4. This is an example of a conventional propulsion system consisting of diesel engine prime mover(s), reduction gears, medium length shafts, and propeller(s). The number of prime movers depends on the application of the vessel. A prime mover rotates the shaft with medium speed and transfers torque through the shaft via reduction gears in order to drive the propeller. The propeller converts torque to thrust at rotational speeds of about a few hundred RPM. The separate diesel generator is designed to operate at a constant speed and supplies electrical power at 60 Hz to the remaining ship loads.

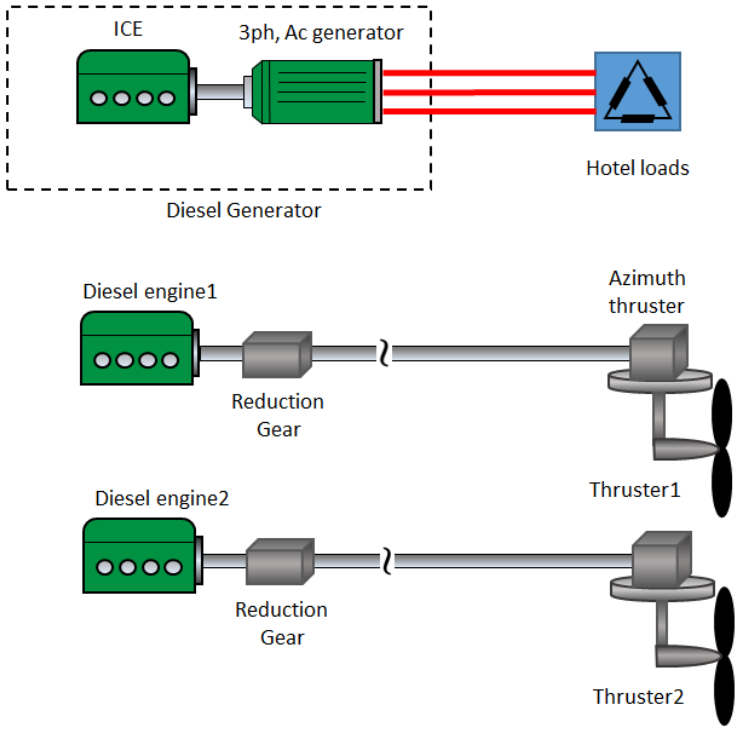

Figure 4: Mechanical propulsion architecture

Another type of propulsion architecture is the diesel electric. A diesel electric architecture is very similar to a series hybrid architecture but it has no energy storage system. Thus, it is not as efficient as a series hybrid architecture. A parallel diesel electric architecture is shown in Figure 5. In this architecture, diesel generator(s) produce three phase AC power which is transferred to the electric motor(s). The electric motor(s) are in parallel with the diesel engine in a parallel architecture.

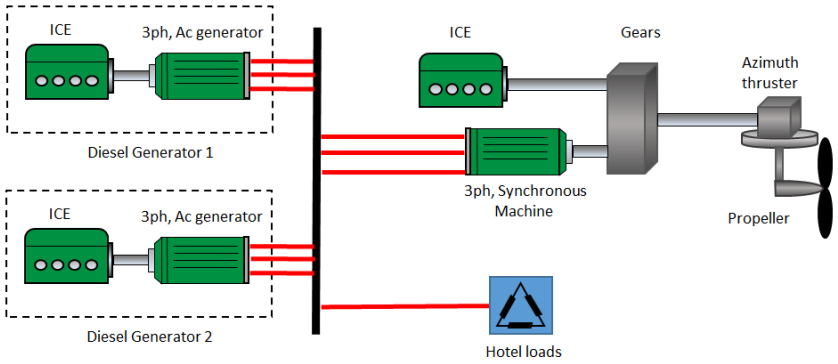

Figure 5: Conventional diesel electric system

A battery electric (pure electric) architecture is widely used in submarines and has become popular for smaller marine vessels in recent years. This design offers significant advantages over other architectures such as higher energy efficiency, lower noise levels, and greater reliability. However, factors such as limited range, high capital cost of the batteries, bulky and expensive charging stations, and the cost of expanding the existing electrical grid have prevented this design from growing quickly. Despite this, the first battery electric car ferry, Norled AS MF Ampere, entered service in the Sognefjord, Norway, in 2015 [13]. It has been estimated that the Ampere annually offsets one million litres of diesel as well as the emission of 570 tonnes of carbon dioxide and 15 tonnes of nitrogen oxide when compared to conventional ferries in service on the same route [14]. This is without considering the well-to-pump fuel cost and GHG emissions.

In the battery electric architecture, the battery ESS is the only source of energy and it services all ship loads (although a backup diesel generator is usually installed in order to satisfy redundancy requirements). This makes the battery electric architecture similar to the architecture of the PEVs. A typical battery electric architecture is illustrated in Figure 6. The BESS is coupled to a bidirectional DC/DC converter in order to charge the battery and step up the voltage. Similar to the series hybrid architecture, the distribution system can be either AC or DC. In the case of a DC distribution grid, electric power is transferred to a DC/AC converter in order to provide the required power for large consumers like propulsion loads. Smaller loads are connected to the grid by means of individual islanding converters. The current trend in the shipping industry is moving towards DC distribution systems because of the flexibility it offers in introducing energy storage, fuel cells, and solar technologies [11].

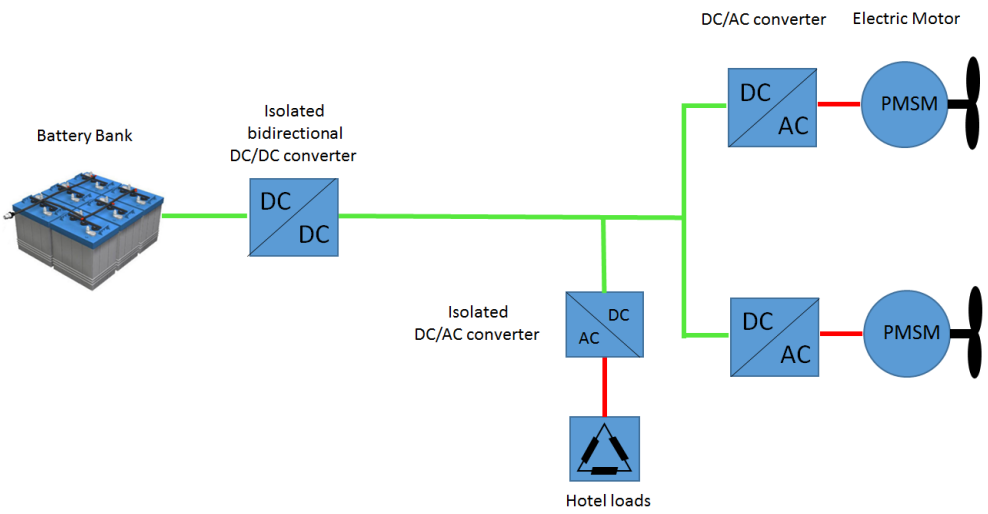

Figure 6: Battery electric architecture with DC bus

Currently, hybrid diesel electric architecture is the most promising architecture and it is the focus of this work. In this architecture, multiple prime movers coupled with gensets are electrically connected to a common busbar to share the power between the propulsion system and service loads. Prime movers are often diesel engines fed by diesel and heavy fuel oil or occasionally gas (LNG tanker) [10]. Other types of prime movers such as gas turbines, steam turbines or combined cycle turbines are also used for high power, high speed vessels. The hybrid electric architecture provides several advantages for vessels like supplying the ship loads with fewer prime movers. This enhances the fuel efficiency noticeably over low and medium speed ranges compared to conventional mechanical power systems. This architecture also reduces the capital investment and improves reliability due to the redundant structure.

The majority of generators installed in vessels are AC synchronous machines. These machines are preferred over other generators mainly due to the excellent power control (active and reactive power) and maturity of the technology. Modern synchronous generators have brushless excitation that reduces maintenance and downtime. The output generator voltage variation must always be kept at an acceptable level. An automatic Voltage Regulator (AVR) controls the voltage and reactive power sharing. Protection relays and circuit breakers are installed on the switchboards to make ensure electrical faults

are detected and isolated from other zones. The design always includes different electrical zones with associated switchboards to improve reliability and redundancy in the system.

In higher power application (usually greater than 5 MW), in order to reduce mechanical and thermal stress on switchgears and busbars, the voltage level is increased to a medium level. This results in lower stress and short circuit currents. The most common voltage levels selected for the main distribution system [15] are 11 kV, 6.6 kV and 690 V. These voltages are associated with total generator capacities of above 20 MW, 4-20 MW and below 4 MW, respectively. In the US with ANSI standard, several additional voltage levels are recognized such as 120 V, 208 V, 690 V, 2.4 kV, 3.3 kV, and 13.8 kV. The voltage drop and future load prediction are important factors that must be taken into account when selecting the main distribution voltage.

In recent years, there has been a strong interest in moving to DC distribution systems. DC distribution has size and cost advantages that make it an attractive option for designers. In DC distribution bulky transformers and large diameter wires are removed or replaced with smaller ones. DC distribution enables the use of compact and lightweight high speed permanent magnet generators and also make it easier to integrate new renewable sources like fuel cells and solar panels. A significant advantage of DC distribution is the fact that it allows generators to operate at different speeds where engines are at optimum fuel consumption. By doing this, fuel consumption can be improved dramatically at low speeds.

1.2.2 Electrified Power and Propulsion Systems

The propulsion architectures of maritime vessels are very similar to terrestrial vehicles. Thus, it is necessary to understand vehicular propulsion systems and the advantages and disadvantages of each architecture. The technology of propulsion system in vehicles can be classified into four different groups as given below

1.2.2.1 Internal Combustion Engine (ICE) Vehicles

Almost all conventional vehicles use ICE for propulsion. There are two types of ICE that transform thermal energy into mechanical energy [16]. The first type is called the Otto cycle and the second is the diesel cycle. The Otto cycle has spark-ignited combustion that is powered by natural gas or gasoline. The diesel cycle has compression-ignited combustion that is powered by diesel fuel. These two cycles have been improving in

parallel, but diesel cycles have better efficiency due to its thermodynamic cycle. The average efficiency of an ICE in practice is about 25% for the Otto cycle and 30% for the diesel cycle considering the optimal operating point.

1.2.2.2 Battery Electric Vehicles (BEVs)

A battery electric vehicle is a pure electric car in which the battery is the only source of energy. The battery provides all propulsion and auxiliary power and can be recharged at a fast charging station or using a charger at home. There are different power system layouts for BEVs and each layout has its own advantages and disadvantages as explained in [16]–[18]. In recent years, multi-machine traction systems have been very popular due to their various operating modes and power optimization.

1.2.2.3 Hydrogen Fuel Cell Vehicles (FCVs)

In this system fuel cell generates electricity and stores it in an energy storage system such as batteries or ultra-capacitors. The most common fuel-cells technology is Polymer Electrolyte Membrane (PEM) which uses stored hydrogen as a fuel and oxygen from the air to produce electricity. Currently, the FCV and BEV are the only potential Zero Emissions Vehicle (ZEV) replacements for the ICE.

1.2.2.4 Hybrid Electric Vehicles (HEVs)

The concept of an HEV uses the idea of optimizing the fuel consumption of internal combustion engine at different loads and speeds by using an electric machine whenever possible. Thus the main objective of hybridization is to keep the ICE operation close to the maximum efficiency point for the longest time possible [19]. Depending on the level of hybridization and electric machine, there are five types of propulsion systems for vehicles: 1) micro hybrid, 2) mild hybrid 3) fuel hybrid, 4) Plug-in Hybrid Electric Vehicle (PHEV) and 5) Extender Range Electric Vehicle (EREV). Table 3 shows the characteristic of each hybridization level. An explanation of these propulsion systems is presented in [19].

Table 3: Characteristics of hybridization levels [19]

Type	Start/Stop system	Power assistant capability	Regenerative breaking capability	Pure electric mode	Charger
Micro hybrid	✓	×	×	×	×
Mild hybrid	✓	×	✓	×	×
Fuel hybrid	✓	✓	✓	✓	×
PHEV	✓	✓	✓	✓	✓
EREV	✓	✓	✓	✓	✓

There are only some HEV drivetrain architectures that are applicable to marine vessels. The propulsion architectures in marine vessels can be split into two main categories, series, and parallel-series hybrid or (power-split) powertrain architectures.

1.2.2.5 Series Hybrid Electric Powertrain Architecture

In a series hybrid architecture, diesel generators or gas turbines generate electricity and provide power for electric motors connected to the propellers. This arrangement eliminates the need for long shafts, clutches, and gearboxes and offers more flexibility for components locations. However, this architecture has disadvantages such as higher energy loss due to energy conversion and a high power rate electric motor. A critical component of this architecture is the ESS which stores the excess energy and releases it whenever needed so the diesel generator can operate at optimum efficiency. This architecture is shown in Figure 7.

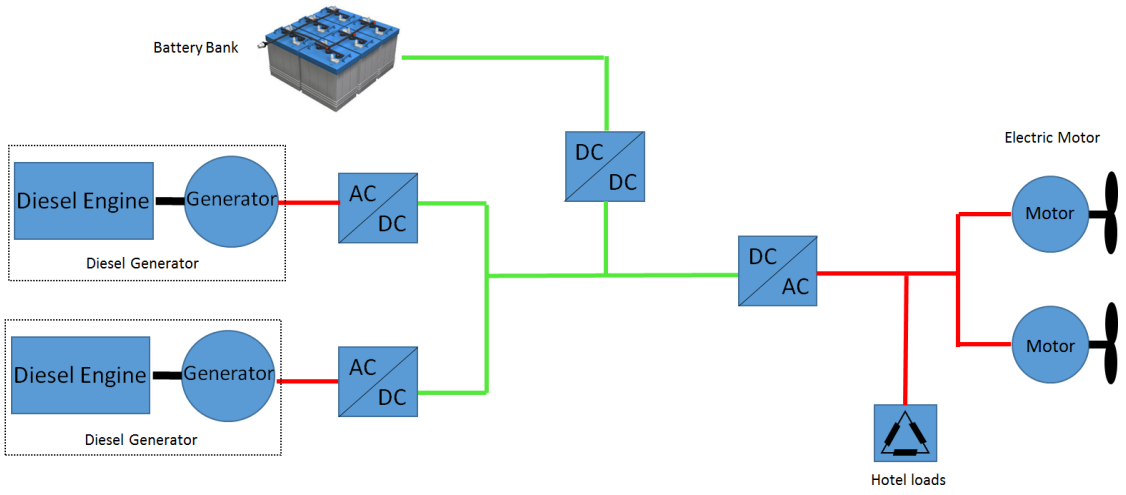

Figure 7: Series hybrid electric drivetrain

1.2.2.6 Parallel-series Hybrid Electric Powertrain Architecture

This architecture combines the features of both series and parallel system, but compared to series it has an additional mechanical link and compared to a hybrid system, the diesel engine can decouple from the propeller. The advantages of this architecture are: 1) both the ICE and electric machine are directly connected to the propeller so less energy conversion is needed so lower losses occur and a lower power rating electric motor is required. The disadvantages of this architecture are the control complexity.

Figure 8 shows the parallel hybrid architecture. In this example, two diesel generators are connected to a busbar with a constant voltage and frequency and a three phase synchronous or asynchronous machine is mounted on a diesel shaft using reduction gears. The electric machine can operate either as a motor or generator and an AC/AC converter provides a connection between the busbar and electric machine. When the required propulsion power is more than the diesel engine was designed for, the synchronous machine works as a motor and provides the extra propulsion power (boost mode). On the other hand, when the diesel engine is working in a lower power range which corresponds to higher Specific Fuel Consumption (SFC), the diesel engine is shut off (pure electric) and the electric motor provides the power. When the demand power is more than the what motor can provide and less than the diesel efficiency point, the electric machine works as a generator and helps the engine to work at its optimum point and excess power is stored in the ESS system (mixed mode). This capability to adjust engine power to match the vessels power demand can significantly reduce fuel consumption and GHG emissions.

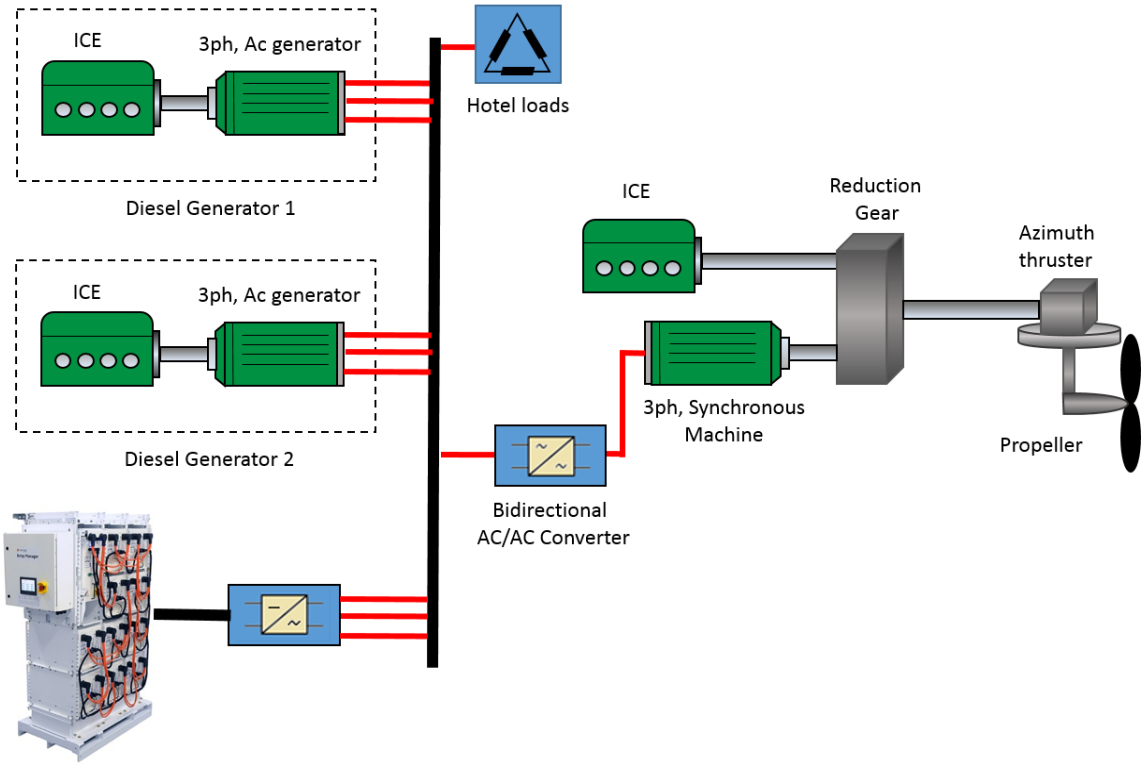

Figure 8: A parallel-series hybrid electric drivetrain

Pure electric vessels are very similar to large terrestrial electric vehicles but with a higher power rating due to the higher power demand. The closest terrestrial applications are buses, trucks, mining trucks and locomotives. The traditional distribution system in these vehicles is a well-proven AC power system. The new emerging solution is DC distribution where AC generators and motors allow for higher efficiency since the generator is no longer locked to a specific frequency. This new freedom of controlling the generator speed opens up numerous ways of optimizing fuel consumption.

Mining trucks are high power terrestrial vehicles that have adopted DC distribution. Mining trucks must work in harsh conditions while providing maximum load. A diesel electric mining truck with a DC distribution system is a new concept, which outperforms mechanical trucks, especially on steep grades. DC distribution makes mining trucks more compact, lighter and easier to repair and maintain, which is a great advantage in remote locations where uptime is critical and work must be done on site. In a mining truck powertrain, a diesel generator acts as a power plant, producing AC power by means of a

traction alternator. A diode rectifier converts the AC power into DC. The DC electrical power passes through the capacitors to two inverters which produce the AC power for the induction motors. The voltage and frequency of the inverters are controlled to provide precise motor torque and speed. Regenerative braking can effectively control the hauler so it reaches 0.5 mph (0.8 km/h) without using hydraulic brakes. AC motor and drive technology is a very efficient way of powering large vehicles. AC drives allow smoother acceleration at low speeds and higher top speeds. AC drives also minimize routine maintenance with their brushless design. Caterpillar 795F AC is an example of an electric mining truck with DC bus, which is shown in Figure 9. This truck uses an 85 L, 3400 hp Cat C175 diesel engine with an AC drive system and Insulated-Gate Bipolar Transistor (IGBT) inverter technology [19].

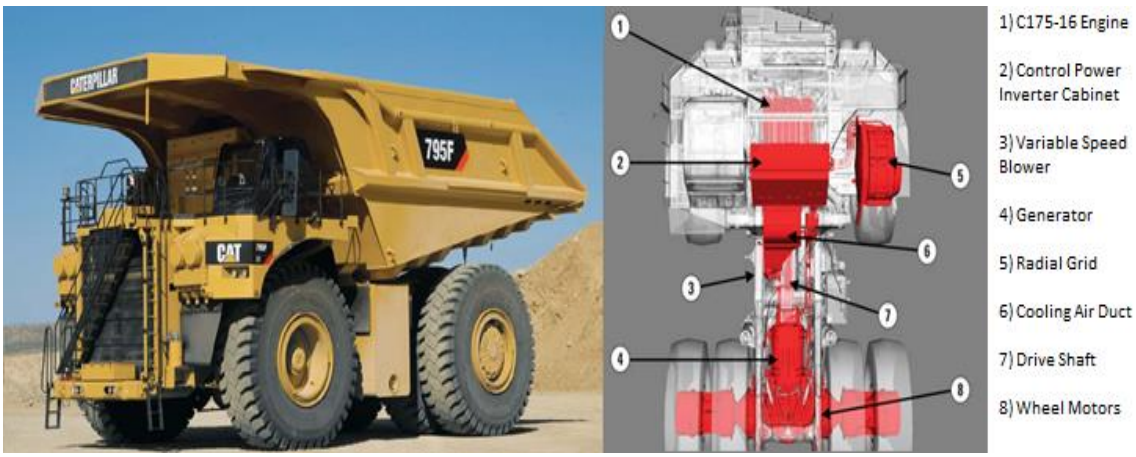

Figure 9: A diesel electric Caterpillar mining truck [19].

1.2.3 Powertrain System Modeling and Model Based Design

Model based design is a method that allows rapid and cost-effective development of a dynamic system like an electric ship. MBD can address problems associated with control systems, signal processing, and communication systems in a common framework for design process while supporting the development cycle. It also allows for the development of the main supervisory controller, enabling integrated control deployment for advanced energy management systems. The MBD in Matlab/Simulink also enables further research on integrated ship power systems using techniques such as Software-in-the-Loop (SIL) and Hardware-in-the-Loop (HIL).

The automotive industry has achieved significant levels of integration using embedded systems for improved performance. The MBD method is a state-of-the-art design technique commonly employed in the automotive industry. Unfortunately, marine industries have been slow to adopt the MBD method for propulsion system design. Therefore, the model developed in Matlab not only provides a platform for further investigation and research on powertrain models, but also enables the analysis of renewable technology integration and control system model. The growing implementation of onboard energy storage systems and renewable energy technologies into IPS requires a higher level of sophistication and system integration. MBD allows these technologies to be evaluated through simulation, and systematically implemented at lower risk. The two approaches used to implement MDB are forward-facing models and backward-facing models.

1.2.3.1 Efficient Electric Power Systems and Drives

Development in electric power system plants can be divided into two parts, the propulsion drive system, and power generation and distribution.

Variable speed electric motor drives provide new opportunities for the employment of electric motor in propulsion drive systems. Semiconductor switches are now capable of handling high voltages and power and they can smoothly control the output torque and speed of motors. A frequency converter is the most common method for controlling the speed of an AC motor. Different topologies can be used in the converter to achieve the required power. The two most common types of converters are voltage source converters and current source converters. These converters can be used in different systems depending on the application.

The generation side of the system uses the same technologies as in the 1980s. However, it has been optimized in design and manufacturing. Recently, a highly efficient distribution system has been introduced for electric ships by merging the various DC links around the vessel and distributing power through a single medium voltage DC main circuit. With this configuration, main AC switchboards, distributed rectifiers, and transformers are eliminated from the system. Moreover, unlike AC distribution, DC distribution has fewer problems with harmonic distortion. Elimination of the harmonics from the AC distribution system usually involves the installation of bulky harmonic filters which in turn introduces

more loss in the system. DC distribution can eliminate a portion of losses in electric propulsion, but this reduction is not sufficient to compensate the extra losses introduced by electric propulsion. Thus besides requiring a highly efficient DC distribution system in electric ships, the power system architecture and components such as converters, controllers, electrical machines and batteries must be efficient.

1.3 Research Contribution

Over the past twenty years, significant research efforts have been devoted to the modeling, simulation, optimization, and advanced control of hybrid electric powertrain systems for terrestrial vehicles [20]–[22]. However, research in these areas for marine vessels is lacking, or relatively superficial with imprecise system performance, cost, and emission models overlooking component interactions and system operation control details.

This dissertation introduces a quantitative, electrified marine propulsion system model with sufficient detail to capture the energy efficiency, emissions and cost of alternative powertrain systems and components to facilitate design optimization, and support cost and emission analysis using the actual operational load profile of a vessel.

Methods are introduced for examining various ship electrification solutions and optimizing powertrain components to match various vessel operating profiles. The resulting powertrain system and component models allow accurate evaluation of the power performance and energy efficiency of traditional and alternative hybrid electric propulsion solutions, supporting both control and system optimization. The developed model is tested for a lobster fishing boat and the work in Chapter 3 was published in the Journal of Ocean Technology [23].

For modeling powertrain systems, an advanced DC/DC converter power loss model and a generic DC/DC modeling tool have been developed. The model can be used to predict the behavior of a DC/DC converter in various hybrid electric powertrain system models to reduce the simulation time without sacrificing accuracy. This work was published in journal Energies [24].

In this work, considerable effort has been devoted to data collection, detailed modeling, and analysis for the Well-to-Propeller (WTP) environmental assessment of NG as a transportation fuel in BC, Canada. Extensive data was collected from active oil and gas

companies in the upstream supply chain in BC and a comprehensive study using these data was conducted. This research provides a better understanding of the quantities and sources of WTP emissions of NG/LNG fuel for marine transportation applications with improved accuracy and confidence. The results of this study have been submitted to a journal for publication.

1.4 Dissertation Organization

In Chapter 2, an emission and cost model for various powertrains is developed. The lifecycle costs of the competing powertrain systems including the investment costs, operation/energy-consumption costs, and the replacement costs of key powertrain components are given for ten-year operation life. The emission cost model uses the Global Warming Potential (GWP) method for emission accounting. A study of the well-to-propeller environmental impact of natural gas as a transportation fuel in BC is also presented.

In Chapter 3, an emission and lifecycle cost analysis of hybrid and pure electric propulsion systems for fishing boats is presented. A new integrated marine propulsion system modeling and simulation method and software tools, and a dedicated mobile data acquisition system are introduced to support the quantitative analysis of energy efficiency, emission reductions, and lifecycle costs of a new or retrofitted fishing boat with hybrid electric and pure electric powertrains, compared with the traditional ICE powered benchmark. Following the automotive industry MBD approach, modeling and simulation of electrified fishing ships using actual operation profiles are conducted. Series hybrid electric and pure electric powertrain system designs with powertrain component models and rule-based system control, including a properly sized electric ESS with an SC or battery, are studied. The total CO_{2e} or GHG emissions and lifecycle costs of various new, electrified boat propulsion system designs are quantitatively evaluated against conventional ICE powered boats with both gasoline and diesel engines.

In Chapter 4, series hybrid and battery electric powertrains are developed and investigated for short-range car deck ferries using the Matlab Simscape™ library. Unlike the fishing boat modeling, the forward-facing approach is used for this passenger ferry. Due to a lack of standardized drive cycles for marine vessels, real operational profiles were collected

from BC Ferries MV Klitsa ferry and compared with the simulation results. An actual diesel engine Fuel Consumption Map (FCM) is implemented in the model and efficient engine and battery sizes are obtained using the optimization algorithm. In Chapter 5, the main findings of this dissertation are summarized, the results are discussed, and recommendations for future work are provided.

2 Lifecycle Cost and Emission Estimation

2.1 Lifecycle Cost Model

The lifecycle costs of competing powertrain systems include the investment cost, operation/energy-consumption costs, and replacement costs of key powertrain components over a projected operation life. In this dissertation, a simple cost model is proposed for different powertrain architectures. The cost model estimates the costs for a given Life Cycle Period (LCP) associated with all components of various architectures such as conventional ICE, hybrid electric and pure electric powertrain. Unlike the other cost models, in this work, we only examined the powertrain cost and not the total cost of building a new vessel. The cost model is based on the assumption that all examined vessels are identical in design (tonnage, hull, propeller etc.) but only different in powertrain architectures. By doing this, many non-necessary cost analyses such as overhaul costs, crew salary, port charge, certification, depreciation and etc. can be removed from the model. The cost model only includes the replacement cost of the battery system in the powertrain over the given LCP of the vessel. A separate battery degradation model is developed which is explained in the next chapter.

The total cost of the system consists of two components: investment costs and operational costs. Investment costs are one-time purchase, installation and training costs of a particular unit in the powertrain system. The operational cost is the cost of day to day running of the system in LCP. The total cost of hybrid electric and conventional ICE powertrain is

$$TC_{Hybrid\ Electric} = n \times Trips \times \sum_{j=1}^{n_t} \sum_{i=1}^{n_G} FC_{ij} \times Fuel\ Cost \times \Delta t_j + OE \qquad (1)$$

where n represent the total number of years in LCP, $Trips$ represent the number of crossing per day, FC represent the fuel consumption, n_G is the number of generators, n_t is the time in second, Δt is the simulations time step, and OE represents other expenses listed in Table 4. Similarly, the total cost of battery electric powertrain is

$$TC_{Battery\ Electric} = n \times\ Electricity\ Cost \times \sum_{d=1}^{180} \mathrm{BESS}_{kWh-consumed_d} + OE \qquad (2)$$

where $BESS$ represent consumed kWh of Battery Energy Storage System (BESS). A more detailed description of some components and operation costs is presented next.

Table 4: System costs

Variables		Conventional ICE Powertrain	Hybrid Electric Powertrain	Pure Electric Powertrain
Investment Costs	Inverter cost	-	$0.21 /W-DC [25]	$0.21 /W-DC [25]
	ESS cost with supercapacitor	-	$5,500 /kWh [26]	$5,500 /kWh [26]
	ESS cost with battery	-	$700 /kWh [27]	$700 /kWh [27]
	ESS installation labor	-	0.15 $/W [25]	$0.15 /W [25]
	Electric motor	-	$17,662 @74kW [28]	$50,476@186 kW [28]
	Charger station	-	-	$25,000
	Genset unit cost	$121,000@238 kW [29]	$11,000 @ 15 kW [29]	-
	Genset installation labor cost	$50 /kW	$50 /kW	-
Operational Costs	ESS operation and maintenance	-	$20 /kW/year [25]	$20 /kW/year [25]
	Fuel cost	$1.3 /L [30]	$1.3 /L [30]	-
	Genset operation and maintenance	$30 /kW/year	$30 /kW/year	-
	Electricity cost	-	-	Varies [31]

2.1.1 Electric Motor and Genset Price

The price of the electric motor and genset varies for different power rating and this needs to be included in the analysis. This has been reflected in our calculation using a linear interpolation model developed by engine manufacturer data. The price of different rating gensets and electric motors shown in Figure 10.

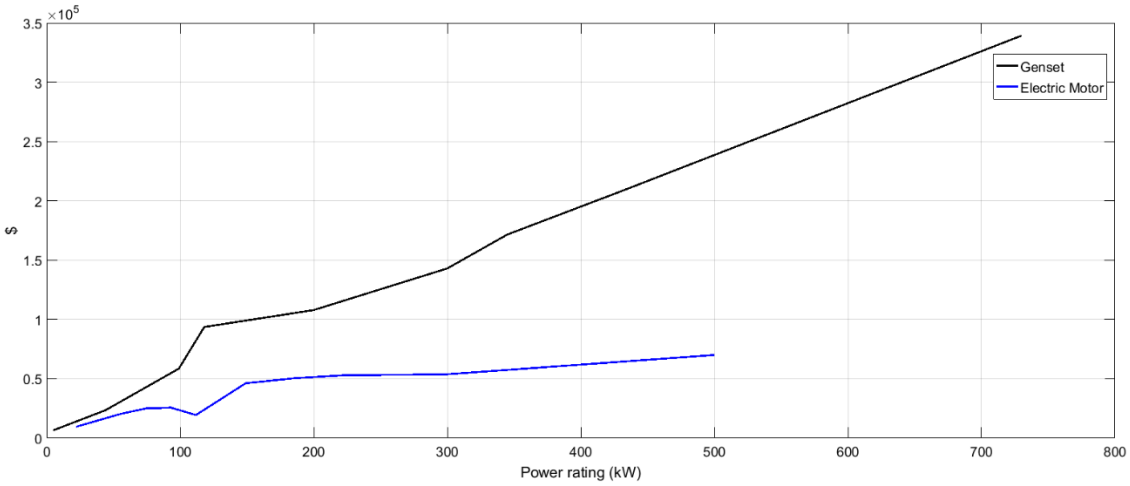

Figure 10: Genset and electric motor prices

2.1.2 Carbon tax

In 2008, BC implemented the first North American carbon tax. After this, carbon taxes gained momentum globally and have been applied in many jurisdictions. From April 2018, the carbon tax is $35 per tonne translated based on the type of fuel consumed [32]. Therefore, the carbon tax is included in the price of fuel in BC and there is no need to calculate it separately. The carbon tax rates for different fuels are given in Table 5.

Table 5: Carbon tax rate for different fuels [32]

Fuel	Tax Rate Based on $35/Tonne of Emissions
Gasoline	7.78 ¢/litre
Diesel (light fuel oil)	8.95 ¢/litre
Natural gas	6.65 ¢/cubic meter

The carbon tax applies to all fuels such as gasoline, diesel, natural gas, heating fuel, propane and coal. This tax will increase yearly by $5 per tonne of CO_{2e} until 2022. To estimate the carbon tax after 2022, we assumed the same increase as shown in Figure 11. In the cost analysis, the carbon tax is added to the fuel price for each year.

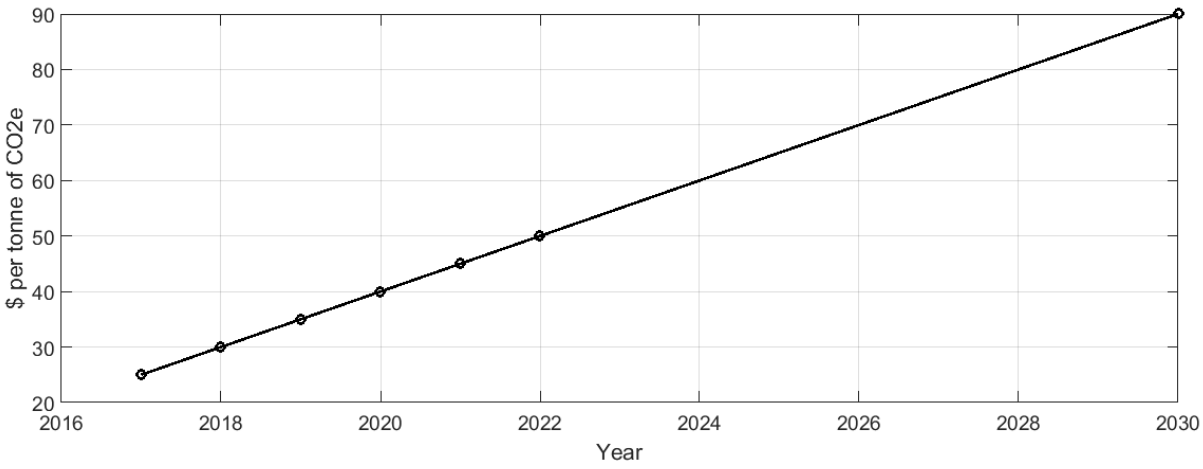

Figure 11: Carbon tax in BC

2.1.3 Fuel price

The cost of fuel varies by region. The Vancouver fuel retail price is selected for use in this study. Figure 12 illustrates the Vancouver average retail price for diesel fuel at self-service filling station for the last four years. The average diesel fuel price in this analysis is 1.3 $/liter of fuel.

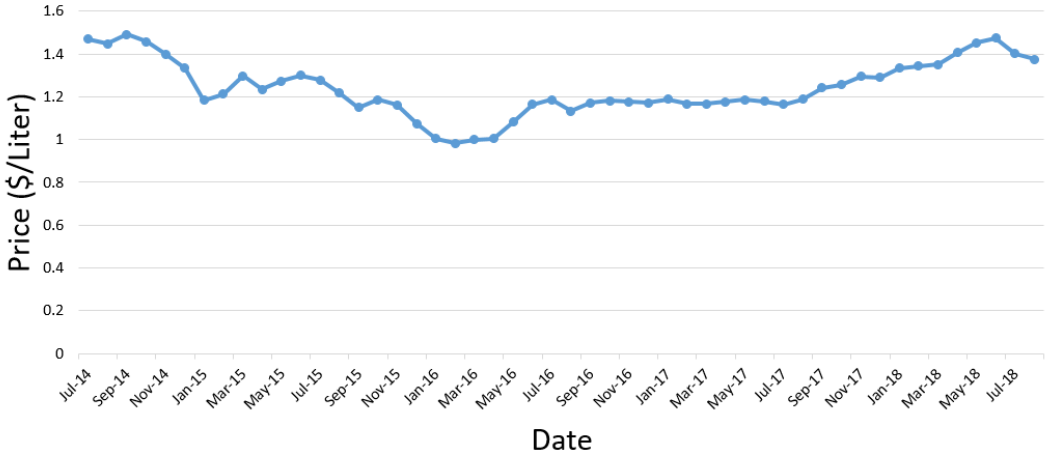

Figure 12: Diesel fuel retail price in Vancouver [28].

2.1.4 Health Costs

One of the largest benefits of air pollution reduction by vessels is human health cost reduction. According to the World Health Organization (WHO), more than 4.2 million deaths were a result of air pollution in 2016 [32]. It is estimated that 16% of lung cancer,

25% of chronic obstructive pulmonary disease, 17% of ischaemic heart disease and stroke, and about 26% of respiratory infection deaths are caused by air pollution worldwide. Accurate estimation of the health cost due to air pollution is a very difficult task mainly due to the range of parameters and lack of data. A more comprehensive presentation of health cost benefit due to vessels air pollution is given in [33]. For the purpose of this analysis, we have ignored the health cost benefits.

2.2 Emission Estimation Model

Emission accounting is a process of estimating emission quantities for different pollutants. Emission accounting for vessels is normally calculated over a fixed period (20 or 100 years) and gives good information about whether goods and passengers are transported in an environmentally friendly manner or not. Emission accounting enables intuitive calculation of pollutions in a specific region; hence provide a powerful supervision tool that can be used for comparison of different vessel powertrain design. In this section, the related literature in marine vessel emissions is reviewed.

There are two types of emission accounting method in use nowadays: top-down method and bottom-up method. Each method has some advantages and disadvantages that we will address here. The top-down method provides information about emission of individual vessel, route and shipping areas based on statistical analysis of vessel operation. On the other hand, the bottom-up method estimates emissions based on individual vessel activity and totals the energy consumption to provide the quantity of emissions. A comprehensive study of these two methods is given in [33].

2.2.1 Top-down Method

Initially, a top-down method was developed based on the assumption of similar emission pattern for different vessels on the same route. This was mainly caused by limited information about vessels maximum engine power, design speed, tonnage or total installed power. However, this was solved by technological advances and the use of information from government and non-government organizations such as IMO and Lloyds Register of Ships (LRS).

The top-down method uses vessels fuel consumption as an input to the model and this data can be obtained by bunker sales data, vessel fuel consumption or simulation data [34] and [35] used bunker sales data collected from local companies. In [34] a regression model was used to relate the bunker consumption to gross tonnage of vessels and sample vessels were allocated to each bin with specific fuel consumption. However, in [35], major shipping routes and its traffic volume is used for calculation of energy consumption for each vessel. After that, both studies used emission factors for calculation of emission. The emission factor is a constant that represents the relationship between pollutants released to the atmosphere with an activity associated with the release of that pollutant [36].

In recent years, advanced top-down emission counting models were developed using individual vessels operation data. In [36], average vessels speed were used to categorize engines operation in three different modes such as cruising mode (over 8 knots), maneuvering mode (1-8 knots) and hoteling mode (below 1 knot). At each mode, the engine has a different emission factor hence this increases the accuracy of emission accounting. In a different study by [36] more advanced and complicated model developed while the effect of other variables like wind direction, wave height, cargo load etc. were included. The model introduced in [36] had a couple of problems. Firstly, all vessel activities were collected by voyage record (voyage log) by captain or deck officer and it was updated once a day which can be considered infrequent as wind direction and waves change continuously. Secondly, the sample time in this model is small which may cause a larger error rate [33]. In [36], a simulation model was developed to create a set of data for emission analysis based on countries, goods types, and routes.

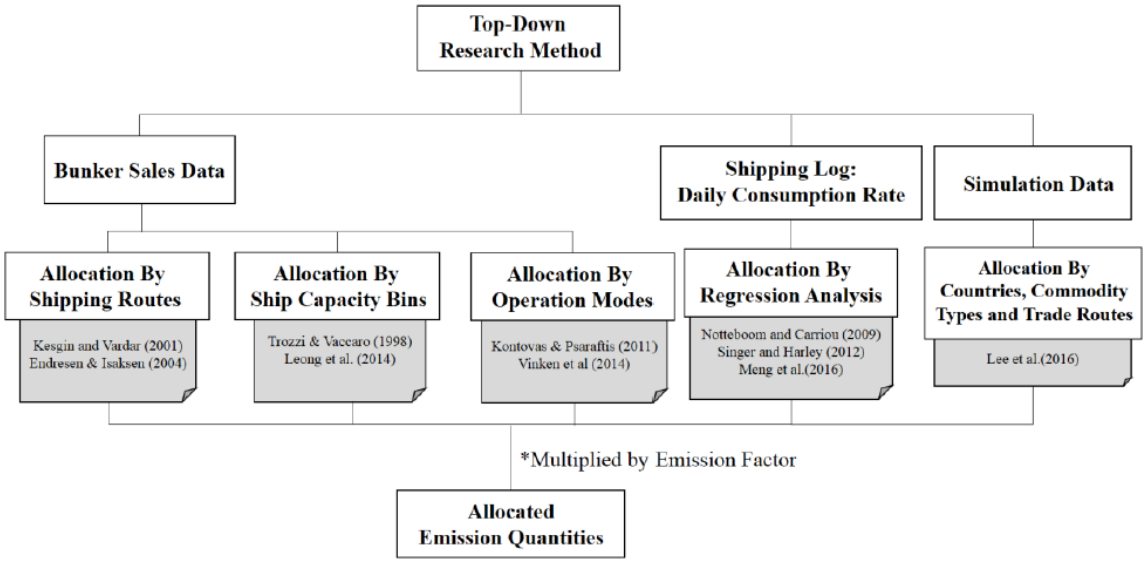

Figure 13: Bottom-up approaches for emission accounting [33]

2.2.2 Bottom-up Method

The bottom-up research method was first used in [36]. This method used individual vessels emission and estimated accumulated total emission with a high accuracy. Currently, there are several types of bottom-up methods available, which all have a similar basic framework developed in [36]. The inputs to these models are normally vessel specifications and its location information. The vessel specification can be obtained from international organizations like IMO or Lloyd's Register of ships (LRS) which provide necessary information like installed engine power, design speed, vessel type etc. Using vessels location data (GPS points), the sailing speed can be calculated for a given time interval. The ratio of sailing speed over the maximum design speed to the power of three defines the vessels load factor. The Load factor equation is presented below

$$Load\ Factor_{Cruise\ mode} = \left(\frac{Cruise\ Speed\ [Knots]}{Maximum\ Speed\ [Knots]}\right)^3 \quad (3)$$

Load factor during each mode should be calculated by modifying the above equation and multiplying the maximum cruise speed by a constant factor in order to reduce the error. After obtaining $Load\ Factor$, total emission for each engine can be calculated as

$$Emission_{mode} = (calls) \times (P_{engine}) \times \left(\frac{hrs}{call_{mode}}\right) \times (LF_{mode}) \times (EF_{engine,gases}) \times (10^{-6}) \quad (4)$$

where $Emission_{mode}$ is metric tonnes emitted from the engine in a specific mode, $mode$ is mode of engine othe peration in any following categories: hoteling, maneuvering, reduced speed zone (RSZ), and cruise, $calls$ is round-trip visits, P_{engine} is the total engine power in kilowatts, hrs is hours per call for each mode, LF_{mode} is load factor for engine in each mode (unitless), $EF_{engine,gases}$ is emission factor for engine for the pollutant of interest in g/kWhr, and 10^{-6} is conversion factor from grams to metric tonnes.

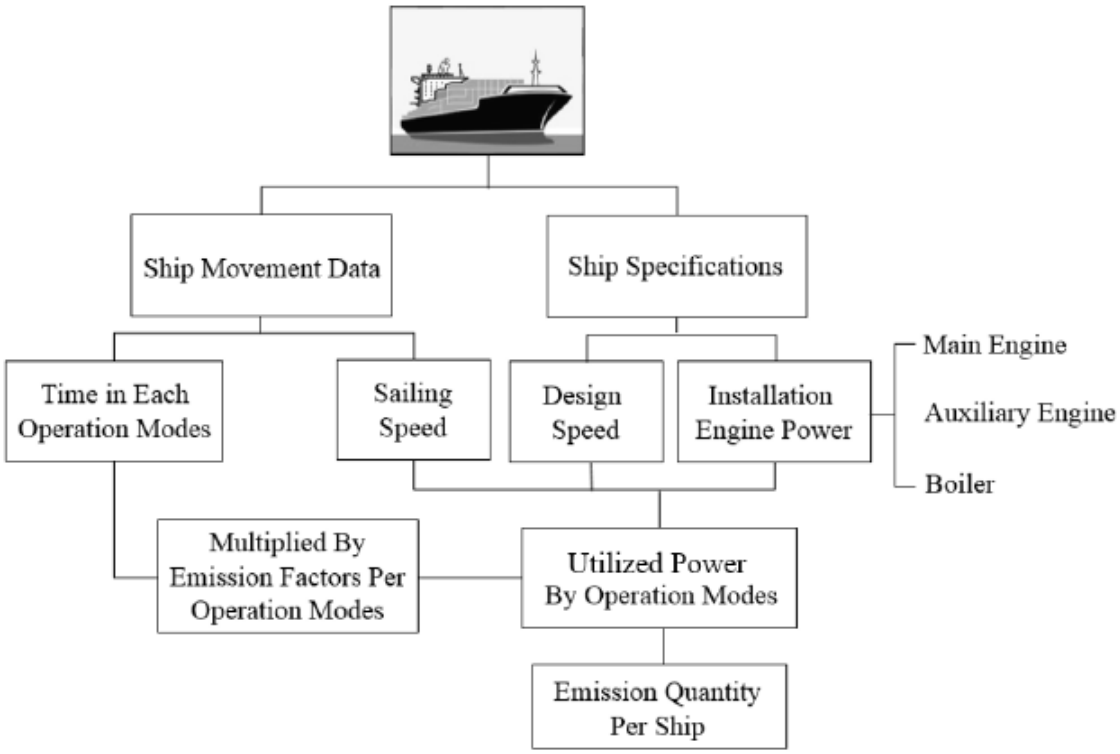

Figure 14: Top-down approaches for emission accounting [33]

Despite higher resolution and accuracy of the bottom-up method in comparison to top-down method, there is a need to develop a technique to solve handling of large Automatic Identification System (AIS) data points and better estimation of auxiliary engine and boiler power. The top-down method requires less effort for data processing and it is faster than the bottom-up method due to the rough estimation of fuel consumption. This method can also include a comprehensive set of variables, such as wind, wave, and the cargo load.

In this dissertation, the bottom-up method with a new approach is used for emission accounting. Due to high variation of load power for selected vessels such as fishing boats, the previous models cannot accurately estimate the actual emission. For this purpose, the engine emission and fuel consumption map given in Advanced Vehicle Simulator (ADVISOR) developed by national renewable energy laboratory for the United States Department of Energy (DOE) written in the MATLAB/Simulink environment is used. ADVISOR is a simulation program for analysis of the performance and fuel economy of light and heavy-duty vehicles with conventional (gasoline/diesel), hybrid-electric, full electric, and fuel cell powertrains. The engines information bank in this software is used for a range of different engine technology and engine size. The collected vessel engine speeds and torque were given as an input to the model and proper values were obtained using a look-up table. The simulation block of the emission model is given in Figure 15. The emission map for each gas is inserted into a two dimensional look-up table in Simulink. When, engine emission data for a selected engine is not available, the total emissions are calculated by multiplying the fuel consumption and the corresponding emission factor given in [37].

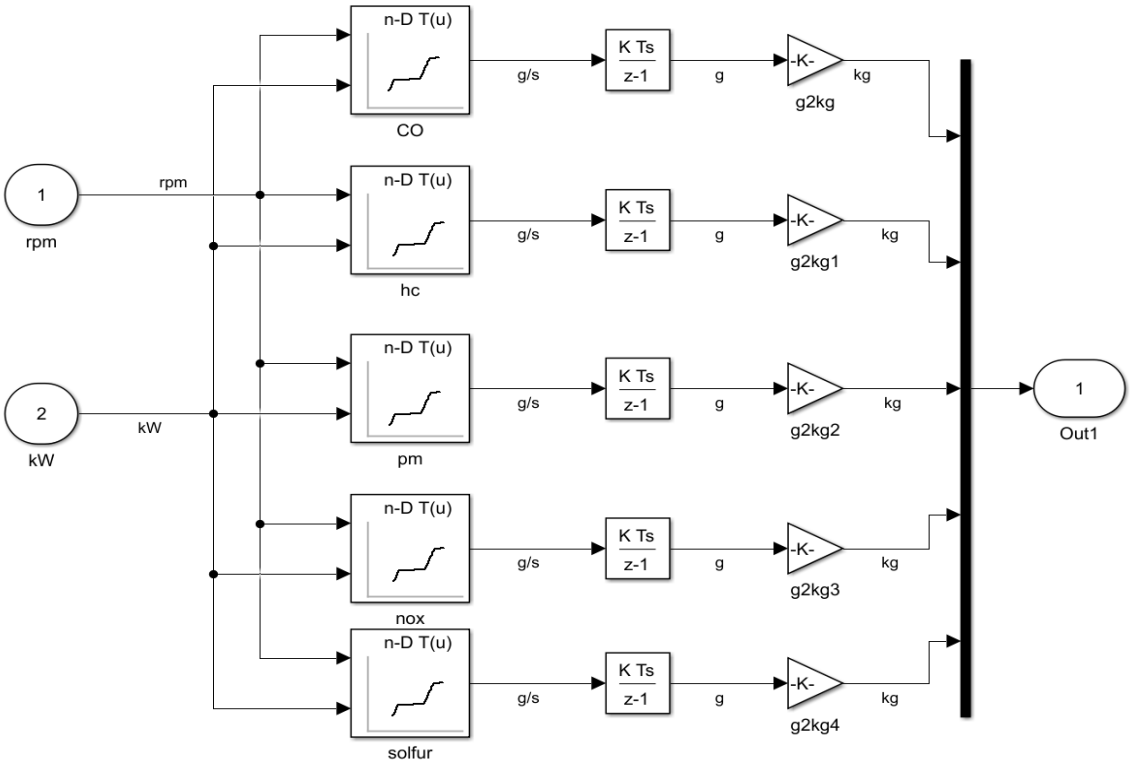

Figure 15: Simulink block diagram of emission model

2.2.3 Well-to-Propeller Environmental Assessment of Natural Gas as a Transportation Fuel in BC

Natural gas (NG) is a potential transition fuel towards green energy systems. It produces higher energy per combustion carbon dioxide (CO_2) molecule compared to other fossil fuels such as oil or coal [38][39]. It is expected that NG will play a significant role as a cleaner and more economical transportation fuel in the future. Canada has abundant natural gas resources as the fourth largest producer of NG in the world. The marketable natural gas production in Canada was over 450 million cubic meters per day (mm^3/d) in 2017, with BC and Alberta contributing 25% and 72% of the total production, respectively [40]. The recently announced major investment in LNG production facilities in BC will boost provincial NG production. In addition, improvements in drilling technology in recent years have resulted in more cost-effective production of unconventional natural gas, leading to increased Canadian production and likely lower NG fuel costs for consumers.

Stricter environmental regulations and increased world energy demand have created an opportunity for increased NG use in the transportation sector including marine applications that represent substantial energy consumption. Lower NG costs in Canada will results in higher adoption rates over the global average. Figure 16 illustrates the NG price trend in Alberta NG which is the largest NG trading hub in Canada [41].

Figure 16: Monthly natural gas prices for Alberta [41]

Most deep-sea shipping and a high percentage of coastal shipping operate on Heavy Fuel Oil (HFO). HFO is a residual product of crude oil and contains a wide range of contaminants such as sulfur, sodium, and ash that are particularly harmful to the environment and human health. Marine Diesel Oil (MDO) and Marine Gas Oil (MGO) are traditional marine fuels known as marine distillates. These fuels have a lower concentration of sulfur compared to HFO and so are considered a cleaner fuel. The evolving and increasingly stricter environmental regulations enforced by the International Maritime Organization (IMO) have led to significant changes in marine fuels and engines. Recent IMO emission regulations limit the sulfur content of fuel to 0.10% by weight in the North America Emission Control Area (ECA) and below 0.5% in all other areas globally [42]. For small and medium-size marine vessels, Ultra-Low Sulfur Diesel (ULSD) fuel has been mandatory as of June 2012.

In comparison to HFO and distillate fuels, NG is a cleaner fossil fuel and results in lower CO_2, SO_x, NO_x, and Particulate Matter (PM). However, methane (CH_4) is the primary component of NG and is a significant GHG emission. The radiative force of methane is 30 times greater than CO_2 over a 100 year time period [43]. Thus, the potential benefits of NG have been challenged considering upstream methane leakage [39], [44]–[49], as well as during the low speed and low load operations of NG engine. Despite the fact that NG is a cleaner fuel, high vent and leakage rates to the atmosphere between production wells and the point of combustion can significantly reduce the environmental benefits.

Assessment of the environmental impact of NG is a very complex task and there is a lack of reliable methods to estimate the associated emissions due to uncertainties. One uncertainty is the amount of fugitive gas emitted into the atmosphere during operation, leading to adjustments in the methane emissions reported by the U.S. Environmental Protection Agency (EPA). The estimated national average production leak rate in EPA reports has increased from 0.16% of production in 2010 to 1.36% in 2011, and 1.25% in 2012. This rate was increased to 1.36% in 2013 and then reduced to 1.33% in 2014 [50][51]. It is estimated that if more than 3.2% of the NG transported from wells to the gas- fired power plants in the US leaks into the atmosphere, the environmental impact would be greater than the equivalent coal-fired plants [52].

This work presents the first effort to systematically estimate the GHG emissions in the upstream supply chain of NG in British Columbia (BC), Canada. BC is the second largest producer of NG in Canada, and an accurate estimation of these emissions can improve the understanding of the NG upstream supply chain emissions in Canada. Similar technologies are used in Alberta, the largest NG producing province in Canada. The assessment covers all areas of the NG supply chain where there are GHG emissions, including fugitive, vented, flared and combustion emissions. Several scenarios are examined to estimate the emission rates. At present, the lifecycle GHG emissions of various transportation fuels are estimated using standard LCA models to assess the environmental impact of alternative fuel paths, including GREET (Greenhouse gas, Regulated Emissions, and Energy use in Transportation) developed and maintained by the Argonne National Laboratory (ANL) of the US Department of Energy [53], and GHGenius [54] developed and maintained by

Natural Resources of Canada (NRCan) with a primary focus on transportation fuels in Canada. Many transportation studies employ these LCAs [55][56][18]. However, neither incorporate detailed GHG emission data and operations from BC NG producers and they do not include marine transportation specific considerations. For example, well completion emissions are flared in Canadian shale gas facilities and venting of unloaded liquids is not permitted in conventional gas production operations in Canada, whereas it is common practice in the US. The LCA of marine transportation fuels in this work is called WTP assessment and covers all stages of the fuel production and usage from feedstock recovery (well) to vessel propellers. To date, the WTP GHG emissions of LNG fuel for marine vessels based on actual fuel consumption has not yet been systematically evaluated, and this study fills this gap. In this work, units of grams of carbon dioxide equivalent released per megajoule of energy (gCO_{2e}/Mj) are considered based on the IPCC Fifth Assessment Report (AR5). This report indicates that the 100-year GWP of methane and nitrous oxide are 30 and 265 times greater than CO_2, respectively.

2.2.3.1 Natural Gas System Analysis

The upstream GHG emissions depend upon the geologic reserve formations and the extraction, transportation, and fuel processing methods employed. Identifying the fuel path is essential for an accurate assessment of the GHG emissions in the upstream supply chain. In BC, there are five main NG production areas located mainly in the northeast of the province. Unconventional gas production accounts for 85% of the production in BC. The largest NG production operation in BC is the Montney area, covering 130,000 km^2 between BC and Alberta. This super condensate area contributed 73% of the total BC NG production in 2016 [18]. With current drilling in Montney, this percentage is expected to increase. Horizontal drilling and multi-stage hydraulic fracturing are common extraction practices in this area. The extracted NG is transported by six main pipeline companies. Enbridge, formerly known as Spectra, has the largest share of the pipeline system in BC and transports NG from the northeast to the lower mainland as shown in Figure 17. FortisBC is the second largest transporter and distributes NG to the lower mainland and Vancouver Island. The pipeline length from Montney to Vancouver Island is approximately 1,300 km.

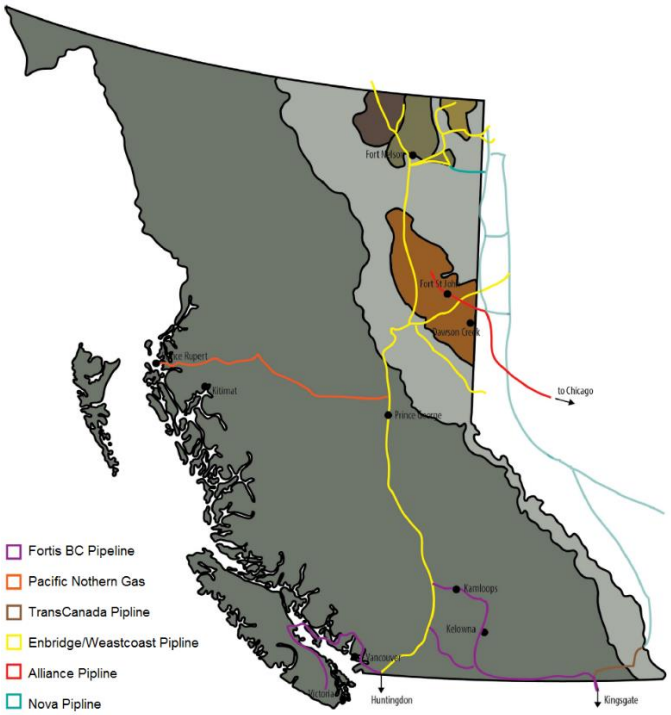

Figure 17: The natural gas pipeline system in BC [58]

2.2.3.1.1 Vessel Description

An accurate evaluation of energy efficiency and GHG emissions of marine vessels must be based on the actual fuel consumption during vessel operation. For this purpose, the fuel consumption of two vessels on the same route is used. One of these vessels operates on diesel fuel while the other operates on LNG fuel. The approximate route is shown in Figure 18. The vessels travel several times per day between the Vancouver Island and Vancouver terminal to transfer goods and passenger.

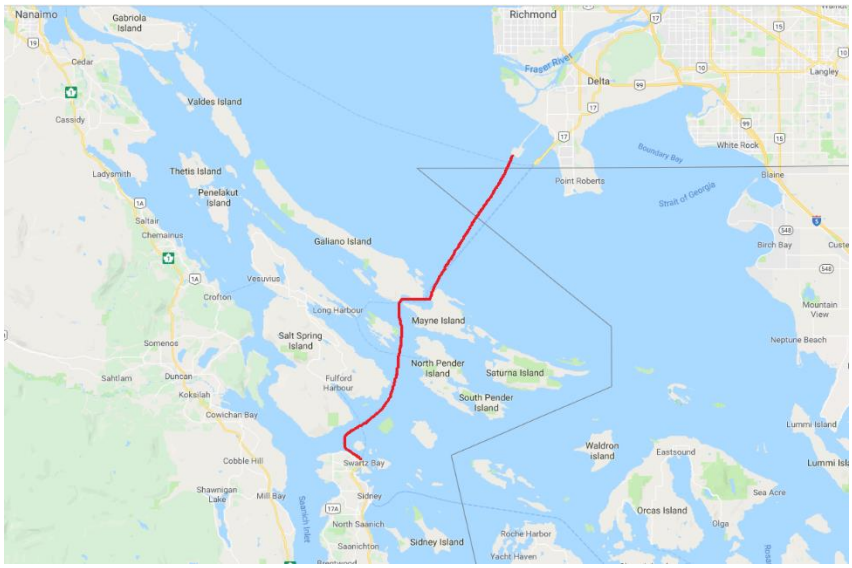

Figure 18: The approximate vessel route

2.2.3.2 LNG Upstream CO_{2e}

In this work, the upstream NG supply chain is divided into extraction and processing, transportation, conversion and storage, and distribution/bunkering, as shown in

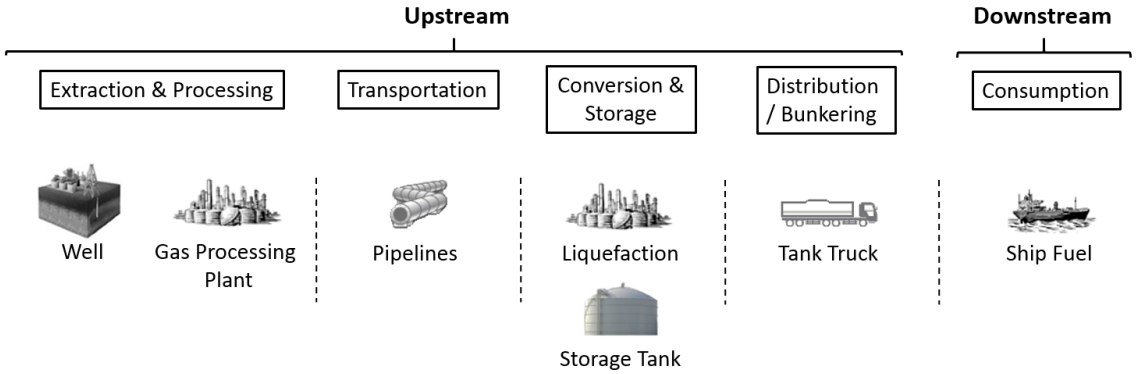

Figure **19**. With this division, the bunkering stage is included in the upstream chain rather than in the downstream chain as in the related literature to better characterize the emission sources of downstream consumption.

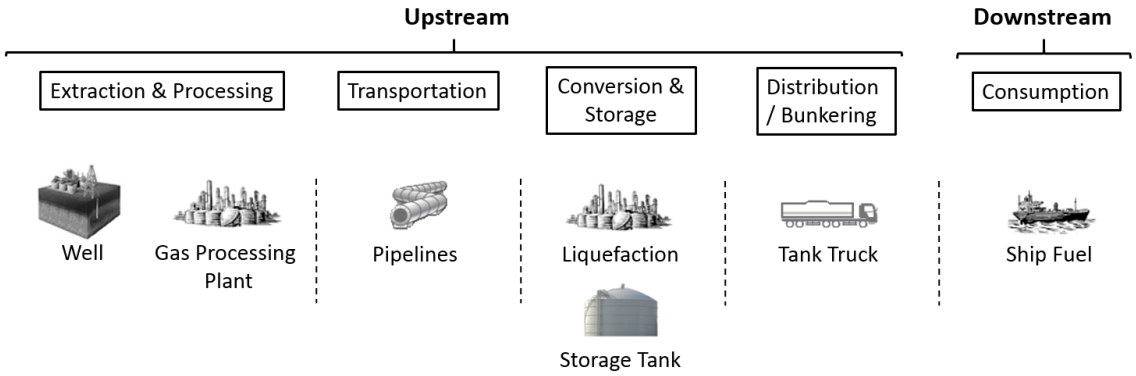

Figure 19: The natural gas supply chain

It is essential for a comprehensive analysis of GHG emissions to consider all emissions produced during the stages in the fuel production and use lifecycle, including fuel consumption, flaring, venting and fugitive gases. In addition to the BC GHG emission data published in [58], forty-seven oil and gas companies in BC were interviewed for this study to have more accurate GHG emission estimates for these companies. The total upstream NG GHG emissions were calculated by adding the carbon dioxide equivalent (CO_{2e}) emissions from each of the four segments shown in

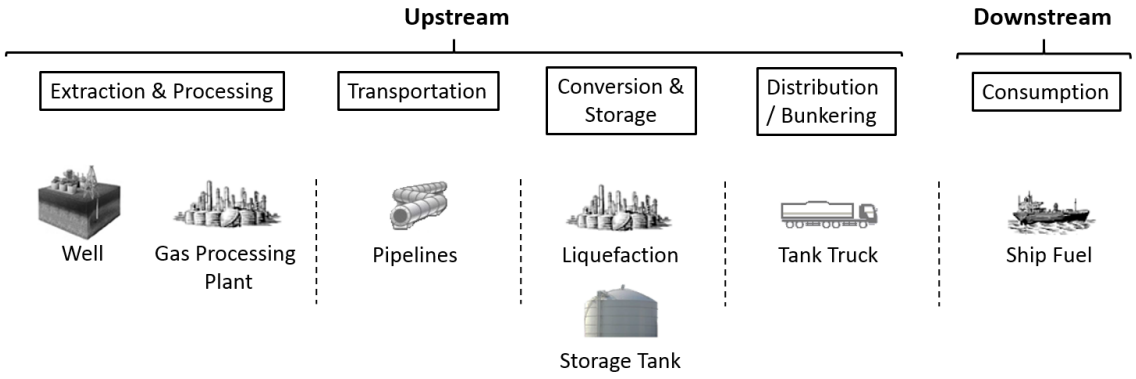

Figure **19**, resulting in estimated total GHG emissions between 9.8 to 10.4 gCO_{2e}/Mj. Details of this analysis for each segment are given below. Note that the BC emission inventory includes only facilities over the provincial reporting threshold of 10,000 tonnes of CO_{2e} per year, so smaller facilities are not considered in this study. This will not have a significant effect on the results given the low number of facilities with emission levels below this threshold.

2.2.3.2.1 Extraction and Processing

Horizontal drilling and multi-stage hydraulic fracturing are common methods of gas extraction in Montney. Recent LCA studies have suggested that unconventional gas extraction methods result in higher emissions than conventional methods [59] [60] [61]. This is mainly because of emissions during well completion. In [60], it was estimated that shale gas has 1.8% to 2.4% higher lifecycle GHG emissions than conventional gas, mainly due to higher methane release during well completion. Figure 20 illustrates the CO_{2e} emissions during extraction and processing for each segment in BC. This shows that fuel combustion during operation contributes about 54% of the total emissions. The second and the third highest emission are related to venting CO_{2e} from fossil fuels and methane venting, accounting for about 15% and 13% of the total emissions, respectively.

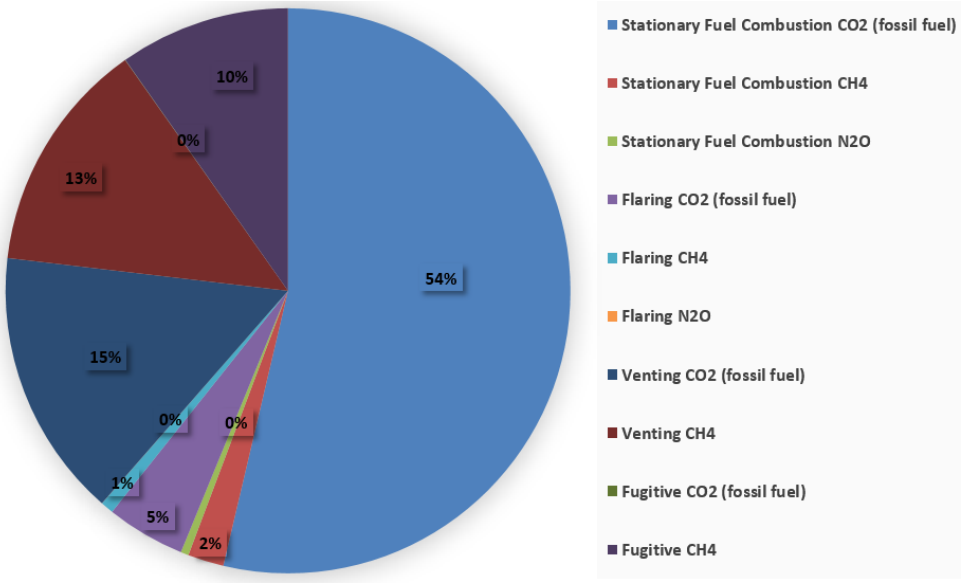

Figure 20: Extraction and processing CO_{2e} per segment

The BC GHG emission repository [58] was used to determine the company emissions during NG extraction and processing shown in Table 6. The total emissions for each company were calculated by adding the emissions from each stage. For example, the emissions for the Alliance Pipeline Company are as follows

Stationary Combustion + Industrial Process + Flaring + Venting + Fugitive = Total

9,098 + 0 + 0 + 1,632 + 1,214 = 12,508

tonnes CO_{2e}

The total extraction and processing emissions from all companies were obtained as 8,972,566 tonnes of CO_{2e}. The total BC NG production in 2015 was 37,873,364 thousand cubic meters [62]. Based on this information and the conversion factors given in Appendix A, the total emissions for extraction and processing is estimated to be between 5.53 to 6.10 gCO_{2e}/Mj. A recent study using mobile collected methane emissions data from oil and gas infrastructure estimated that the Montney area contributes 111,800 tonnes of methane per year to the atmosphere [47]. This is about 43% higher than the value given in the BC emission inventory used in this analysis. Taking this into account, the estimated extraction and processing emissions would be 6.40 to 6.82 gCO_{2e}/Mj. In another study using airborne measurements of oil and gas infrastructure in the Red Deer region of Alberta, Canada, methane emissions were estimated to be 25% to 50% greater than government estimates [49].

Table 6: BC company GHG emissions in 2015

Company	**Type of Company**	**Pipeline GHG (tonnes CO2e)**	**Emissions (tonnes CO2e)**
Aitken Creek Gas Storage ULC	NG	0	47,070
Alliance Pipeline Ltd.	NG	12,508	0
AltaGas Ltd.	NG	0	85,157
ARC Resources	Oil	0	0
Black Swan Energy	NG	0	47,416
Bonavista Energy Corporation	NG	0	67,919
British Columbia Hydro and Power Authority	N/A	0	0
Canadian Natural Resources Limited	NG	0	1,264,479
Canbriam Energy Inc.	NG	0	111,213
Cequence Energy Ltd.	NG	0	11,325
Chevron Canada Resources	NG	0	39,596
Chinook Energy Inc.	NG/Oil	0	53,379
ConocoPhillips Canada Resources Corp.	NG	0	331,118
Crew Energy Inc.	NG	0	92,850
Devon Canada Corporation	NG	0	5,539
Direct Energy Marketing Ltd.	Unknown	0	111,827
Encana Corporation	NG	0	900,761
Endurance Energy Ltd.	Unknown	0	602,952

Enerplus Corporation	Unknown	0	43,295
EOG Canada Oil & Gas Inc.	Unknown	0	34,253
FortisBC Energy Inc.	Transportation	136,382	0
Harvest Operations Corp.	Oil	0	0
Husky Oil Operations Limited	NG	0	114,045
Imperial Oil Resources Ltd.	Unknown	0	0
Kelt Exploration	Unknown	0	0
Keyera Corporation	NG	0	40,091
Lightstream Resources Ltd.	Unknown	0	9,953
Lone Pine Resources Canada Ltd.	NG	0	6,748
Murphy Oil Company Ltd.	NG	0	177,411
Nexen Energy ULC.	NG	0	92,089
Pacific Northern Gas Ltd.	Transportation	39,019	0
Painted Pony Petroleum Ltd.	NG	0	46,566
Pengrowth Energy Corporation	NG	0	34,732
Penn West Petroleum Ltd.	NG/Oil	0	76,047
Polar Star Canadian Oil and Gas Inc.	Unknown	0	23,815
Progress Energy Canada Ltd.	NG	0	979,105
Quicksilver Resources Canada Inc.	Unknown	0	15,151
Ramshorn Canada	NG	0	23,157
Shell Canada Limited	NG	0	362,850
Spectra Energy Midstream Corporation	NG	0	250,873
Spectra Energy Transmission	Transportation	1,500,642	2,800,790
Suncor Energy Inc.	NG	0	20,937
Taqa North Ltd.	NG/Oil	0	48,058
Tourmaline Oil Corp.	Unknown	0	0
TransCanada PipeLines Ltd.	Transportation	234,513	0
Veresen Midstream General Partner Inc.	Oil	0	0
Whitecap Resources Inc.	Oil	0	0
Total		1,923,063	8,972,566

2.2.3.2.2 Pipeline Transportation

The emissions from pipelines are mainly due to the burning of fossil fuels at the compressor stations and methane leaks. Compressor methane losses account for about 46% of the total methane emissions in the stations while compressor-packing vents contribute about 17% of the total compressor methane losses [22]. The remaining emissions are due to pneumatic actuators and controllers, engine crankcases, wet seal vents, and slop tanks. Stricter

maintenance practices and more energy efficient compressors can reduce pipeline emissions. The emissions of the five main pipeline companies in BC including FortisBC, Pacific Northern, TransCanada, Enbridge, and Alliance, are considered in this study and the total emissions were calculated by adding the pipeline emissions from these companies given in Table 6. The emission contribution of each company is shown in Figure 21. The total emissions related to NG management, pipelines, and transportation are estimated to be 1.31 gCO_{2e}/Mj. NOVA Gas Transmission Ltd has a short pipeline with limited activity in BC, and so is not included. The total pipeline emissions are 13% lower than that obtained value for Canadian NG pipeline emissions using GHGenius [54]. This is due in part to stricter environmental regulation in BC and newer facilities [63].

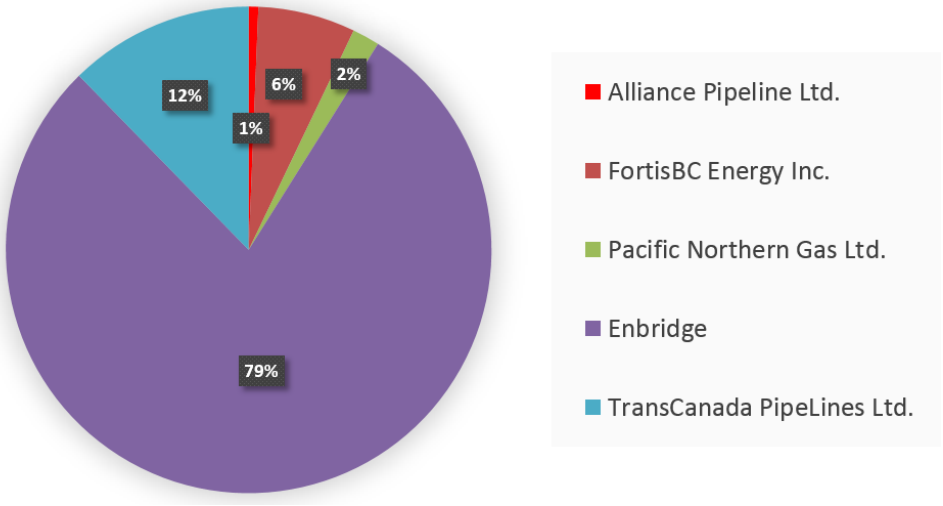

Figure 21: Pipeline company emission contributions in BC

2.2.3.2.3 Conversion and Storage

The energy density of NG is less than that of diesel fuel, so a larger fuel tank is required for vessels with NG engines. Natural gas is stored in liquid form at a temperature of approximately -160º C with volume reduced by a factor of 600 [64]. Before liquefaction, any impurities and contaminants are removed from the gas, and the liquefaction is done in a coolant chilled by large refrigerators. Liquefied natural gas (LNG) is a clear, colorless, and safe liquid that is easy to store and transport. It is kept in insulated tanks during transportation and storage until it is ready for loading onto a ship or vehicle.

There are five NG liquefaction processes in use today, propane pre-cooled mixed refrigerant (C3MR), AP-X large train cycle, optimized cascade, Shell double-mixed refrigerant (DMR), and mixed fluid cascade [64], and each of these processes have different efficiencies and production capabilities. Liquefaction of NG is an expensive process in terms of energy and cost, accounting for up to 50% of the total plant costs, while refrigeration accounts for 30% to 40% of the costs.

Emissions and energy use at NG liquefaction facilities are a function of the leakage rate, type of motors (electric or gas) and facility efficiency. Unfortunately, little data is available on the emissions and the energy requirements of the liquefaction processes and facilities, and further study is needed to obtain more accurate estimates of these emissions. LCAs such as GREET and GHGenius combine liquefaction with pipeline transportation emissions. Using the 3.38 gCO_{2e}/Mj given by GHGenius 5.0 [54] for liquefaction and BC pipeline transportation, emissions from the NG liquefaction process are estimated to be 2.1 gCO_{2e}/Mj.

2.2.3.2.4 Bunkering

Four different types of LNG bunkering systems are used, fixed shore facilities, portable tank transfer, tanker trucks, and LNG barge carriers, as shown in Figure 22. LNG bunkering systems depend on many factors, such as berth characteristics (turns, depth, and hazards), vessel design, fuel demands, and availability. LNG bunkering using tanker trucks is the most favorable method in terms of flexibility and capital investment. Tanker truck bunkering is currently employed by BC Ferries. The main reason for not using other systems are high tidal deviations on the west coast of Canada and limited berthing space.

In this work, it is assumed that the current LNG storage facility at Mt. Hayes, Vancouver Island, provides the LNG fuel for the vessel. The emissions from tanker trucks used in transporting LNG to the vessel are relatively small in comparison to the overall upstream emissions and so are ignored. However, the methane leakage during bunkering is significant and so must be included. There is a lack of methane emission data for marine vessel bunkering, so the available LNG station leakage data for LNG powered ground transportation given in Table 7 and obtained from [51], [65] are used in this work for marine vessels. Unlike LNG fuel stations, the marine bunkering method employed does

not produce boil-off gas because the Mt. Hayes facility is connected to the Vancouver Island NG distribution grid so the boil-off gas is captured and fed into the grid. LNG delivery, continuous station, fuel tank, and fuel nozzle leakage will occur, so the total bunkering emissions are estimated to be 0.89 gCO_{2e}/Mj.

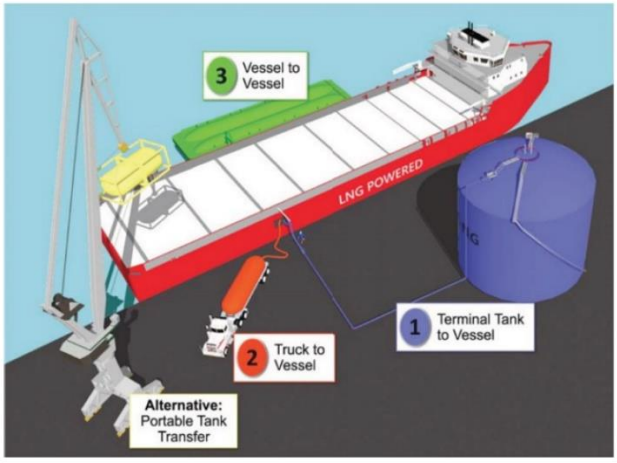

Figure 22: The four different bunkering methods [66]

Table 7: LNG station methane leakage (Ch_4 g/Mj)

	LNG delivery	Manual vent	Boil off gas from the tank	continuous station	Fuel tank	Fuel nozzle
LNG station (Ch_4 g/Mj)	0.015	0.013	0.011	0.002	0.011	0.002

2.2.3.3 LNG Downstream CO_{2e}

During the downstream use of NG as a marine vessel fuel, NG engines are the main contributors to CO_{2e} emissions. Therefore, accurate estimation of engine emissions is essential for precise lifecycle assessment. An NG engine emits less CO_2 than a diesel engine [56], mainly due to the gas composition with lower hydrocarbons. Although this implies a lower environmental impact, the potential benefit can be compromised by methane leakage or the release of unburned methane from the engine. The level of emissions and methane leakage depend on the age and technology of the engine.

NG engines can be classified into three basic types: spark-ignited, dual fuel, and direct injection. A spark-ignited engine uses a spark plug to ignite a mixture of NG and air. This type of engine has high thermal efficiency due to the high specific heats for lean fuel-air mixtures [67]. These engines meet IMO Tier III standards but are sensitive to gas quality and methane slip. Dual fuel engines operate on NG and/or a secondary fuel, such as a distillate fuel. These engines use a pilot fuel to start the combustion process and this fuel is less than 5% of the total consumed with modern technology. A dual fuel engine is an attractive option for ship owners as it provides flexibility in fuel type, cost, and availability. Dual fuel engines also meet IMO Tier III but are sensitive to gas quality and methane slip. A direct injection engine operates on a diesel cycle with high pressure. Natural gas is injected at the top of the compression stroke. The modifications required to convert a regular diesel engine to direct injection NG engine are minimal, thus providing great potential for retrofitting existing diesel engines to NG direct injection. However, direct injection engines do not meet the IMO Tier III standard. Recently produced direct injection engines use advanced combustion control technologies which have resulted in a 10% performance increase over traditional direct injection engines [68]. A comprehensive study of marine NG engines is given in [69].

The emissions and fuel consumption of diesel engines also depend on the engine load. The powertrain architecture is one of the key factors in determining this load. The four main powertrain architectures for marine vessels are shown in Figure 23. Figure 23-A illustrates the conventional architecture in which the diesel engine is directly connected to the propeller via a speed reduction gearbox. In this case, the engine provides all the propulsion power required by the vessel with no power flow flexibility. In the series hybrid electric powertrain architecture shown in Figure 23-B, the engine is coupled to a generator that produces electricity, and an electric motor is coupled to the propeller with the speed adjusted using a variable frequency drive. Multiple generators and motors can be used. An ESS can provide additional energy for propulsion when needed, or can be charged using excess engine power. This allows the engine to operate in its most efficient speed and torque output zone. A series powertrain can better serve vessels with dynamically varying loads such as tugboats. In the parallel hybrid electric powertrain architecture shown in Figure 23-C, the engine and electric motor are both connected to the propeller through

mechanical links, and the electric motor can operate either as a motor or a generator. A bidirectional converter provides power from the bus-bar to the motor/generator, and an electric ESS provides or stores energy. This powertrain system allows the engine size to be reduced to an optimal value. A parallel hybrid powertrain architecture is suitable for vessels dominated by static propulsion loads, such as ferries sailing on calm water, to avoid mechanical-electric-mechanical energy conversion losses.

In a battery electric or pure electric powertrain architecture as shown in Figure 23-D, the battery ESS is the only source of energy to meet the propulsion needs of the vessel. This is similar to battery powered or Pure Electric Vehicles (PEV). In this system, the battery ESS is coupled to a DC/DC converter to provide power for the electric motor(s). For small and short-haul vessels, this design offers high energy efficiency, low noise, and good reliability, but clean electric power and long battery life are essential for this architecture to be beneficial. Factors such as limited traveling range, high battery cost, bulky and expensive fast-charging stations, and the cost of expanding existing electrical grids have restricted the adoption of pure electric vehicles and vessels.

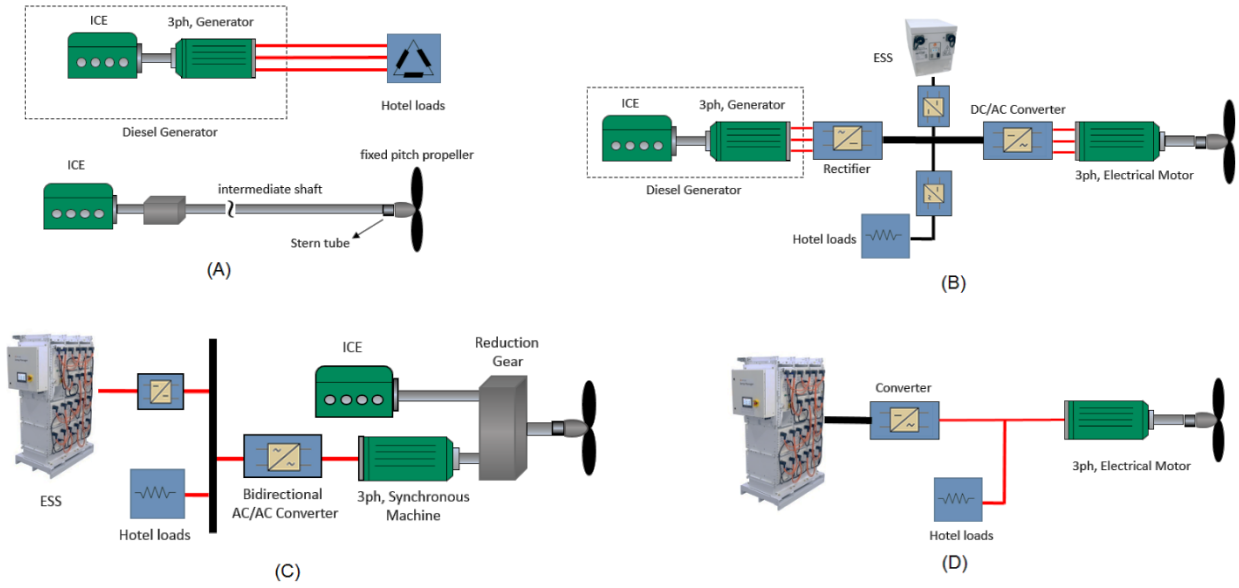

Figure 23: Four powertrain architectures

In this work, engines emission factors are obtained using the Total Energy and Environmental Analysis for Marine Systems (TEAMS) model [70] and from [71], except

for the spark-ignited NG engine. The factors for this engine have been adjusted to reflect manufacturers observations and are given in Table 8. The fuel consumption of a new LNG powered vessel and a diesel fuel vessel of similar size operating on the same route was obtained. These values have been used in the model to calculate the emissions of the different engine technologies and the results are given in Table 9.

Table 8: Engine emission factor in grams per Megajoule of fuel burned [71]

	Diesel	**Compression-Ignited Natural Gas**	**Spark-Ignited Natural Gas**
NOx	2.351	2.351	2.351
PM_{10}	0.070	0.070	0.001
SO_x	0.246	0.009	0.0003
CH_4	0.004	0.004	0.087
N_2O	0.002	0.002	0.002
CO_2	80	73	55

Table 9: Vessel emissions per crossing (kg)

Fuel Type	**NO_x**	**PM_{10}**	**SO_x**	**CH_4**	**N_2O**	**CO_2**	**CO_{2e} ***
Diesel	201	5.95	0.80	0.37	0.16	6,257	6,519
Compression-Ignited NG	201	0.06	0.02	7.42	0.16	4,743	5,210
Spark-Ignited NG	19.0	0.43	0.02	53.4	0.16	4,743	6,409

* CO_{2e} is based on three main gasses: CH_4, N_2O, CO_2

2.2.3.4 Results and Discussion

2.2.3.4.1 Total Fuel-cycle Emissions Results

The total well to propeller CO_{2e} emissions per vessel crossing for three scenarios and three different types of engines for the NG pathway in BC were calculated and the results are given in Table 10. Scenario 1 represents the analysis given previously without any changes in the amount of emissions, Scenario 2 includes an additional 43% in methane leakage during extraction and processing of NG according to the approach recommended in [10], and Scenario 3 represents the worst case which is the 43% increase in methane leakage during extraction and processing and an additional 2.22 g/Mj of leakage during engine combustion [30]. The total CO_{2e} was obtained using the emissions produced at each stage of the fuel pathway based on the energy consumed each crossing. The upstream CO_{2e}

represents the emissions from the extraction, processing, transportation, conversion, and distribution of the fuel, and the downstream CO_{2e} includes emissions from the main and auxiliary engines of the marine vessel.

Table 10: Total well to propeller CO_{2e} per crossing for three scenarios

	Fuel Type	Downstream CO_{2e} (kg/crossing)	Upstream CO_{2e} (kg/crossing)		Total CO_{2e} (kg/ crossing)	
			Lower bound	Higher bound	Lower bound	Higher bound
Scenario 1	Diesel	6,519	1,369	1,571	7,889	8,091
	Compression-Ignited Natural Gas	5,210	838	887	6,048	6,097
	Spark-Ignited Natural Gas	6,409	838	887	7,247	7,296
Scenario 2	Diesel	6,519	1,369	1,571	7,889	8,091
	Compression-Ignited Natural Gas	5,210	913	949	6,123	6,159
	Spark-Ignited Natural Gas	6,409	913	949	7,322	7,358
Scenario 3	Diesel	6,519	1,369	1,571	7,889	8,091
	Compression-Ignited Natural Gas	10,686	913	949	11,600	11,636
	Spark-Ignited Natural Gas	10,505	913	949	11,419	11,455

The upstream emissions for diesel fuel were obtained using the default setup for marine diesel fuel using GHGenius 5.0 [54]. In all three scenarios, the largest contributor to emissions is the marine engine. Thus, improvements in engine design and efficiency will have a major effect on total emissions. With diesel fuel, upstream emissions account for about 22% of the total emissions for all three scenarios. In the first scenario, the compression-ignited NG engine has 27% lower emissions than the diesel engine, and 13% lower than the spark-ignited NG engine. In the second scenario, the extra methane leakage increased upstream emissions by 7% for the compression-ignited NG engine, resulting in less than 1% increase in the total CO_{2e} emissions per vessel crossing. These results indicate that the compression-ignited NG engine is the best option for the first and second scenarios.

However, the increased engine methane leakage in the third scenario leads to 39% higher CO_{2e} emissions compared to the diesel engine.

2.2.3.4.2 Air Quality Comparison

The emission details for each scenario are now examined.

Table **11** presents the upstream and downstream emissions per vessel crossing based on the actual fuel consumption of the vessel. The N_2O and CO_2 emissions mainly come from the downstream operation, and the methane emissions depend on the engine technology employed. For instance, the CH_4 emissions for a spark-ignited natural gas engine in the downstream are significantly higher than in the upstream, while for a compression-ignited NG engine, the upstream emissions are slightly higher than the downstream emissions. A significant portion of the emitted NO_x comes from the downstream engine combustion which depends on the operating temperature of the engine. Higher cylinder temperatures produce greater NO_x emissions. For this reason, a diesel engine with a high operating temperature produces more NO_x emissions than an equivalent Otto cycle engine. The use of NG fuel also reduces the sulfur oxide (SO_x) emissions by 99% due to the very low NG sulfur content.

Table 11: Total fuel cycle emissions in Kg per crossing

	Gases	Diesel	Compression-Ignited Natural Gas	Spark-Ignited Natural Gas
Downstream	NO_x	201	201	19
	SO_x	0.80	0.02	0.02
	CH_4	0.37	7.4	53
	N_2O	0.16	0.16	0.16
	CO_2	6,258	4,743	4,743
	CO_{2e}	**6,514**	**5,210**	**6,409**
Upstream	NO_x	3.36	N/A	
	SO_x	1.87	N/A	
	CH_4	15.39	5.2	
	N_2O	0.019	0.010	
	CO_2	910	396	
	CO_{2e}	**1,382**	**556**	
Total	NO_x	204	201	19

	SO_x	3	0.02	0.02
	CH_4	16	12.7	59
	N_2O	0.18	0.2	0.17
	CO_2	7,167	5,139	5,139
	CO_{2e}	**7,895**	**5,766**	**6,964**

2.2.3.5 Discussion

The results in this study clearly demonstrate the advantages of LNG as a marine fuel compared to diesel fuel. The use of other fuel pathways and bunkering methods may lead to different results. For example, the upstream CO_{2e} or GHG emissions with LNG fuel in the first scenario can vary by about 6% depending on the pathways and bunkering methods, ranging from a low of 9.81 gCO_{2e}/Mj to a high of 10.38 gCO_{2e}/Mj. These results are about 55% lower than the default value given by the GHGenius software for marine diesel fuel. For the second scenario with 43% additional methane leakage, LNG is still a better option with 50% lower total upstream emissions.

For the third scenario, the high methane slip from downstream engine operations can offset the environmental benefits of NG as a marine fuel. It is thus important that the engine technology employed minimizes the methane slip. Engine manufacturers have recently reported improvements that lower methane slip during combustion [72]. Further, the research team at the University of Victoria is developing integrated NG engine hybrid electric propulsion technology with dedicated controls to address this issue. In the upstream, the majority of emissions come from NG extraction and processing. The results in [47] indicate that old NG infrastructure is more prone to leaks in comparison to younger wells. Using low-bleed devices to reduce fugitive methane from pneumatic valve operation can reduce emission in extraction and processing. The NG emission lifecycle can also be improved by controlling direct methane leaks from fuel unloading operations during LNG delivery and bunkering.

Another important environmental impact of NG fuel besides methane leakage and emission is water consumption during the process of hydraulic fracturing, also known as fracking, in which a large quantity of pressured fluid is used to create fractures in rocks. More than 90% of the fluid is water and the rest are proppants and chemical additives [73]. An

analysis of water consumption and wastewater treatment for NG extraction is needed to evaluate the impact and sustainability of NG as a marine fuel.

2.2.3.6 Conclusion

This work presented a new method to evaluate the lifecycle environmental impact of NG as a marine fuel for British Columbia, Canada using data from NG producers and suppliers in the province. Several scenarios were considered in evaluating the resulting emissions. The results obtained indicate that NG is a desirable marine fuel in BC only if proper engine technologies are used. NG generates less air pollution and has a lower environmental impact than diesel fuel. British Columbia has strict environmental regulations, and the majority (more than 97%) of the electricity used in the NG pathway comes from renewable energy sources such as hydro. If NG fuel is considered as a bridge to future all-electric powered vessels, then it must be used carefully. The results of this study showed that high methane leakage during NG engine operations can offset the environmental benefits of NG as a transportation fuel.

3 Electrified Propulsion for Fishing Boats

Maritime transportation emits about 961 million tonnes of CO_2 equivalent, accounting for 2.8% of global GHG emissions [6]. This is more than the total emissions produced by Canada in 2013 [74] and this number is expected to increase to 5% by 2050 [75]. Depending upon future Gross Domestic Product (GDP) and socio-economic and energy efficiency, the growth rate could be higher than this predicted value. To address this issue, international maritime organization standards, referred to as Tier I, Tier II and Tier III, were introduced to set limits on NO_x and SO_x emissions from marine vessels.

The strict and evolving environmental regulations enforced by regional and national governments as well as the IMO has forced ship owners to seek alternative solutions to meet these standards while trying to lower associated operational expenses at the same time. Electric and hybrid-electric propulsions have been proven in a range of vessel types over the last few decades as one of the most efficient powertrain architectures. The fuel saving potential of electric propulsion in comparison with mechanical propulsion is a strong driver for the adoption of electric propulsion for many of these vessels. The fuel saving is largely due to the fact that many vessels usually have a very dynamic load profile and seldom operate at the maximum power of the ICE with best energy efficiency. The hybrid electric propulsion systems can use its ESS to store surplus energy from the ICE when it is not needed and return it to the system when required. In these systems, the size of the ICE can be reduced, and the ICE can operate at its maximum power and efficiency. The maritime industry is also moving fast to maintain peace with current hybridization and electrification demand.

Although hybridization and electrification of vessels is an appealing solution for different vessel types, it may not be the best option for many vessels that spend most of their time at a constant speed with a constant power load and long sailing distance. The optimum powertrain architecture for vessels should be selected based on their specific designs and operational load profiles. This means that naval architects need to consider a different vessel classification type from those recognized by classification societies, i.e. the International Association of Classification Societies (IACS). For electrification, naval architects need to classify the ships and boats based on their load profiles and select a proper powertrain architecture that best suits the power demand.

Unlike the other publications that prescribe a powertrain for all vessels, the focus of this work and the produced results are based on a specific type of fishing boats. These boats have a very dynamic load profile and this makes them an excellent candidate for hybrid and electric propulsion systems [4][5]. In this work, a specific load profile of two lobster fishing boats has been introduced using their statistical operation data. Series hybrid electric and battery electric powertrain architectures are modeled, and performance of these design variations are examined based upon the obtained load profiles. The MBD methodology employed in this work, however, is generically applicable to all different types of marine vessels as long as their operation profiles are established.

3.1 Modeling of Fishing Boat Operation Patterns

3.1.1 Fishing Boats and Their Operation

Fishing boats have a dynamic load profile. Commercial fishing boats are capable of hauling a catch of thousands of kilograms of fish per voyage. Larger fishing boats that operate in higher depth have advanced equipment and facilities where the fish can be prepared and stored for sale. These vessels are also equipped with amenities for workers for a long stay on the ocean and they can do the job of several smaller boats. The location of fishing, method of capture and duration of the trip can also vary significantly each trip. For this purpose, two different lobster fishing boats, similar to the vessel shown in Figure 24, have been selected for this study. These boats typically have a single diesel engine that provides all power used aboard. The power is distributed via a direct mechanical link, as well as hydraulic and electrical systems from the main engine to various appliances aboard the vessel. These typically include propulsion, trap-haulers (winches), power steering, water pumps, navigation electronics, and heaters.

Figure 24: A typical Canadian east coast lobster fishing boat [78]

Each boat operates approximately 6 hours per day. The total operational hours of each boat is estimated around

$$6\ \frac{hours}{day} \times 30\ \frac{days}{month} \times 6\frac{months}{year} = 1080\ \frac{hours}{year}$$

Detailed information about the two fishing boats is given in Table 12.

Table 12: Detail information of the studied boats.

	Boat 1	**Boat 2**
Length:	12.2 m	13.7 m
Beam:	5.2 m	3.66 m
Displacement:	15 tonnes	15 tonnes
Engine:	300 kW	242 kW
Max speed:	14 kt	16 kt
Cruise Speed:	10 kt	13 kt
Engine RPM at cruise:	1,600 RPM	1,200 RPM
Propeller:	5 blades, 0.76mx0.66m	4 blades, 0.6 m/0.66 m
Daily operation time:	6 hrs	6 hrs
Yearly operation time:	1,080 hrs	1,080 hrs

3.1.2 Current Fishing Boat Powertrain Configurations

At present, smaller fishing boats have a conventional mechanical powertrain with a gasoline or diesel engine connected to the mechanical drivetrain. Some larger vessels may have a hydraulic drive system to improve the torque characteristics over mechanical drive

and use an additional generator for hotel loads. The current mechanical powertrain of small fishing boats is illustrated in Figure 25, and used as the benchmark in this study. This powertrain architecture represents a conventional propulsion system, consisting of prime mover(s), reduction gears, medium length shafts, and propeller(s). The prime mover drives the shaft at medium speed and connects to the propeller through reduction gears to obtain appropriate speed and higher torque. The propeller works at several hundred revolutions per minute (RPM) and produces thrust. Meanwhile, the hydraulic pump attached to the diesel engine provides power for the trap hauler and power steering. A representative trap-hauler consumes an average of 8.7 kilowatt power based on the manufacturer specifications. A small alternator attached to the engine meets the remaining electrical loads in the boat.

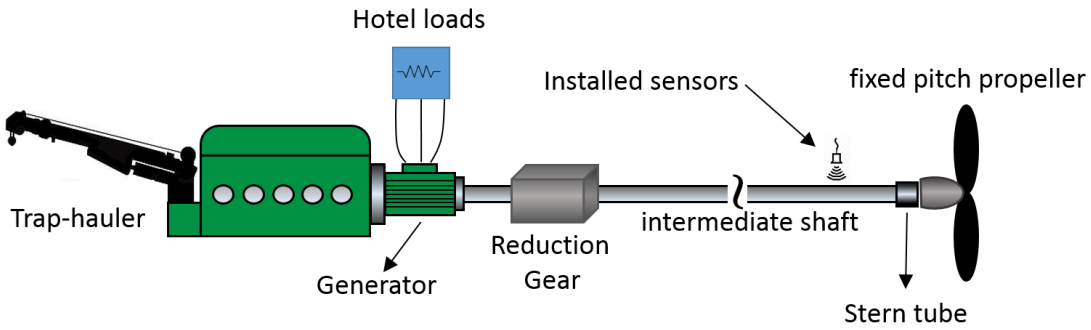

Figure 25: Pure mechanical propulsion system

3.1.3 Acquisition System Description and Data Collection

Evaluation of energy efficiency, GHG emissions, and operation costs of a marine vessel needs to be based upon their actual operations. To accurately assess the engine performance, speed and torque sensors have been mounted onto the propeller shaft of the vessels under study for representative operation days, as shown in Figure 26.

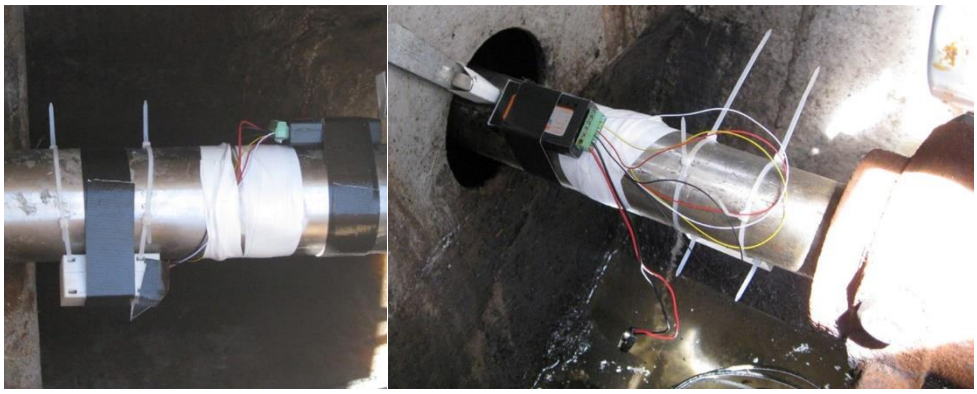

Figure 26: Strain gauge installations

Figure 27 through 32 illustrate the collected data from two fishing boats. The data acquisition system was installed on both vessels and shaft torque and speed data were collected for simulation and model validation. The collected data enable a direct comparison between the current mechanical powertrain and the two proposed powertrain architectures. Operational data was collected over the summer of 2017 and one representative mission profile was identified as a good representation of the boats daily operational variability.

Given that both boats are under operation as lobster fishing vessels, the similarity in the load profile is expected. Figure 29 and Figure **32** illustrate the required vessel engine power. Travelling to the fishing zone from the wharf accounts for the sustained peaks at the beginning of the collected torque and rpm data. Upon arriving at the fishing zone the Captain brings the boat to a stop to work on each trap, and moves to the next afterwards as illustrated in Figure 29 andFigure **32**. This process accounts for the intermittent peaks and negative torques before each stop. After all traps have been serviced, the vessel returns to the wharf. This process accounts for the sustained peak near the end of the collected torque and rpm data. Finally, the vessel motors around the wharf unloading the catch, traps, and gear before docking. This process accounts for the smaller peaks at the end of the collected torque and rpm data.

In designing a traditional, mechanical marine propulsion system, the power spectrum approach is commonly used for accessing the propulsion power and determining the engine size of marine vessels. However, the addition of sizable battery ESS and the optimal energy

management in a hybrid electric powertrain system have changed the needed design approach and demand consideration on the "time series" of power consumption. This is due to the fact that energy produced by the ICE can be stored in the ESS and used at a different time. The time series data of power and energy demands allow optimal energy management and power control to be developed through global optimization of energy use during the complete trip using Dynamics Programming (DP). This is the foundation and one of the principal advantages of hybrid electric propulsion technology, and the approach is commonly used in the automotive industry for the development of hybrid and plug-in hybrid electric vehicles. Using this approach, the power and torque pulses of a vessel over a very short duration can be satisfied by borrowing the stored energy and power from the ESS without oversizing the engine to accommodate these transient loads. The hybrid electric powertrain system handles transient loads without oversizing the engine(s), and ensuring properly sized engine(s) to operate mostly at the preferred speed and torque with peak fuel efficiency. This is particularly the case for smaller vessels, such as the fishing boats included in this study.

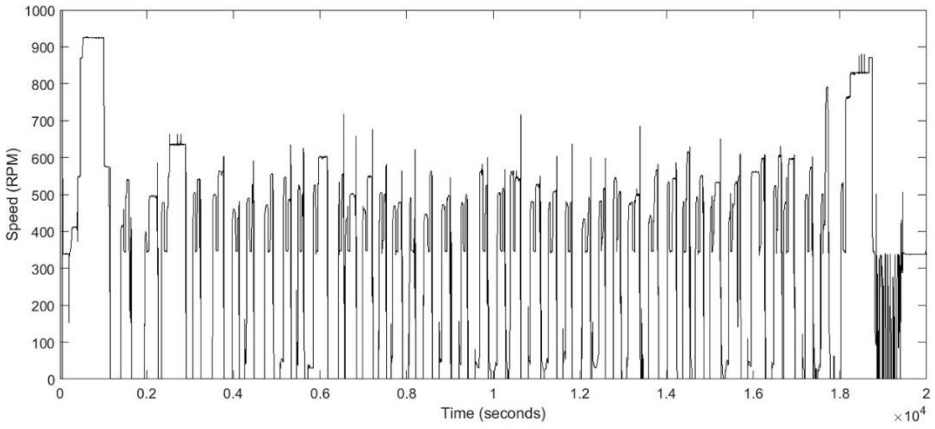

Figure 27: Propeller speed for boat 1

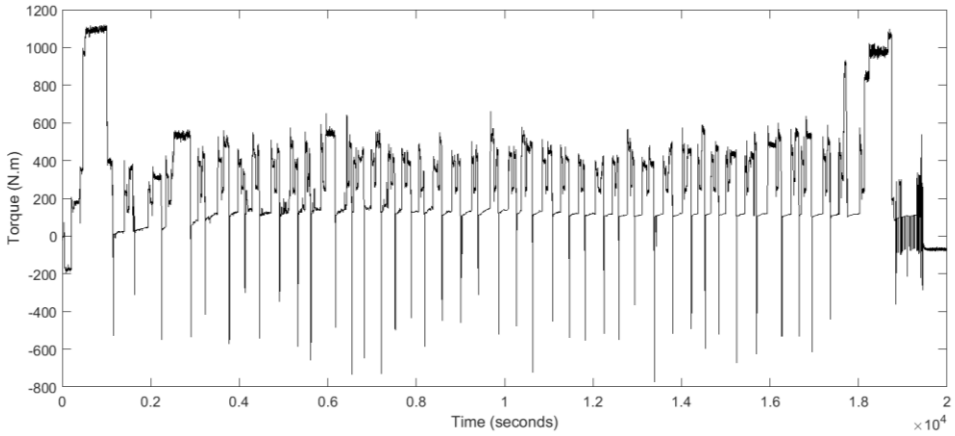

Figure 28: Shaft torque for boat 1

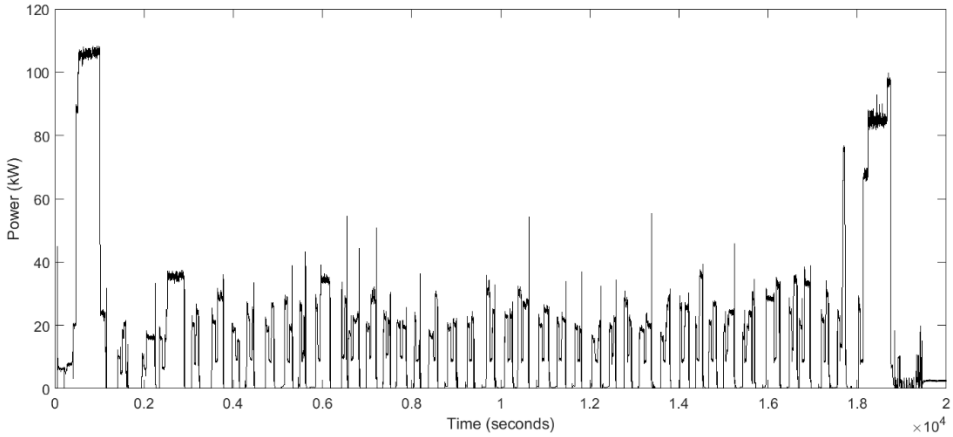

Figure 29: Engine power for boat 1

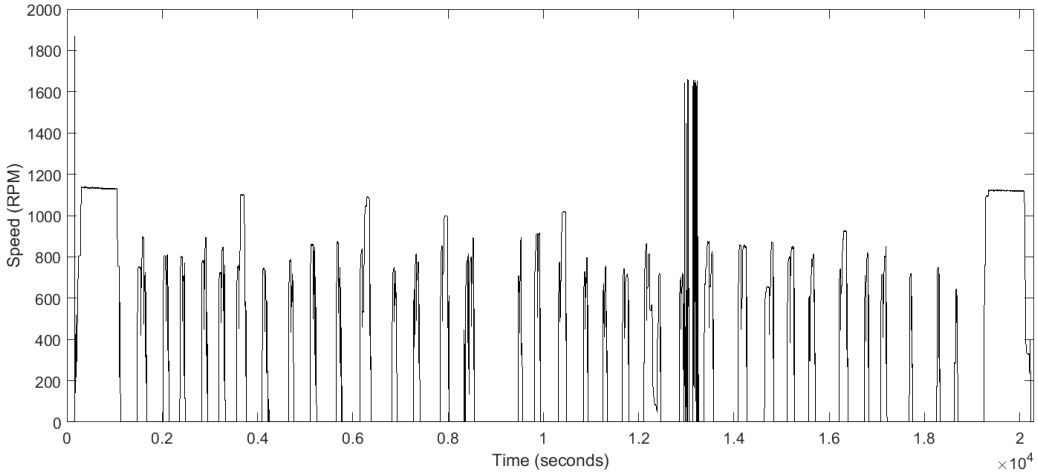

Figure 30: Propeller speed for boat 2

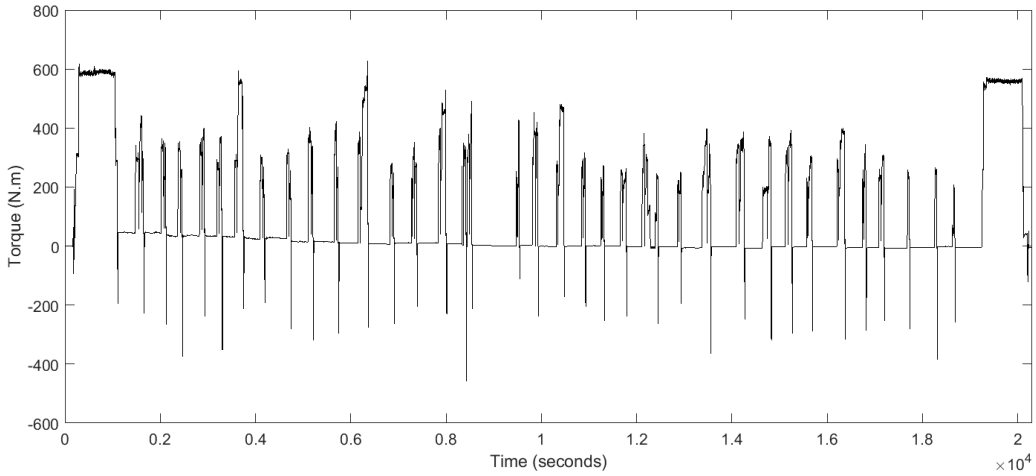

Figure 31: Shaft torque for boat 2

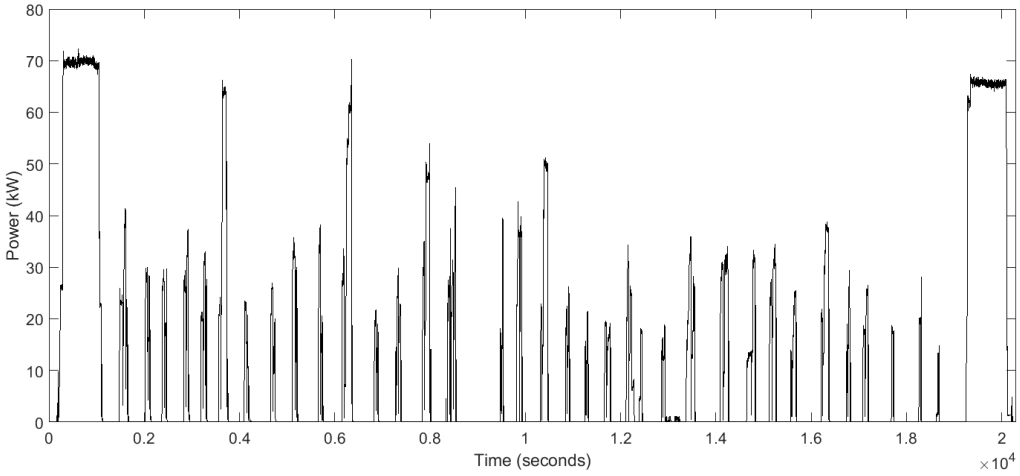

Figure 32: Engine power for boat 2

3.2 Hybrid Electric Power Systems

3.2.1 Advantages of Advanced Hybrid Electric Propulsion Systems

The proposed series hybrid electric powertrain system design is depicted in Figure 33. Advantages of this powertrain system design include longer diesel engine lifetime, flexibility in powertrain component layout, higher system energy efficiency, and the possibility of using a smaller ICE. These would result in noticeably improved fuel consumption over the low/medium speed ranges. The hybridization also increases the dynamic response of the boat and reduces engine noise.

The DC power system used in this powertrain has some obvious advantages over a traditional AC system. The DC power system uses the same well-proven AC electrical machine as a generator and motor while increasing the overall system efficiency. The DC power system improves the diesel engines efficiency and reduces its fuel consumption due to variable speed generation. The ICE can operate at optimal fuel consumption as ICE and rotor are not mechanically coupled. More weight and space is saved in the DC power system and the connection of generators in parallel is simpler in comparison to the AC power system. The current trend in the shipping industry is towards DC distribution systems because of the flexibility they offer in introducing energy storage, fuel cell, and solar technologies [11].

3.2.2 Proposed Series Hybrid Architecture

Figure 33 illustrates a schematic of the series hybrid powertrain system with a DC bus. The power from the synchronous generator is rectified to DC voltage. Other loads, including hydraulic pumps and auxiliary (hotel) loads, are connected to the DC bus via DC/AC inverters. The ESS is also connected to the DC bus by an internal DC/DC converter. A three-phase electrical motor is fed through the DC bus via an electric driver and rotates the propeller at the desired speed. The battery and supercapacitor have been selected to be used in the ESS. The supercapacitor was studied because a supercapacitor ESS, unlike a battery system, has none or very little degradation over a high rate of charge and discharge with dynamic load changes of the type of boats studied in this work. More discussion on supercapacitor ESS is given in the following section.

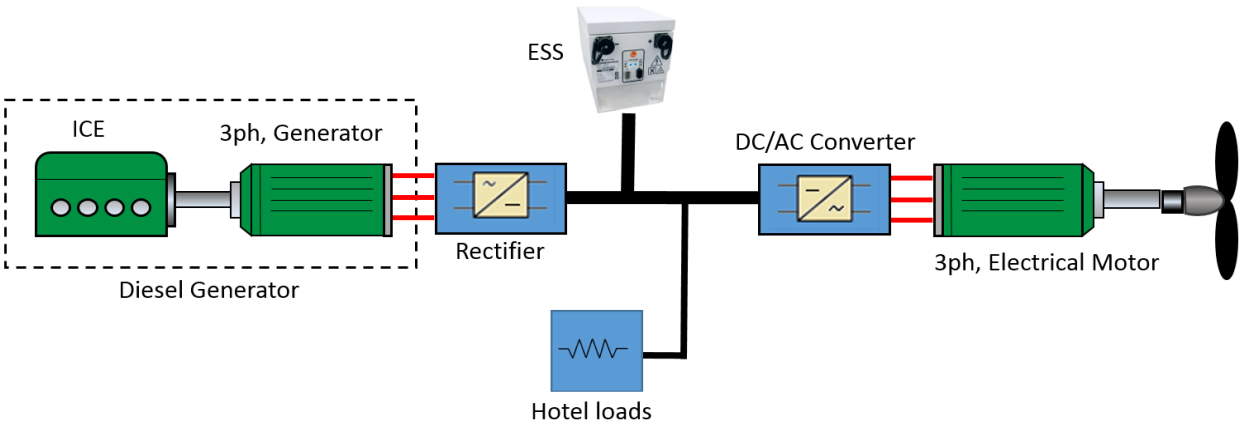

Figure 33: Series hybrid electric propulsion system

3.3 Battery Electric Powertrain

3.3.1 Advantages of Battery Electric Fishing Boats

Pure battery electric powertrain systems offer unique advantages over other architectures such as higher energy efficiency, lower noise levels, and greater reliability. Factors such as high capital cost, the need for proper battery cooling mechanisms, bulky and expensive fast charging stations, and the high cost of expanding existing electrical grid infrastructure in some cases have limited the widespread adoption of this design. The number of battery electric vessels are increasing rapidly. The first battery electric car ferry, the Norled AS MF Ampere, entered service in Sognefjord, Norway, in 2015 [13]. It has been estimated that it annually offsets the use of one million litres of diesel which translate to the emissions of 2,680 tonnes of carbon dioxide and 37 tonnes of nitrogen oxide [79].

3.3.2 Pure Battery Powered Powertrain System

The proposed battery powered powertrain architecture is illustrated in Figure 34. The Battery Energy Storage System (BESS) is coupled to a DC/AC converter to step up the voltage and provide power for the rest of the system. Similar to the series hybrid electric powertrain architecture, the power distribution system can be either AC or DC. In the case of a DC distribution grid, electrical power is transferred to a DC/AC converter to provide power for propulsion. Auxiliary loads can also be connected to the AC or DC bus. In the case of the DC bus, extra DC/AC inverter(s) is needed to provide power for the AC loads aboard.

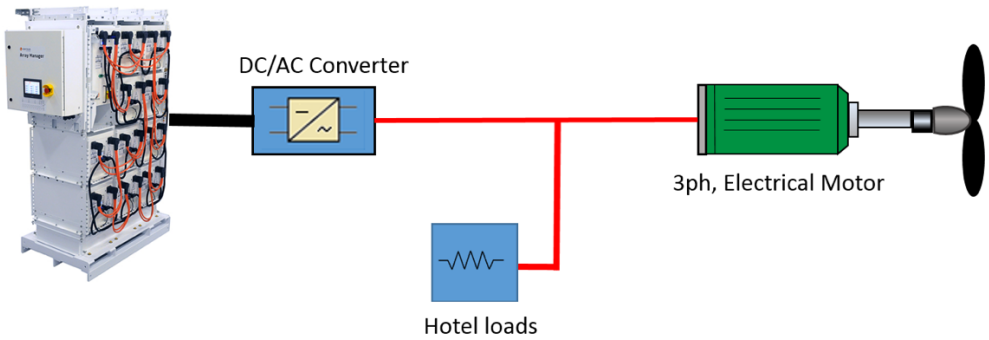

Figure 34: Pure battery electric propulsion system

3.4 Key Component Modeling

The core of this study is to develop a powertrain system model with sufficient resolution to capture the dynamic behaviour of all critical powertrain components to optimize the size of the ICE and ESS. The developed model must be computationally efficient so that it can be used in the system design optimization. For this purpose, according to [80], many high frequency dynamics related to the converter models can be replaced with a more straightforward power loss model and little impact on modeling and simulation results. The Model Based Design (MBD) approach that is widely used in the automotive industry has been using in this work to form the powertrain system model of the marine propulsion system, and implemented in MATLAB/Simulink. The complete powertrain system model consists of blocks of powertrain system component models as illustrated in Figure 35. These components are connected to form the complete powertrain system of different powertrain system architectures, such as the hybrid electric powertrain system architecture detailed in Figure 35 to capture power flow or power loss of the system. Methods for constructing MATLAB/Simulink models are explained in various reference books.

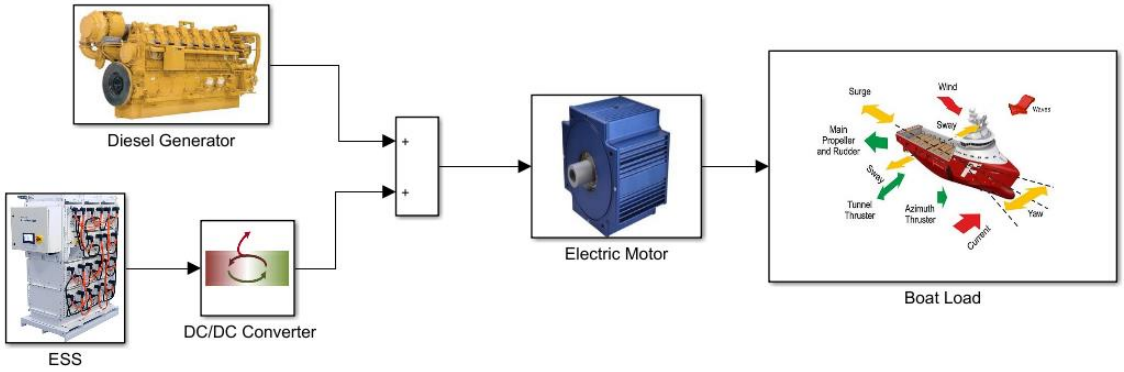

Figure 35: Different components of a hybrid electric architecture.

3.4.1 ICE Model

In this work, the gasoline and diesel engine performance and emission models are based on the models in the Advanced Vehicle Simulator (ADVISOR), developed by the US DOE's National Renewable Energy Laboratory [81]. As a MATLAB/Simulink based simulation program for rapid analysis of the performance and fuel economy of light and

heavy-duty vehicles, the engine powertrain component models in ADVISOR fit the engine specifications of the fishing boats well. The engine Fuel Consumption (FC) was calculated for every step of the simulation for given power and torque demands from the powertrain control system. To capture the dynamics of the engine model, a linear first order transfer function was employed [82]–[86]. Similarly, an engine actuator and controller transfer function along with a feedback loop were implemented and parameters tuned up within the range given in [83]. The simulated engine model in MATLAB/Simulink is shown in Figure 36.

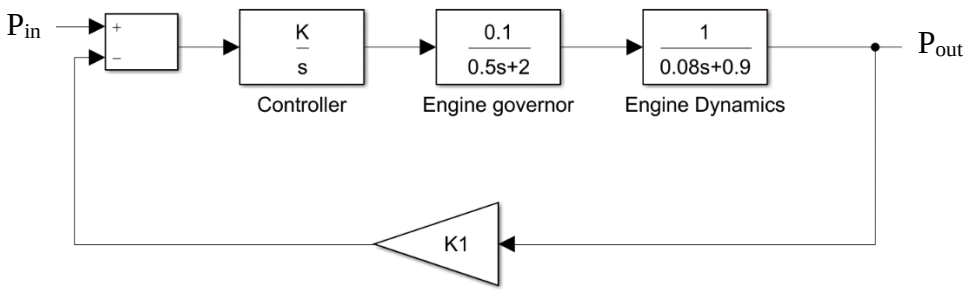

Figure 36: Engine model transfer functions.

3.4.2 DC/DC Converter Power Loss Map

DC/DC converters have taken much attention in recent years, mostly because of their applications in hybrid electric vehicles and renewable energy systems. In these systems, power constantly flows between the ESS (usually a battery) and the rest of the system. This converter is an essential component for power management in an electrified boat. A hybrid electric powertrain uses DC/DC converters to transfer the excess power from the genset to the ESS and the reverse. In general, power converters can be divided into four types as shown in Table 13.

Table 13: Types of converter systems

Type of conversion	**Converter system**	
AC-to-DC	Rectifiers (Uncontrolled) (Diodes)	Fixed AC to Fixed DC (Line Commutation)
	Rectifiers (Controlled) (SCRs, IGBTs, MOSFETs, GTOs)	Fixed AC to Fixed or Variable DC (Line or Forced Commutation)

DC-to-DC		Fixed (or variable) DC to Variable (or fixed) DC
DC-to-AC	Inverters (Uncontrolled)	Fixed voltage DC to Fixed AC
	Inverters (Controlled)	Fixed (or variable) DC to Variable ac
AC-to-AC	AC Voltage Controllers	Fixed to variable AC
	Cyclo Converters	Fixed AC to variable voltage and frequency (usually less than input frequency)

The voltage doubler boost converter shown in Figure 37 is modeled and simulated to produce an accurate power loss model for the DC/DC converter, to account its power use and to remain computationally efficient. In simulating its power loss, the voltage and current across each element of the circuit are calculated. The simulated chief waveforms this circuit are presented in Figure 38.

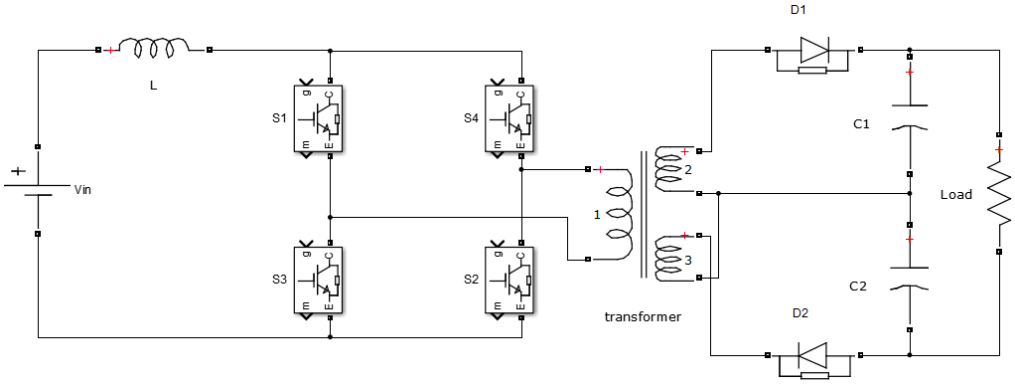

Figure 37: A generic voltage doubler boost converter

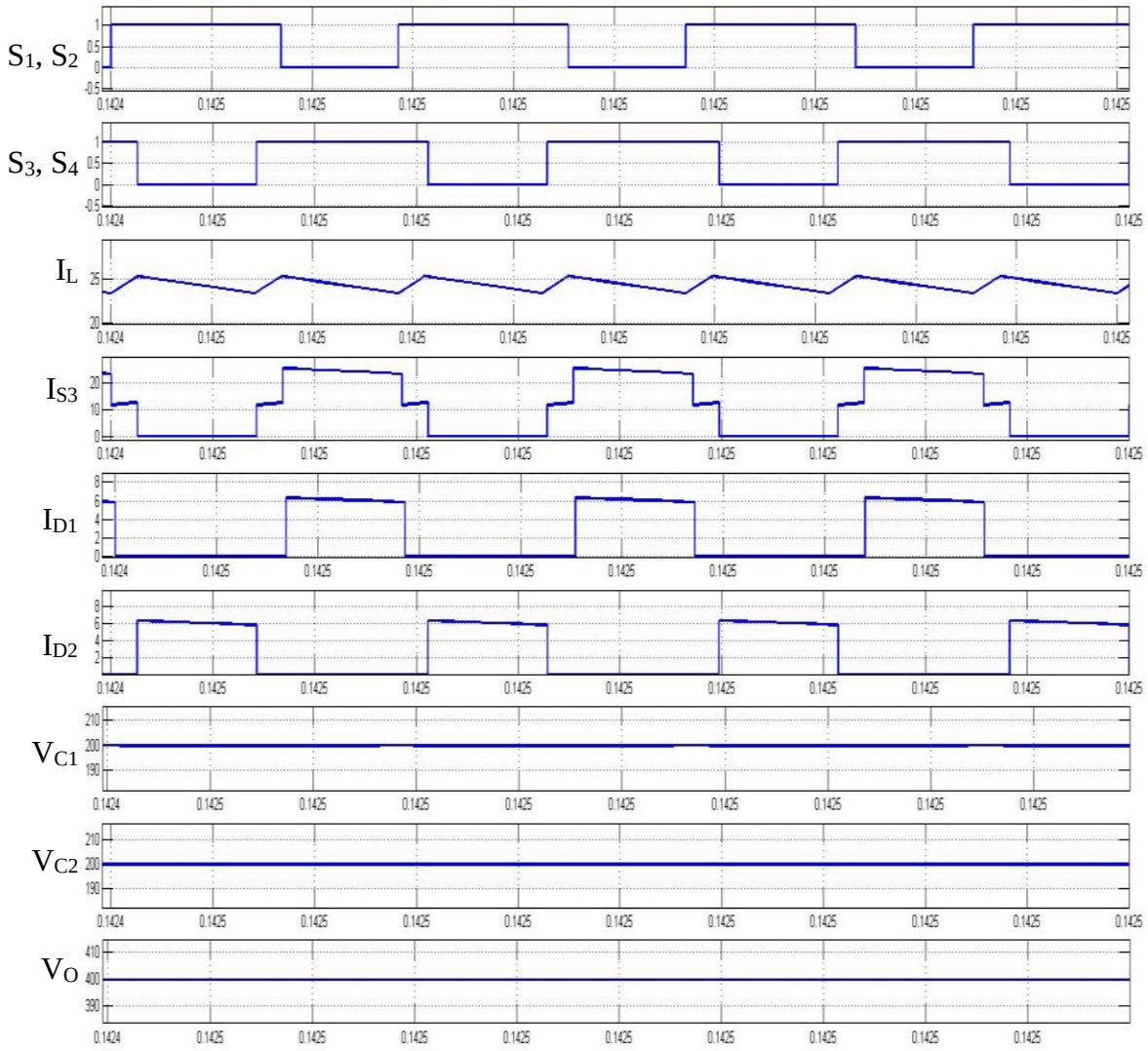

Figure 38: Gate signals and primary waveforms

For this converter, switch turn on/off loss, switch conduction loss and diode conduction loss are considered. The total switching loss of the converter can be calculated by using the fall (t_f) and rise (t_r) time available on the data sheet [87]. In this work, we assumed that switch voltage and current have a linear behavior shown in Figure 39.

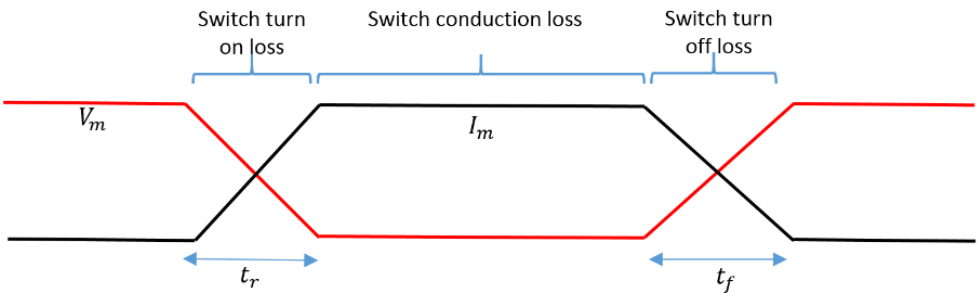

Figure 39: Switch voltage and current

Therefore, the losses can be calculated as follows

$$P_{switching\ loss} = P_{t_r} + P_{t_f} = \left(\frac{1}{6} V_m I_m (t_r + t_f) f\right) \times n_s, \quad (5)$$

where V_m and I_m are maximum voltage and current across the switch and f is the switching frequency. The conduction loss is determined by the on-resistances of the switch $(R_{ds\ ON})$ and the transistor RMS current (I)

$$P_{switch\ cond} = \left(R_{ds\ ON} \times I^2_{T(rms)}\right) \times n_s \quad (6)$$

The antiparallel diode loss is equal to

$$P_{diode\ loss} = \left(V_F\ I_{F\ av} + R_F {I_F}^2_{rms}\right) \times n_D \quad (7)$$

In addition, a high frequency transformer is used between the switches and capacitor for isolation and voltage translation requirements. The main transformer losses consist of copper losses, eddy current losses and hysteresis loss in the core of the transformer. In this work, it is assumed that the total transformer loss is 1% of the net output power. Moreover, power losses in inductor and capacitors are ignored and ideal components are considered. When the voltage across the diode is negative and the diode is in reverse-bias mode, it is assumed that the diode is open circuit and no power loss during this mode is considered.

The converter efficiency map is shown in Figure 40. The input voltage has changed from 22 V to 42 V and the output power varied from 500W to 1000W. The converter power loss is

$$P_{converter\ loss} = P_{diode\ loss} + P_{switch\ cond} + P_{switching\ loss} \quad (8)$$

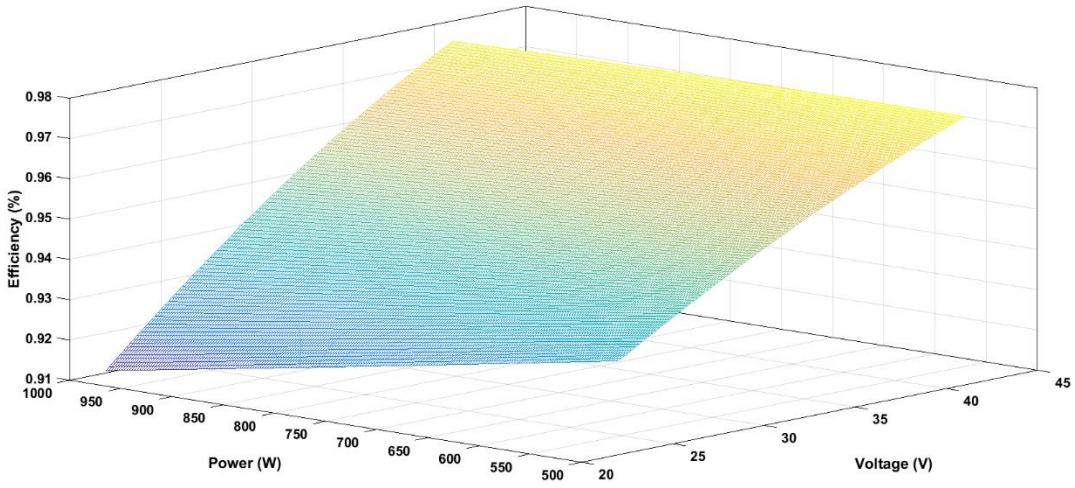

Figure 40: Efficiency map of the DC/DC converter

3.4.3 Battery ESS Model

A lithium-ion battery is a typical choice over standard nickel-cadmium and offers largest energy density for weight. Lithium-ion has a very low maintenance; an advantage that most other battery chemistries cannot claim. Lithium-ion batteries are being used in increasingly complex configurations with very challenging duty cycles and usually selected as the desired battery chemistry. Due to the large amount of energy required in vessels, BESS in vessels are enormous and consequently costly. That is why it is important to predict the battery capacity fade using battery degradation model. Yet, developing such a model for practical applications is a new concept and a challenging task for industry. In this section, two models are developed to estimate the battery degradation. Each approach are explained and results are presented.

Model 1

A BESS is an essential part of the hybrid electric and pure electric powertrains. A lithium-ion (Li-ion) battery was selected as a suitable candidate due to high energy density, low self-discharge rates, and wide applications in maritime industry [79]. The battery performance model has been extensively discussed in the literature. A comprehensive review of the battery system is given in [88]. A more simplified model, which is required for system modeling is given in [89]. In [90] the equivalent circuit parameters of a battery

is optimized and using experimental data, an equivalent circuit model is developed. By using an equivalent circuit model and passive elements such as a capacitor, a resistor and an inductor, the approximate behaviour of the battery can be estimated. The Thevenin equivalent circuit model was selected to represent the battery dynamics since it can simulate battery performance for various chemistries, including valve-regulated lead-acid (VRLA) [91], nickel metal hydride (Ni-MH) [92], and LiB [93]. The battery Thevenin equivalent circuit is shown in Figure 41.

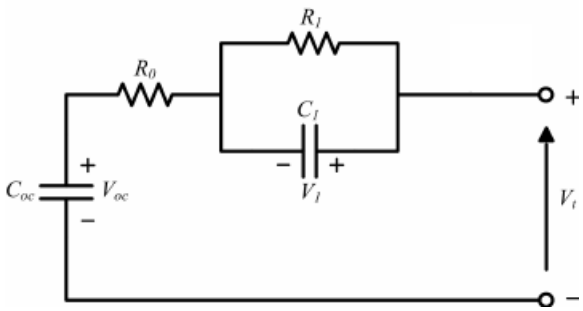

Figure 41: Thevenin equivalent circuit for the battery system

Since the introduction of Li-ion battery in the 1990s, the performance, lifecycles and costs have improved significantly. A comprehensive cost analysis of Li-ion battery technology for a BEV is given in [94]. The cost of Li-ion battery has dropped from CDN$655 per kWh in 2008 to about CDN$394 per kWh in 2014. It is also predicted that battery cost may drop to CDN$264 per kWh in 2020 and CDN$197 per kWh in 2025 [94]. In this work, CDN$700/kWh is used for battery pack cost based on harsh marine conditions and the data from a leading marine battery ESS manufacturer.

The lifecycle costs of the hybridized and electrified propulsion system consist of various costs of all powertrain components, including their investment costs, the costs of fuel and/or electric energy, and the replacement costs of key powertrain components within the projected lifetime. Among those, the batteries have a shorter life and need to be replaced within the lifecycle of the system. The hybrid electric boat has a smaller BESS and a shallow depth of discharge (DOD), thus last for longer time. For shallow DOD, a lithium-ion phosphate battery can last for about ten years, before its charging capacity drops by 20%. With proper battery sizing at 30 kWh to work with a 40kW diesel engine, the battery pack in this study is expected to cover the ten-year lifetime of the hybrid electric

powertrain. The proper use of the BESS is controlled by the energy management system of the hybrid electric powertrain. The battery pack of representative HEV, Toyota Prius, has been reported to have an average of thirteen years of operation life [95].

The BESS of the pure electric powertrain provides all propulsion energy that can be calculated from the measured power load of the boat, leading to a much larger battery and a deep DOD. During the six hours of boat operation under the obtained load profile and total energy consumption, the State of Charge (SOC) of the BESS is controlled between 15% and 95% between each deep charge at night. For six hours of operation, the BESS needs to have a capability of 97 kWh. At 80% deep DOD of each operating day, the battery will last about 1,000 cycles [96], equal to five years under the more demanding working condition. In this work, the battery life of pure electric boat was based upon similar studies on pure electric vehicle (PEV) [96], and more accurate battery life and lifecycle cost predictions can be made using the accurate battery performance degradation model and given load profiles, forming our future work.

Model 2

Over the past years, several models have been introduced for lithium-ion battery capacity fade [97]–[100]. These models are based on different methods, such as parasitic side reactions [100], solid-electrolyte interface formation [99], and resistance increase [98]. All these models require extensive data collection to assess the battery capacity fading process. Moreover, the majority of these models require calibration and complex calculation. In Wang et al. a semi-empirical life model is proposed considering the impacts of four parameters such as time, temperature, depth of charge, and discharge [97]. The semi-empirical model can adequately estimate the battery degradation using the Arrhenius equation. This equation can also be used in battery dynamic degradation

$$Q_{loss} = Ae^{-(\frac{e_a+B.C_{rate}}{RT_{Bat}})}(A_h)^z \tag{9}$$

where Q_{loss} is the battery capacity loss (the initial capacity of the battery is normalized to 1), A is the pre-exponential factor, e_a is the activation energy (J), R is the gas constant (J/(mol. K)), T is the absolute temperature (K), A_h is the Ah-throughput, C_{rate} is the

discharge rate, and B is the compensation factor of C-rate. Based on the cumulative damage (Fatigue) theory [101].

The pre-exponential factor and other constant variables in the above equation must be determined by experiment. In [102], an experiment was performed using a lithium iron phosphate ($LiFePO_4$) battery cell to calibrate the unknown parameters and verify the accuracy of the model. The battery was charged and discharged at 0.3C and 1.5C rates, respectively, from zero to 100% SOC. To calculate the parameters, the above equations are modified as follows

$$A_h = \left(\frac{Q_{loss} e^{\frac{E_a + B.C_{rate}}{RT_{Bat}}}}{A} \right)^{\frac{1}{z}} \tag{10}$$

and

$$\dot{Q}_{loss} = zAe^{-(\frac{e_a + B.C_{rate}}{RT_{Bat}})} (A_h)^{z-1} \tag{11}$$

Adding these gives

$$Q_{loss,p+1} - Q_{loss,p} = \Delta A_h z A^{\frac{1}{z}} e^{-(\frac{e_a + B.C_{rate}}{zRT_{Bat}})} Q^{\frac{z-1}{z}}{}_{loss,p} \tag{12}$$

where $Q_{loss,p+1}$ and $Q_{loss,p}$ are the accumulated battery capacity loss at times t and $t+1$, and ΔA_h is the Ah output during t_p to t_{p+1} which is defined as

$$\Delta A_h = \frac{1}{3600} \int_{t_p}^{t_{p+1}} |I_{Bat}| \, dt. \tag{13}$$

Experimental data were used to obtain the unknown parameters using a least squares fit method which gives

$$Q_{loss} = 0.0032 e^{-(\frac{15162 + 1516.C_{rate}}{RT_{Bat}})} (A_h)^{0.824} \tag{14}$$

Then the predicted capacity fade from the simulations was checked against the experimental results and accuracy of the model proven for different C rates. This result is illustrated in Figure 42.

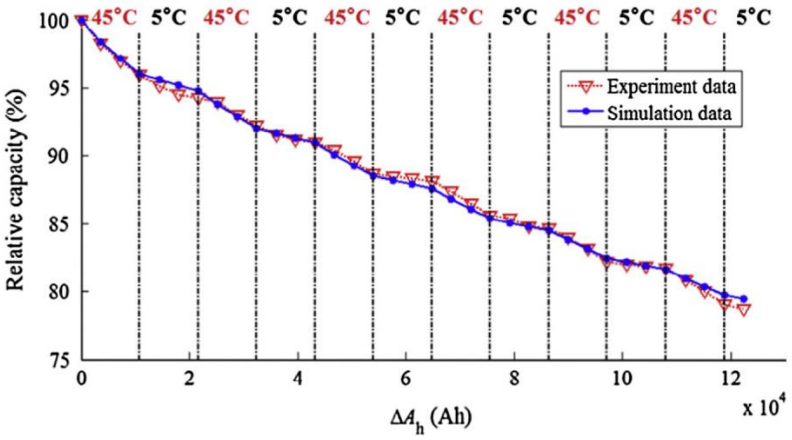

Figure 42: Verification of the battery degradation model [102]

The explained model is implemented in MATLAB/SIMULINK environment and two different power loads fed to the model in order to estimate power capacity loss in the battery system. Simulated model is shown in Figure 43.

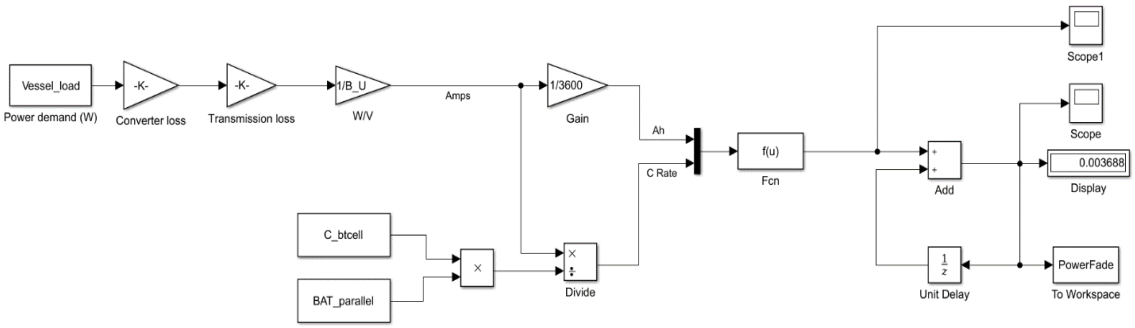

Figure 43: Simulated battery degradation model

The results obtained for this model using load profile given in [102], confirmed the accuracy of the model. However, when the model was tested for two different vessels load profiles and adjusted battery size, the results were not acceptable. First, thr passenger ferry load profile explained in the next chapter (MV Klitsa) was input to the model and then a fishing boat load profile was input to the model. In each case, the results were not realistic.

3.4.4 Supercapacitor ESS Model

In-depth reviews on supercapacitors and their modeling can be found in [25][26]. Conventional capacitors have features similar to supercapacitors, but their volumetric energy density is about two orders of magnitude lower and the cycle life is only half that of the supercapacitors [105]–[107]. The cycle life of a supercapacitor is also slightly affected by its operating temperature and voltage [108]. In this work, the operating temperature and voltage of the supercapacitor are assumed to be constant. This is a reasonable approximation as cooling seawater at about 12°C can be used for the thermal management of ESS and a controller can keep the voltage constant. Supercapacitors have low internal resistance, long cycle life, and high power density, and these advantages make supercapacitors an excellent candidate for the fishing vessels with dynamically changing power loads. A supercapacitor block in MATLAB/Simulink was implemented to capture the dynamic behaviour of the supercapacitor and its interaction with other powertrain components. This computationally efficient model can provide acceptable supercapacitor behaviour accuracy.

3.4.5 Electric Motor Transfer Function

Using motors governing differential equations, the transfer function of an electric motor can be derived [109]. The motor torque equation can be written as

$$T_m(t) = j\frac{d^2}{\mathrm{dt}}\theta(t) + B\frac{d}{dt}\theta(t) \tag{15}$$

where j is the moment of inertia, B is the friction constant, and $\theta(t)$ is the motors angular position. The motors back Electromotive Force (EMF) voltage equations is given by

$$e_b(t) = K_b\frac{d}{dt}\theta(t) \tag{16}$$

where K_b is the EMF constant. Motor input voltage can be written as

$$e_a(t) = R_a\, i_a(\mathrm{t}) + L_a\frac{d}{dt}i_a(t) + e_b(t) \tag{17}$$

where K_b is the EMF constant and R_a is the armature resistance, L_a is the armature inductance and i_a is the armature current. By assuming a zero initial condition and then using a Laplace transform we have:

$$\frac{w(s)}{E_a(s)} = \frac{K_t}{(L_a s + R_a)(Js + \mathrm{B}) + K_b K_t} \tag{18}$$

The electric motor parameters are given in Table 14.

Table 14: Motor parameters

Armature resistance ($\boldsymbol{R_a}$)	Armature inductance $\boldsymbol{L_a}$	Moment of inertia ($\boldsymbol{J}$)	Friction constant (**B**)	Torque constant ($\boldsymbol{K_t}$)	EMF constant ($\boldsymbol{K_b}$)
2 Ω	0.5 H	0.02 Kgm^2	0.2 Nms	0.015 Nm/A	0.01 Vs/rad

3.5 Optimal Sizing of the Generator and Battery ESS

The aim of powertrain component optimization is to find the optimal sizes of the genset and battery ESS for proper powertrain system design. The optimization of any maritime vessels powertrain system should provide a design that meets all vessel performance and regulatory requirements while minimizing the cost and fuel consumption of the vessel. The fishing boat powertrain system optimization problem is formulated as a Multi-Objective Optimization (MOO) problem with conflicting design objectives of minimizing the overall lifecycle costs (both capital and operational) and minimizing GHG emissions at the same time. The design constraints of the formulated MOO problem include

$$P_{DG} + P_{ESS} = P_{demand} \tag{19}$$

$$0 \leq P_{DG} \leq P_{DG_{max}} \tag{20}$$

$$P_{ESS_{Min}} \leq P_{ESS} \leq P_{ESS_{max}} \tag{21}$$

where P_{DG} is the power generated by the diesel generator, P_{ESS} is the power provided by the ESS, and P_{demand} is the given vessels power demand.

3.5.1 Emission Reduction Objective

The global warming potential method for calculating the impact of all released gases at a future time (e.g. 100 years) is been used to calculate the total equivalent CO_2 emissions of the vessel. The total equivalent CO_2 formulated as

$$CO_{2_{e\ TOTAL}} = FC \times y \times trips \times K_f \times n \tag{22}$$

where n is the number of vessel operating days, FC is the engine fuel consumption per trip, y is the number of years, $trips$ is the number of vessel trip per day and K_f is the emission factor for marine diesel given in [37]. The total CO_{2e} is calculated based on the GWP values of different gases given in the fourth assessment report of Intergoverntheе mental Panel on Climate Change (IPCC) [110]. The GWP values of CO_2 and two other related gases are given in Table 15.

Table 15: Global warming potential of three gasses

GHG emissions	CO_2	CH_4	NO_2
GWP	1	25	298

3.5.2 Overall Lifecycle Cost Objective

The total cost of the hybrid electric and battery electric powertrains are

$$TC_{Hybrid\ Electric} = n \times days \times trips \times \sum_{j=1}^{n_t} \sum_{i=1}^{n_G} FC_{ij} \times Fuel\ Cost \times \Delta t_j + OE \tag{23}$$

$$TC_{Battery\ Electric} = n \times Electricity\ Cost \times \sum_{d=1}^{180} \mathrm{BESS}_{kWh-consumed_d} + OE \tag{24}$$

where Δt is the simulations time step, n_G is the number of installed gensets, n_t is the simulation time, $trips$ is the number of crossing per day, n is the number of years, $days$ is the number of operating days in a year, FC is the fuel consumption, and OE represents other expenses listed in

Table **16**.

3.6 Results and Analysis

3.6.1 Component Interactions

The proposed hybrid electric and pure electric propulsion system models are computationally efficient for estimating the energy efficiency and emissions of different design options, thus supporting the propulsion system design optimization. The model could capture the component interactions and interdependencies with a sufficient level of detail. The powers derived from the generator and ESS for the hybrid electric system are shown in Figure 44. Initially, the ESS and genset provide power for travelling to the fishing zone from the wharf at full power of about 60 kW. When the vessel reaches a lobster trap, the propulsion power drops to zero but the genset continuously works at its maximum power (13 kW) to charge the ESS. When the ESS reaches its maximum SOC, the charging stops and the genset follows the power demand (black solid curve). The supercapacitor SOC, current and voltages are shown in Figure 45. At present, the duration of the simulation spans more than six hours of operation, due to the need for the genset to fully charge the ESS at the start or end of the trip. A better and more preferred alternative is to obtain this full charge using “plug-in” charge capability from the electric power grid at the shore. The present setting is used to facilitate a fair energy use comparison.

Figure 46 illustrates the response of the engine and supercapacitor to abrupt changes in the vessels power requirements. As the vessels power increases, the engine tends to increase power output, however, due to engine inertia and engine time lag, this response is slow. At this moment, the ESS responds first and provides power until the engine power catches up.

Table 16: System costs

Variables		Conventional ICE powertrain	Series hybrid with SC ESS	Pure battery powered
Investment Costs	Inverter cost	-	$0.21 /W-DC [25]	$0.21 /W-DC [25]
	ESS cost	-	$5,500 /kWh[26]	$700 /kWh [27]
	ESS installation labor	-	$0.15 /W [25]	$0.15 /W [25]
	Electric motor	-	$8,000	$8,000
	Charger station	-	-	$20,000
	Charger station Transformer	-	-	$5,000
	Diesel generator unit cost	$121,000 @238kW [29]	$11,000 @ 15 kW [29]	-
	Diesel generator Installation labor cost	$50 /kW	$50 /kW	-
	Total	132,900$	$226,150	$56,250
Operational costs	ESS operation and maintenance	-	$20 /kW/year [25]	$20 /kW/year [25]
	Fuel cost	$1.121 /L	$1.121 /L	-
	Diesel generator Operation and maintenance	$30 /kW/year	$30 /kW/year	-
	Electricity cost	-	-	Varies [31]

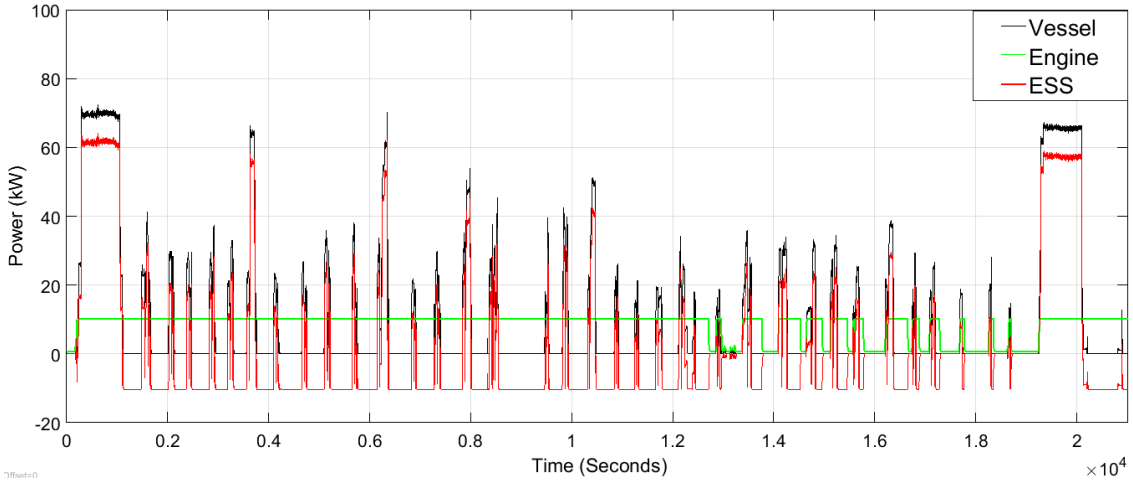

Figure 44: Generator power, ESS power, and vessel demand power.

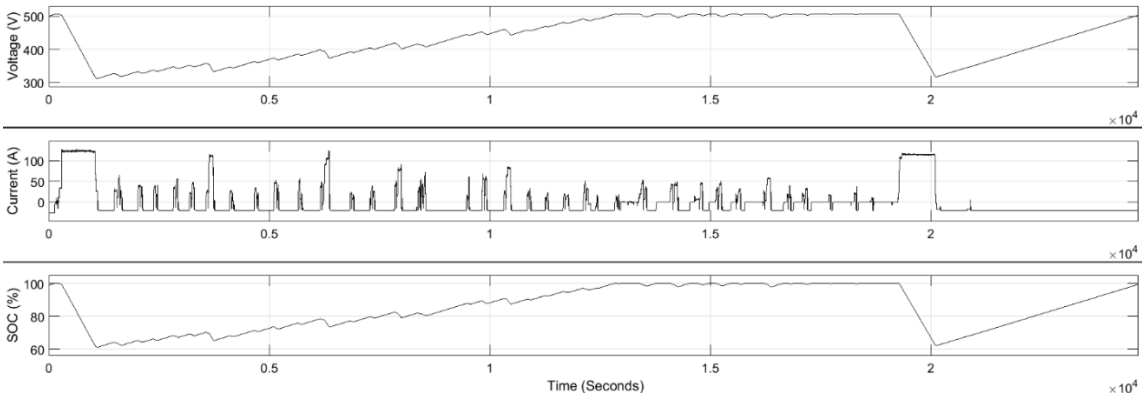

Figure 45: Supercapacitor voltage, current and SOC (%) during a trip

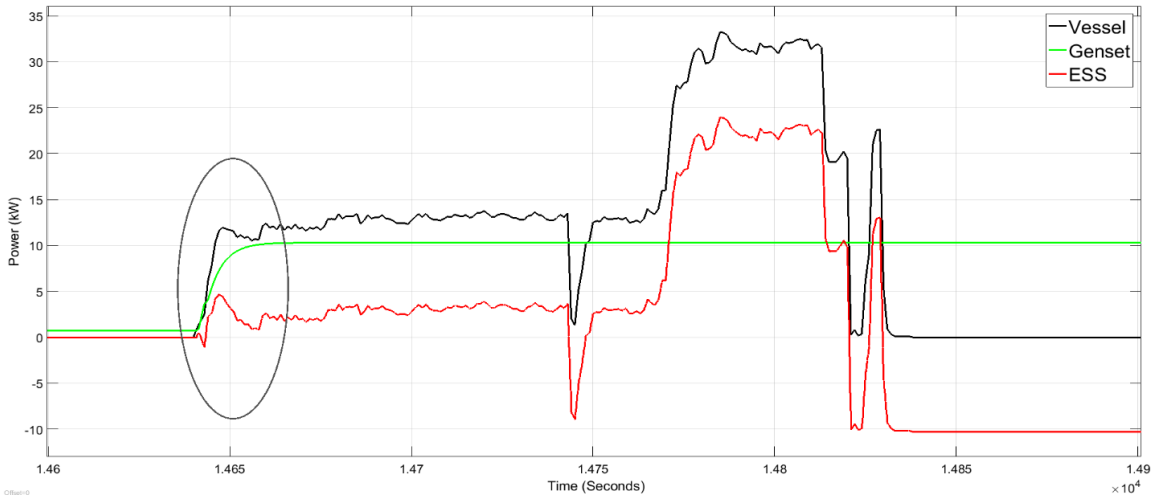

Figure 46: Response of the diesel generator and ESS to abrupt changes in vessels power requirements

3.6.2 Optimal Engine and ESS Size

The Pareto optimal solutions of the multi-objective optimization can provide various optimized engine sizes under different design trade-offs on the overall lifecycle costs (investment and operation) and the equivalent CO_2 emissions over a ten-year period. For a given design preference with a proper weight on the lifecycle costs and equivalent CO_2 emissions, the optimized engine and ESS sizes can be determined. The proposed approach provides a set of solutions for the series hybrid electric powertrain system design, referred to as the Pareto optimum [111], as shown in Figure 47. Pareto optimization was performed to maximize the CO_{2e} reduction and minimize the system cost. As the size of the ESS increases, the cost of the system increases. A larger ESS results in a smaller engine and

lower CO_{2e} emissions. Different levels of hybridization are possible, and each Pareto optimum point represents an optimal solution of the hybrid powertrain system for a given design trade-off decision.

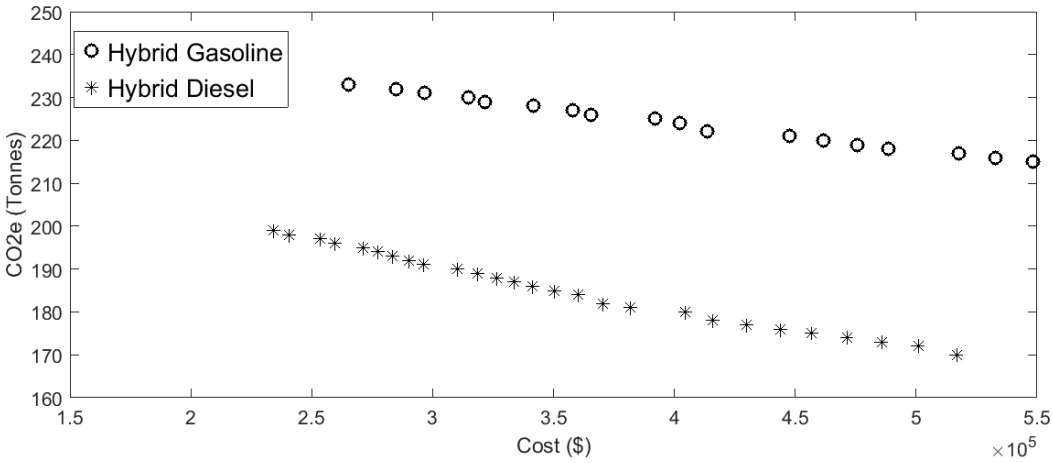

Figure 47: Pareto optimum solutions for two systems.

The total CO_2 equivalent emissions and the lifecycle costs of the conventional ICE powered boat with gasoline and diesel engines, the series hybrid electric boat with gasoline and diesel engines and battery/SC ESS, and the pure electric boat with battery ESS have been projected, using the collected vessel operation data and the newly-developed powertrain system models. Figure 48 illustrates the simulation results of lifecycle costs and emissions under different powertrain systems.

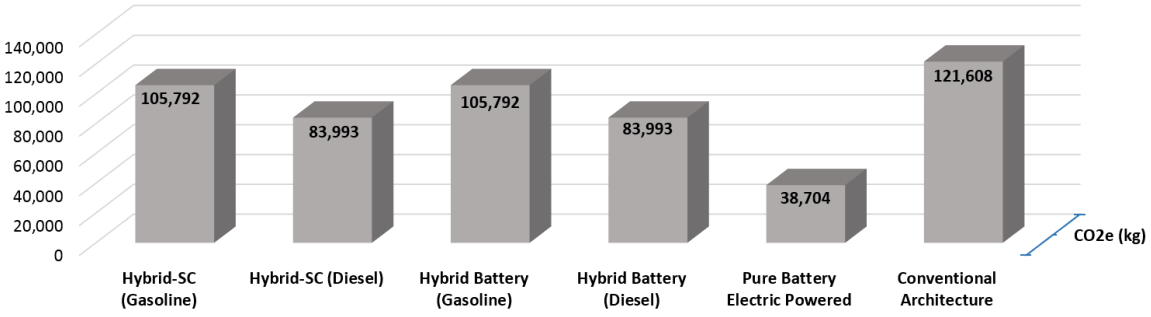

Figure 48: Emission comparison of different architectures over a ten year period.

The new hybrid electric boat design and the battery powered pure electric boat design showed considerable GHG emissions reduction and favorable lifecycle cost savings. The

pure battery powered powertrain has the lowest CO_{2e} emissions and the highest overall costs in comparison to other powertrain systems. The hybrid electric powertrain system with supercapacitor ESS emits the same amount of CO_{2e} as a hybrid powertrain with battery ESS and diesel engine, and has a higher overall cost due to the higher cost of the supercapacitors.

Similarly, the gasoline engine hybrid electric powertrain system with a battery ESS is less expensive than the same system with a supercapacitor ESS. The lifecycle cost of the hybrid electric powertrain system with a gasoline engine is slightly higher than the same system with a diesel engine due to the higher efficiency of diesel engines. The pure electric powertrain system with a battery ESS presents the lowest CO_{2e} emissions among all alternative powertrain systems due to the low emissions of the North American electric power generation that blends at about 0.3794 Kg/kWh [40][41]. In contrast, the conventional powertrain system of the fishing boat has the highest lifecycle cost and CO_{2e} among all powertrain architectures.

3.7 Conclusions

In this work, the hybrid electric and pure electric powertrain system designs for a specific class of fishing boats are proposed, and their performance, energy efficiency, and lifecycle cost are modeled and quantitatively analyzed. Dedicated data acquisition systems have been installed on two representative fishing boats to collect their daily operational data for accurate powertrain system performance, energy efficiency and lifecycle cost prediction and comparison, against the conventional fish boat powertrain system to reveal the benefits of fishing boat powertrain system hybridization and electrification. The lifecycle cost and GHG emissions of hybrid electric, pure electric and conventional mechanical powertrain systems are quantitatively compared using the simulation results.

Moreover, the engine and ESS size are optimized for different powertrain architectures under existing technical and operational constraints of fishing vessels. Simulation results indicated that the hybrid electric powertrain architecture with BESS can ensure lower lifecycle cost and reduced GHG emissions in comparison with the conventional mechanical powertrain. Simulation results also showed that significant reduction in GHG emissions

can be achieved using the pure electric powertrain with a battery ESS, although the lifecycle cost of this system was higher than the hybrid electric powertrain system with a battery ESS due to battery performance degradation under heavy use and large depth of charge/discharge.

4 Electrified Propulsion for a Passenger Ferry

While there has been significant research on the simulation, optimization, and analysis of different hybrid electric terrestrial vehicle architectures [20]–[22], similar research for marine vessels is lacking. Moreover, relevant studies in this area either focus on overall system optimization and ignore component interactions or offer detailed (albeit isolated) analyses of different subsystems. This chapter introduces a system level model of sufficient detail to capture all component dynamics, facilitate design optimization, and support cost analyses. Moreover, due to a lack of standardized drive cycles for marine vessels, real data has been collected for small car-deck ferries. In the next section, a description of BC Ferries MV Klitsa, including its mechanical propulsion architecture, is given. In Section 4.3, series hybrid powertrain and battery electric powertrain architectures are proposed as replacements for the traditional mechanical architecture. These new architectures are modelled using MATLAB-Simscape library and the results are validated using the data collected from the MV Klitsa. In Section 4.4, key components modeling is described and in Section 4.5 optimization problem and constraints are represented. The discussion of the results, overall cost, and GHG emissions are compared with current mechanical systems in Section 4.6.

4.1 System Description and Data Collection

Ferries, unlike other marine vessels such as tugboats, have a very predictable load profile. They usually have a routine schedule and this makes them an attractive case study for modeling and investigation. In addition to having a predictable load profile, the MV Klitsa has other advantages such as available space for battery installation and the fact that it operates in sheltered waters. Lower environmental variability also makes the MV Klitsa an

ideal choice for research on ship hydrodynamics. The MV Klitsa is a car-deck ferry that was built in 1972 and operates between Brentwood Bay and Mill Bay on southern Vancouver Island [114]. It has a total installed power of 700 hp with a maximum speed of 10 knots. The passenger capacity of the ferry is about 150 people and it can carry 19 cars per voyage.

In terms of daily routine, the vessel makes 18 crossings of 5.7 km each, 8 in the forenoon and 10 in the afternoon. In addition, between the forenoon and afternoon crossings there is a one-hour mid-day layover during which the vessel is secured in Brentwood Bay. More information about the ship is given in Table 17.

Table 17: MV Klitsa information [114]

Built:	1972, Vancouver
Overall Length:	47.55 metres (156')
Maximum Displacement:	450 tonnes
Car Capacity:	19
Passenger & Crew Capacity:	150
Maximum Speed:	10.0 knots
Horsepower:	700
Amenities:	Accessible car deck lounge

The MV Klitsa is currently equipped with two 14 litre Detroit Series 60 diesel engines, each coupled to an azimuthing thruster system. A separate 50 kW diesel generator provides electrical power for all other ship loads. After finishing its daily routine the ship is secured in Brentwood Bay, connected to shore power (cold ironing), and all engines are shut down [115].

The current powertrain architecture of the MV Klitsa is illustrated in Figure 49. This architecture is an example of a conventional propulsion system consisting of prime mover(s), reduction gears, medium length shafts, and propeller(s). The prime mover rotates the shaft with medium speed and transfers torque through the shaft via reduction gears in

order to drive the propeller. The propeller converts torque to thrust at rotational speeds on the order of a few hundred RPM [116]. The 50 kW diesel generator is designed to operate at constant speed and supplies electrical power at 60 Hz to the remaining ship loads. The location of each diesel engines is shown in vessel layout in Figure 50.

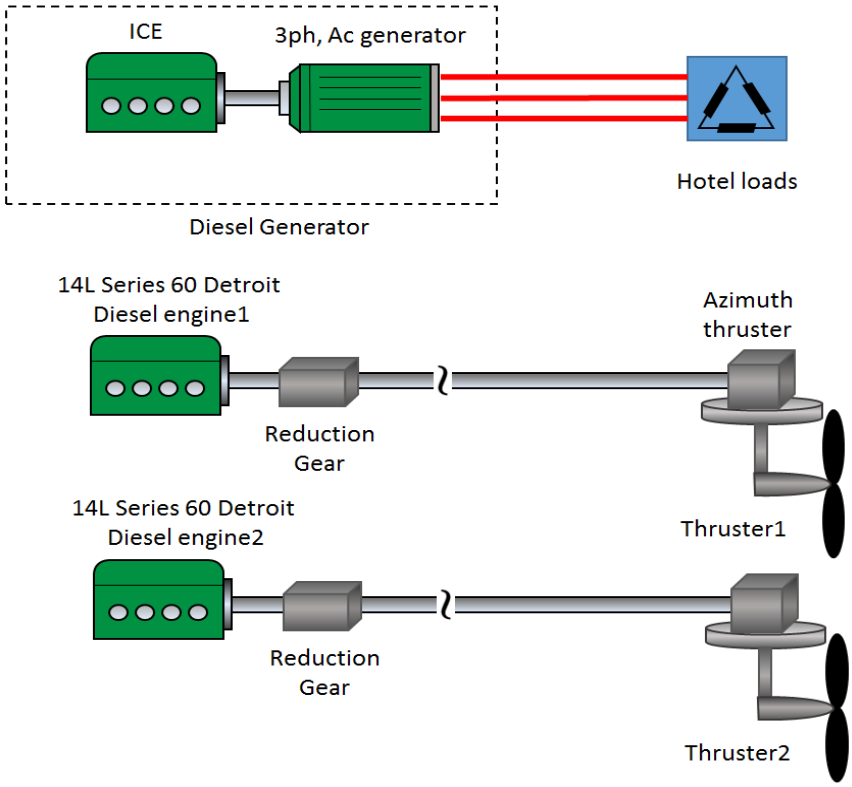

Figure 49: Current powertrain architecture for MV Klitsa

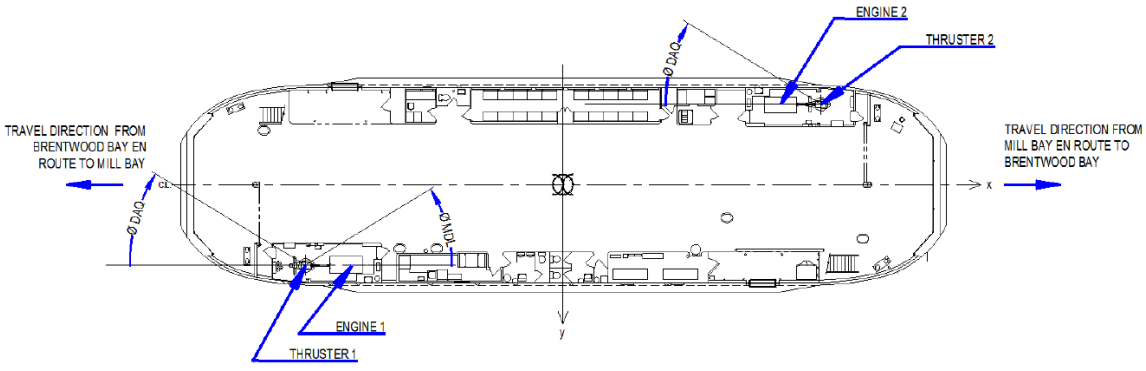

Figure 50: MV Klitsa design layout

A data acquisition system has been installed onboard the MV Klitsa in order to obtain the data required for simulation and model validation. The input torque, power, and speed of each propeller, ship velocity during transit, angle of the azimuthing thrusters, and output power of the 50 kW diesel generator have all been collected. These measurements enable a direct comparison between the current mechanical powertrain and the proposed powertrain architectures.

The data was collected over a two-month period and three representative mission profiles were identified as a good representation of the ship operational variability. Figure 51 shows the low, medium and high load profile for vessel engine. The engine maximum power varies between 170kW to 90kW for steady state condition. In the case of MV Klitsa, the engine power variation is mainly due to the time schedule and less by environmental factors due to its operation in sheltered water. Figure 52 illustrates the ship velocity corresponding to ship power shown in Figure 51. As expected, higher engine power corresponds to higher vessel speed and lower travel time.

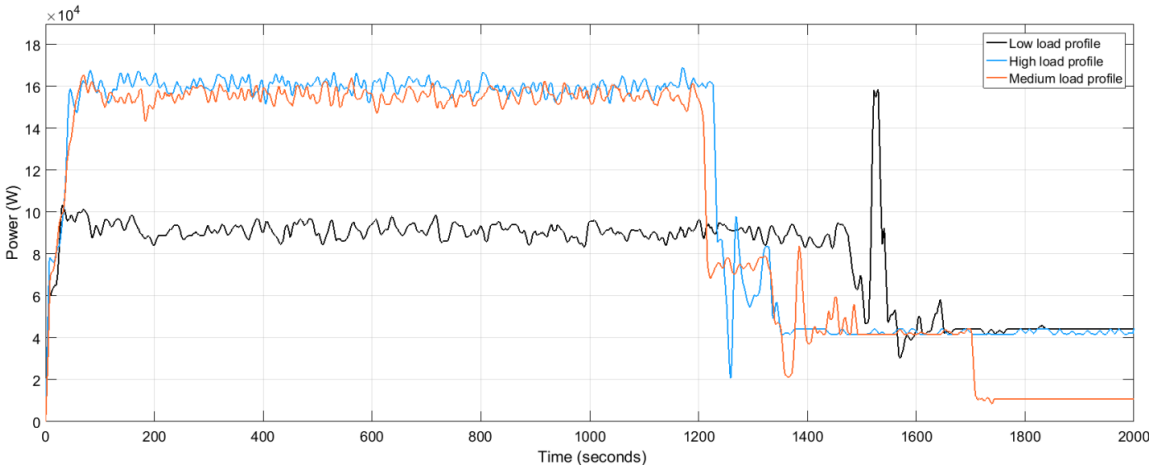

Figure 51: Diesel engine output power for low, medium and high load profile.

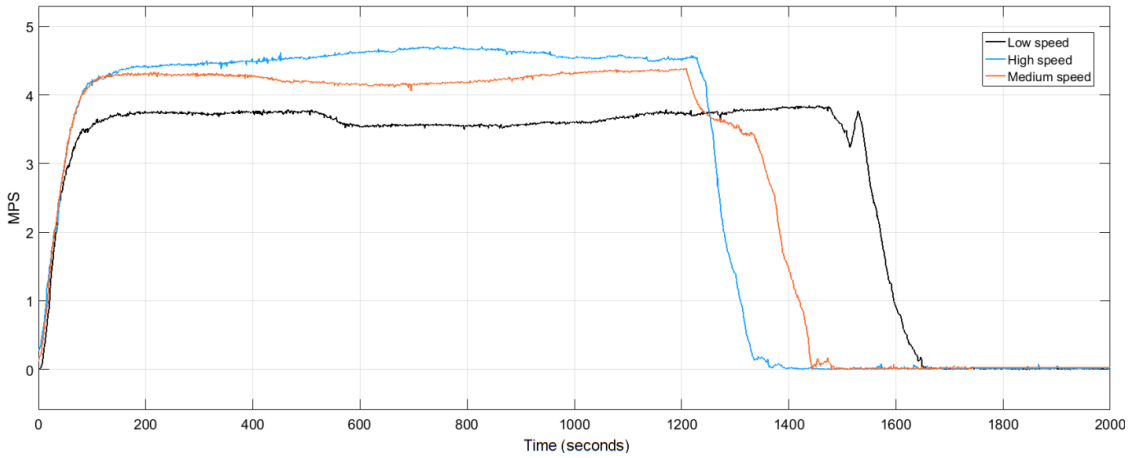

Figure 52: Ship velocity for low, medium and high speeds.

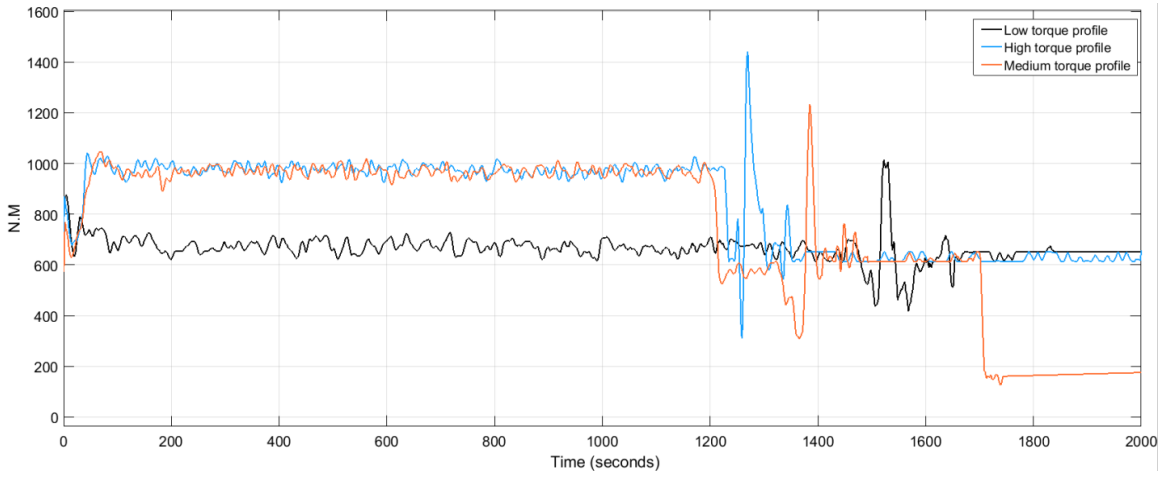

Figure 53: Diesel engine output torque for low, medium and high torque profile.

Engine torque pulses can be observed in Figure 53 when the MV Klitsa nears either Mill Bay or Brentwood Bay. These pulses represent the short bursts of power required to maneuver the ship into alignment with the jetty at either terminal. While the MV Klitsa is pushing into the jetty during loading and unloading, the engines are working at slightly more than their idle speed. The torque pulses that are characteristic of a vessel maneuvering into a jetty are of major significance since they often require oversizing the engines to accommodate for this transient load. This is one of the major advantages of hybrid electric

propulsion since the plant can better tolerate transient loads without oversizing the engine and increasing fuel consumption. The three navigational trajectories taken by the vessel for each respective load profile are shown in Figure 54. Two of the three load profiles run from Mill Bay to Brentwood Bay, illustrated with red and green arrows respectively. The third profile runs in the reverse direction with its course plotted with blue arrows.

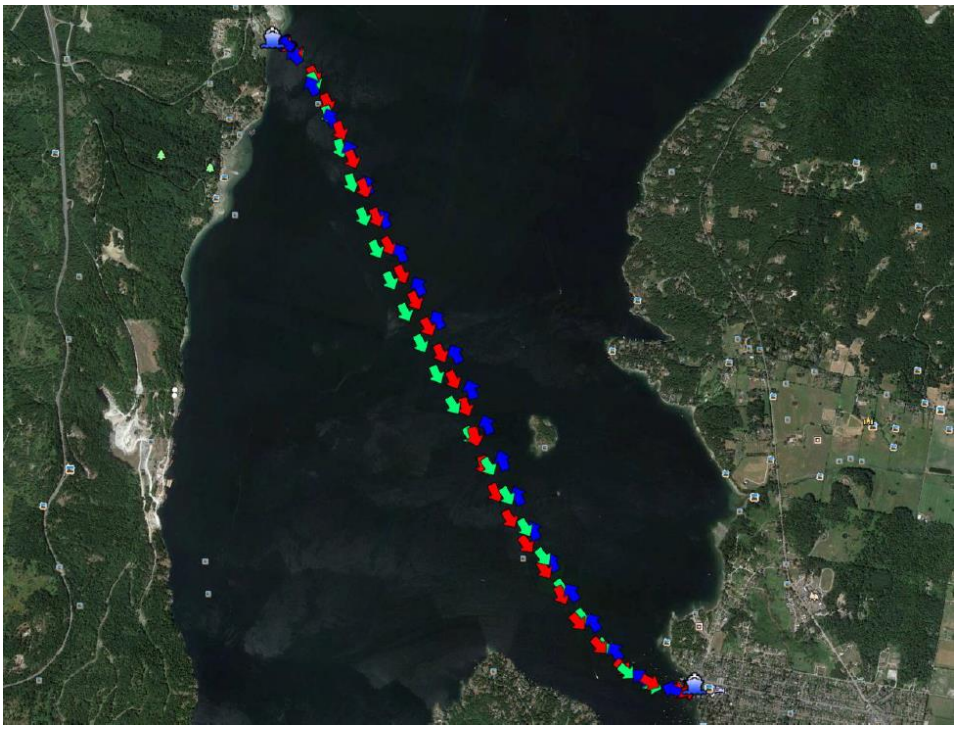

Figure 54: Course and heading data for the three load profiles [115]

4.2 Proposed Powertrain Architectures

The choice of a powertrain architecture depends on vessel types and the operational profile of the vessel. Finding the optimal architecture for a particular vessel, however, is generally not an easy task. Designers must take into account many factors like availability of technologies at the time of construction and design flexibility. In this work, series hybrid and battery electric architectures are investigated for application onboard the MV Klitsa while keeping the existing hull and propeller system.

4.2.1 Series Hybrid Architecture

The proposed series hybrid architecture is depicted in Figure 55. One of the great advantages of series hybrid architectures is flexibility in the location of equipment. The lack of need for a long shaft line allows the diesel generators to be placed wherever is ideal. The common electrical grid would provide several advantages for the MV Klitsa such as servicing ship loads with a smaller number of prime movers; which would result in noticeably improved fuel efficiencies over the low and medium speed ranges. Moreover, this design can maintain the level of redundancy, which is an important design factor, especially in passenger vessels which are required to always have a redundancy of 50% of the total propulsion demand [117].

The series hybrid architecture has higher efficiency especially at the low speed range when compared to tradition mechanical propulsion. This happens when the diesel engines are working in a lower power range which is corresponded to a higher fuel consumption. As mentioned before, any electric propulsion designs introduce extra electrical losses due to electrical components such as electric motors, converters, generators, and transformers [118]. Depending on the vessel operating profile, these losses at full power can outweigh the benefits of switching to a series hybrid architecture. Therefore, extra care must be taken before selecting a series hybrid architecture for a given ship design. However, there are still several other arguments in favour of a series hybrid architecture such as lower noise and better dynamic response.

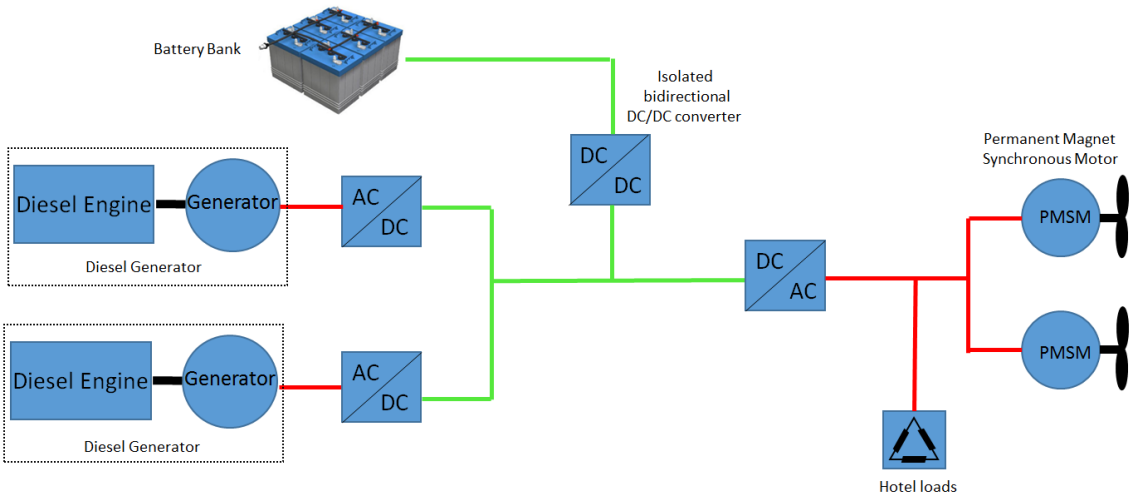

Figure 55: The proposed series hybrid architecture.

4.2.2 Pure Battery Electric Architecture

Pure battery electric architectures have become quite popular for passenger ferries in recent years. They offer significant advantages over other architectures such as higher energy efficiency, lower noise levels, and greater reliability. However, factors such as high capital cost, the need for proper cooling mechanisms, bulky and expensive fast charging stations, and (in some cases) the cost of expanding the existing electrical grid have limited the implementation of this design. Despite this, the first battery electric car ferry, the Norled AS MF Ampere, entered service in Sognefjord, Norway, in 2015 [13]. It has been estimated that it annually offsets the use of one million litres of diesel fuel which translate to the emission of 570 tonnes of carbon dioxide and 15 tonnes of nitrogen oxide when compared to conventional ferries in service on the same route [14].

In a battery electric architecture, the BESS is the only primary source of energy and it services all ship loads, although a backup diesel generator is usually installed to satisfy redundancy requirements. This makes the battery electric architecture very similar to the architecture of the EREV currently available on the market. The BESS is the main source

of energy like a diesel generator in a series hybrid architecture. However, a BESS has a very high efficiency over its entire operating range when compared to a diesel generator.

The proposed battery electric architecture for the MV Klitsa is illustrated in Figure 56. The BESS is coupled to a bidirectional DC/DC converter in order to charge the battery and step up the voltage. Similar to the series hybrid architecture, the distribution system can be either AC or DC. In the case of a DC distribution grid, electrical power is transferred to a DC/AC converter to provide power for big loads like propulsion. Smaller loads are connected to the grid by means of individual converters. The current trend in the shipping industry is moving towards DC distribution systems because of the flexibility they offer in introducing energy storage, fuel cell, and solar technologies [11].

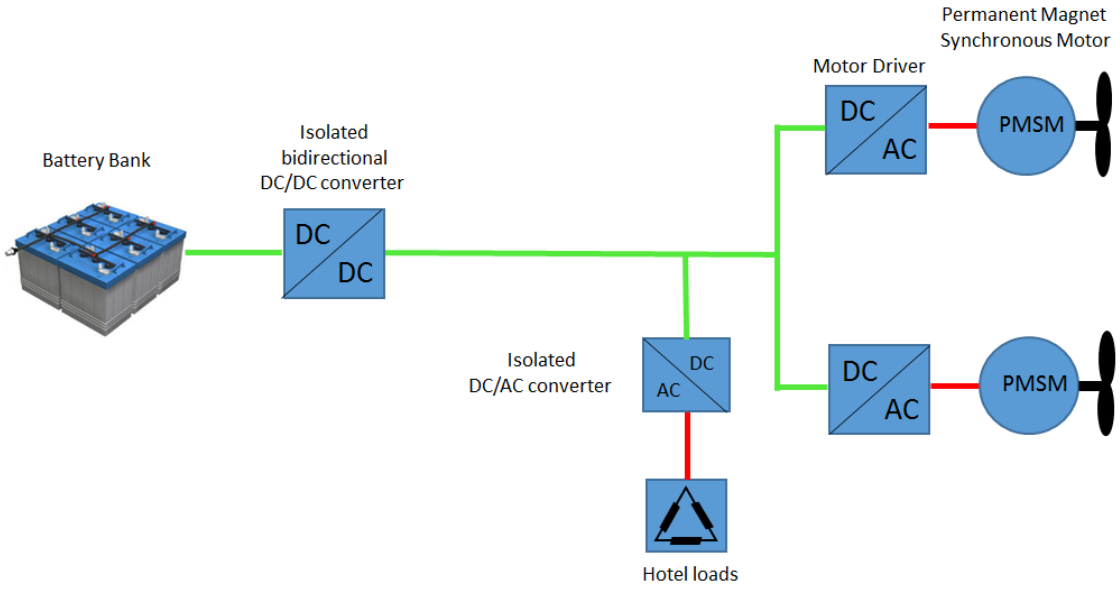

Figure 56: The proposed battery electric architecture

4.3 Key Component Modeling Using Simscape

In this section, the developed powertrain model for the MV Klitsa is explained. A different approach of modeling using Simscape library is used to expedite the modeling time for

different powertrain architectures. Simscape block libraries contain a range of prebuilt blocks that represent engineering components. These blocks are also expandable to represent the unique engineering needs using Simscape language to define customized components. The developed model in MATLAB/Simulink is shown in Figure 57. The detail description of this model is explained next.

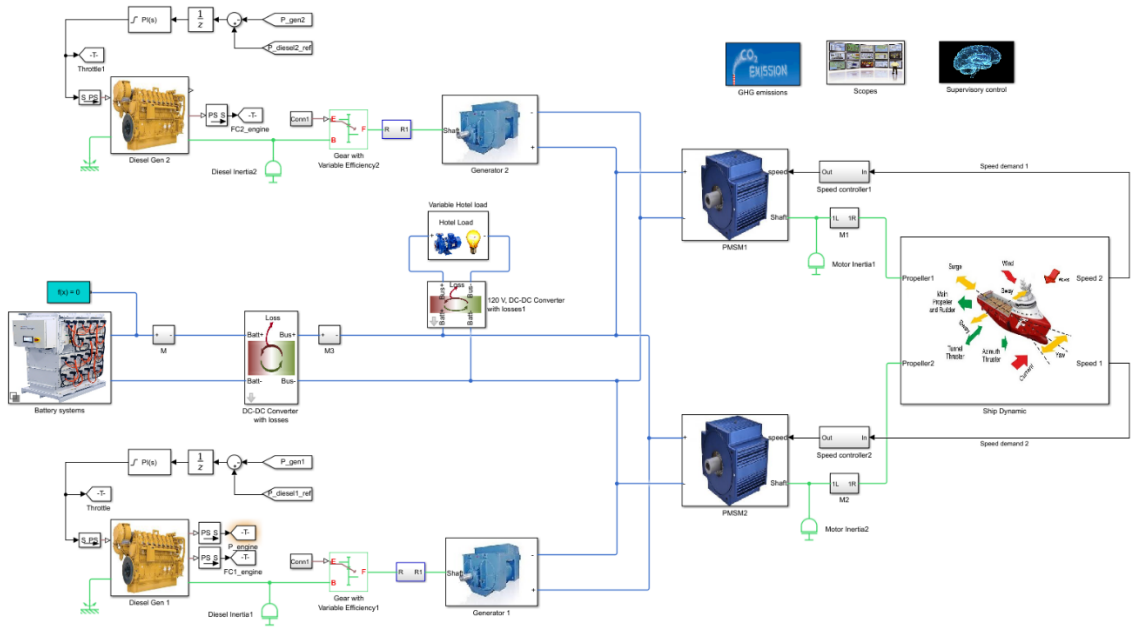

Figure 57: Simulink model in MATLAB

4.3.1 ICE Model

The generic engine model block available in the library is used to represent the diesel engine. For higher accuracy in the engine model, we have used an actual fuel consumption map of Detroit diesel engine [13] shown in Figure 58. The range of speed and torque from fuel consumption map is placed in the model and tabulated power data and linear interpolation are used to calculate the engine output torque. A discrete PI controller as shown in Figure 59 provides required throttle for the engine and controls the output power with respect to the reference power (collected data). A simple gear block model with

constant efficiency also is attached between the diesel engine and generator to represent the gears between these two components.

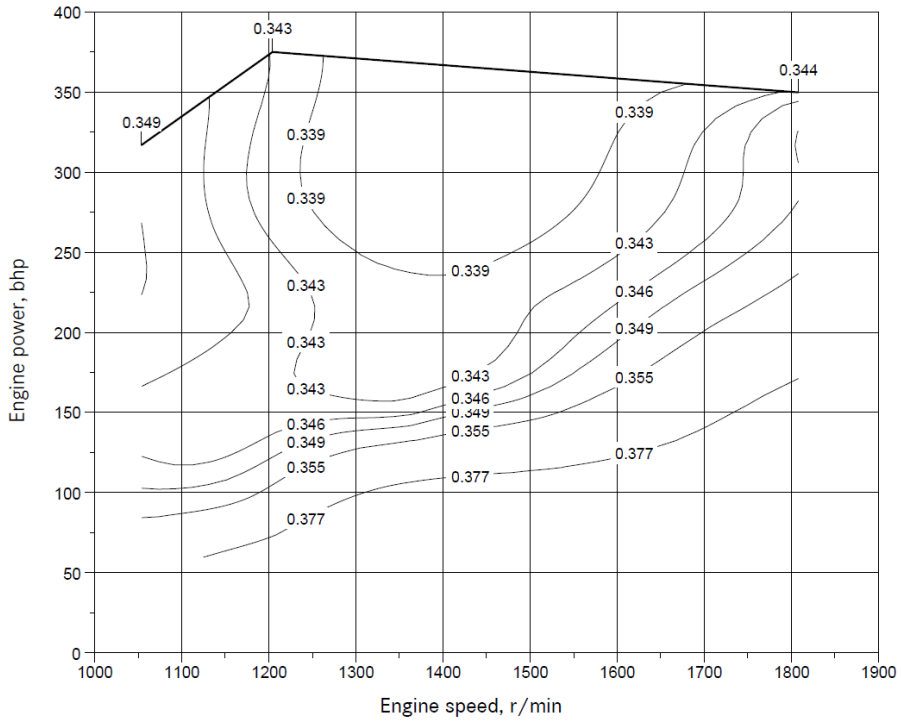

Figure 58: Fuel consumption map, [lbm/bhp-h] [13]

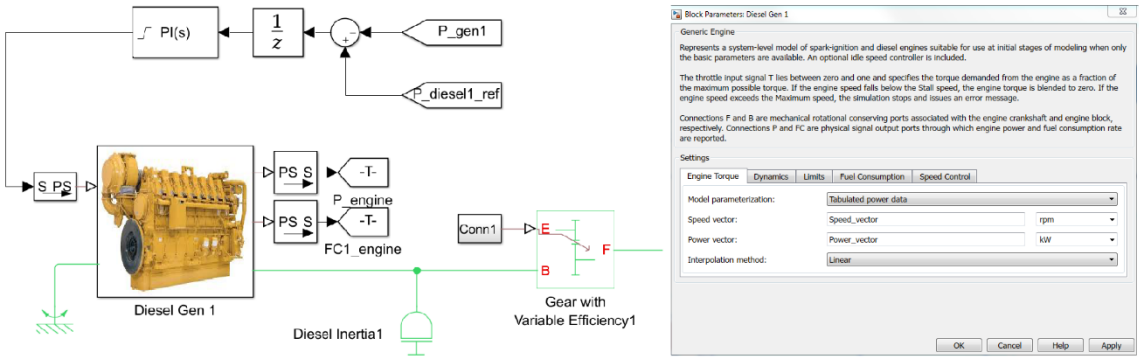

Figure 59: Engine model and parameters

4.3.2 Battery Model

BESS is a key component of the hybrid and pure electric powertrain in marine vessels. lithium-ion is a typical choice over standard nickel-cadmium and offers largest energy density for weight. In addition, Lithium-ion has a very low maintenance, an advantage that

most other battery chemistries cannot claim. Lithium-ion batteries are being used in increasingly complex configurations with very challenging duty cycles and are usually selected as the desired battery chemistry. A simple prebuilt battery model in Simscape shown in Figure 60 is used to represent the battery ESS. Finite mode for battery charge capacity parameter is selected to represent the battery as a series resistor and a charge-dependent voltage source. In this mode, the battery voltage is a function of charge and is defined as

$$V = V_0 \left(\frac{SOC}{1 - \beta(1 - SOC)} \right) \tag{25}$$

where SOC is the state-of-charge, V_0 is no load voltage at full charge and β is a constant that is calculated so that the battery voltage is V_1 when the charge is AH_1. Above equation relates the output voltage to SOC. Since SOC is defined as a ratio of current charge over rated battery capacity, the output voltage is also related to the remaining charge in the battery. The SOC equation defined as follow [119]

$$SOC\%(t) = \frac{Q_0 - \int_{t0}^{t} I_b(\tau)\, d\tau}{Q_0} \times 100 \tag{26}$$

where Q_0 is the battery charge capacity, $I_b(t)$ is the battery current, and $\int_{t0}^{t} I_b(\tau)\, d\tau$ is the battery charge delivered over the time interval $[t_0, t]$ with the battery assumed to be at full charge at time t_0. One advantage of using this model is the small number of parameters in the battery model.

The energy holding capacity, or cycle life, of the Li-ion battery is affected by its operating temperature, depth of discharge (DOD), and charge/discharge currents. The performance degradation and capacity fade of the battery under different use patterns needs to be taken

into account for lifecycle costs of the BESS. In this work, for hybrid electric propulsion, as in automotive applications, it is assumed that the BESS needs to be replaced after a 20% reduction on its energy holding capacity or capacity fade. During vessel operation under the obtained load profile and total energy consumption, the SOC of the BESS is between 40% and 95%. For 40% DOD, a Lithium-ion battery is expected to cover the ten-year lifetime of the hybrid electric powertrain.

For Pure electric powertrain architecture, BESS needs to provide all power required by the vessel and have a deeper DOD. The BESS is charged using a fast charger facility installed onshore which is assumed to be located in Brentwood Bay. The battery size in this architecture should provide power for nine consecutive transits. During vessel operation under the obtained load profile and total energy consumption, the SOC of the BESS is between 20% and 100% between each deep charge. During the one-hour noon layover, the batteries have a chance to fully charge using the fast charger station. For five hours of operation in the morning, the BESS needs to have a capability of 1538 kWh. At 80% deep DOD of each operation twice per day, the battery will last about 500 cycles [96], equal to one and a half years under the more demanding working condition. By doubling the BESS size and reducing the DOD, it is assumed that the battery can last for three years.

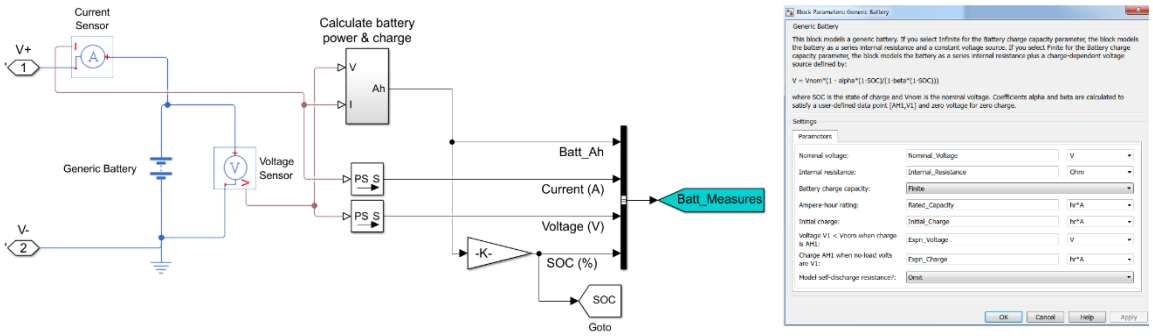

Figure 60: Battery model and parameters

The weight of the battery ESS is an important design factor in the automobile industry, but it can be ignored in marine transportation mainly due to the heavy weight of the vessels. For example, the MV Klitsa ferry has a maximum displacement of 450 tonnes and a maximum ESS battery weight considering 12.4 kg per kWh of energy of 18,800 kg, which is about 4% of the total weight.

4.3.3 DC/DC Converter Power Loss Model

The DC/DC power loss model used in this model is the same as in the previous chapter.

4.3.4 Electric Machine Model

Two high performance permanent magnet motors (PMM) drive the MV Klitsa azimuthing thrusters at reference (i.e. data) speeds and torques. The prebuilt Simscape permanent magnet electric machine shown in Figure 61 is used as a motor and generator in this work. This block has an inherent closed loop system which facilitates the simulation. The PMM output torque and power illustrated in Figure 62. Output torque and power are in a close approximation with actual data. This ensures that the PMM can provide enough power and torque for MV Klitsa to reach its desired speed.

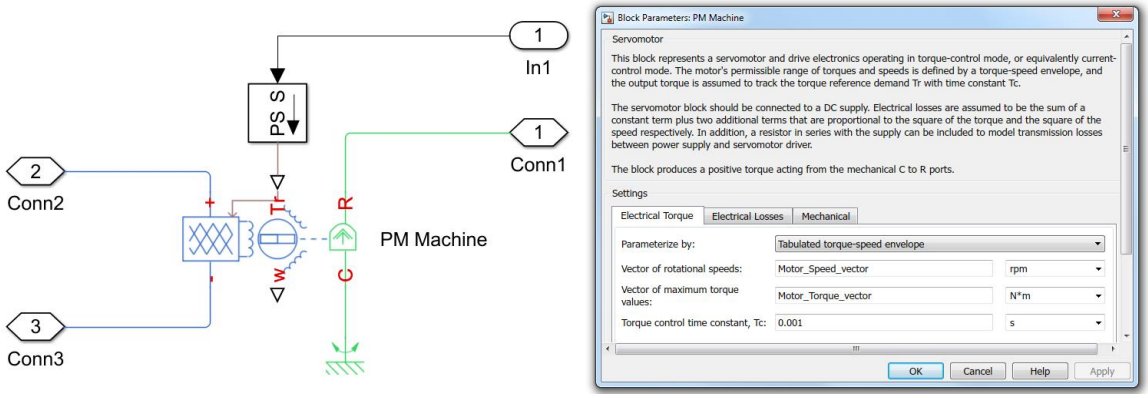

Figure 61: Electric machine model and parameters

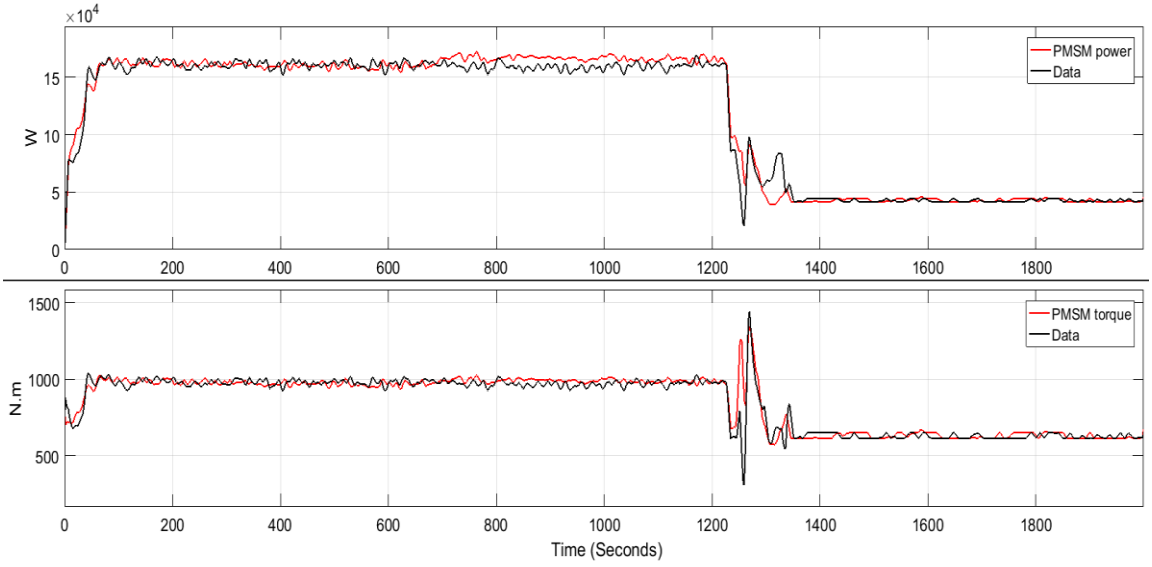

Figure 62: PMSM output power and torque

4.3.5 Vessel Speed

The simulated vessel speed requires to follow the reference vessel speed to make sure that vessel can arrive in the terminal on time. Vessel speed can be calculated using the following equation

$$P_{prop} = P_s \ \ \eta_s = R_{ship} \ V \tag{27}$$

where P_{prop} is actual propeller power, P_s is the shaft power, η_s is shaft efficiency, V is vessel velocity and R_{ship} is the total resistance of the vessel [120]. The total resistance of a vessel in calm waters can be expressed as the summation of four main resistance components: fractional resistance, wave making resistance, eddy resistance, and air resistance. The wave making and eddy components can then be combined into a single component called residuary resistance. A simple way to express the total resistance is given in ITTC-78 and [120] and expressed as

$$R_s = \ C_{TS} \ \frac{1}{2} \rho \ V^2 \ S_s \tag{28}$$

where C_{TS} is the total MV Klitsa resistance coefficient, ρ is the water density, and S_s is the wetted surface. C_{TS} for the MV Klitsa was calculated using vessel data provided by manufactuthe rer and computational fluid dynamics (CFD) software [121].

4.4 Diesel Generator and Optimal Battery Sizing

4.4.1 The Optimization Problem

The general problem of optimizing component sizes can be expressed as a minimization problem in which cost (both capital and operational) and CO_{2e} emissions are the objectives. The constraints on this problem are

$$\begin{aligned} Min \quad & Obj_1 = Cost\left(P_1, P_2, P_b\right) \\ & Obj_2 = CO_2\left(P_1, P_2, P_b\right) \\ St. \quad & \left\{P_1 \in Z \mid 0, \left[65:15:370\right]\right\} \\ & \left\{P_2 \in Z \mid 0, \left[65:15:370\right]\right\} \\ & P_1 + P_2 + P_b = 370 \\ & P_b \in [0, 370] \end{aligned} \tag{29}$$

where P_1 and P_2 are engine one and two rating powers and P_b is the BESS power. It is clear that the optimization problem has two computationally expensive black-box objectives, three mixed design variables and a linear constrain which is difficult to solve with conventional optimization methods. Therefore, in order to simplify this problem, a transformed optimization formula is presented and shown as follows

$$\left.\begin{aligned} P_b &= 370 - P_1 - P_2 \\ P_b &\in [0, 370] \end{aligned}\right\} \Rightarrow 0 \le 370 - P_1 - P_2 \le 370 \tag{30}$$

$$\begin{aligned} Min \quad & Obj_1 = Cost\left(P_1, P_2\right) \\ & Obj_2 = CO_2\left(P_1, P_2\right) \\ St. \quad & \left\{P_1 \in Z \mid 0, \left[65:15:370\right]\right\} \\ & \left\{P_2 \in Z \mid 0, \left[65:15:370\right]\right\} \\ & P_1 + P_2 \le 370 \end{aligned} \tag{31}$$

This optimization problem is transformed into simpler equations with a two-dimensional bi-objective integer solution including a simple inequality constraint and two complex objectives that need to be analyzed by Simulink. After removing the infeasible solution from the results, there are 92 feasible cases with a simulation time of eight minutes each. In the post processing stage, a non-domination sort is used to capture the Pareto frontier as follows

$$f_{obj}^{i} = \frac{rawf_{obj}^{i} - rawf_{obj}^{\min}}{rawf_{obj}^{\max} - rawf_{obj}^{\min}} \tag{32}$$

$$G_i = 1 - \max_{j}\left(\min_{obj=1,2}\left(f_{obj1}^{i} - f_{obj1}^{j},\ f_{obj2}^{i} - f_{obj2}^{j}\right)\right) \tag{33}$$

where $rawf_{obj}$ is the original objective value and f_{obj} is the normalized value. The pseudo code is summarized below.

Enumeration of the Pareto frontier

```
Begin
  Input P1 and P2 and assign the integer values between 0 and 370.
  Generate the grid sample points in the range [0, 370].
  for i =1 to 371×371
    Delete the infeasible points based on the true integer ranges of P1 and P2.
    Delete the infeasible points based on the inequality constraint.
  end
  Save the feasible 92 points in the database.
  Run the simulation on the 92 cases and get the objective values.
  Save and normalize the objective values based on (32).
  Carry out the non-dominated sorting process based on (33).
  Select the G values that are bigger than 1.
  Return the Pareto set and the corresponding solutions.
End
```

Additional constraints and formulation of the optimization problem are given next.

4.4.2 Constraints for MV Klitsa

The simulation model and optimization problem for the MV Klitsa requires the following additional limitations to satisfy physical laws and safe operating requirements.

- Mechanical power balance: The motor output torque and speed must follow the reference (collected data) propeller torque and speed.

- The variation in vessel speed during steady state operation should stay within the limit (±3 km/h). This ensures that the MV Klitsa can complete a given transit in the prescribed time.
- The diesel generator output power should not exceed its maximum rating power.
- The CO_{2e} emission should not exceed the CO_{2e} emissions of the current mechanical architecture.
- The battery power rating must be sufficient to provide enough power for each case including pure battery system and follows the following equation

$$\sum_{j=1}^{n_{BESS}} P_{BESSj} = \sum_{i=1}^{n_G} P_{Gi} - \underbrace{\max}_{t}[P_{demand}] \tag{34}$$

- The BESS state of charge should not exceed its minimum limits of 50% for a hybrid powertrain and 20% for a pure battery architecture, respectively.

4.4.3 Total Cost Function

The total hybrid series architecture cost is the sum of the fuel costs of all generators and other expenses

$$TC_{Hybrid\ series} = n \times days \times trips \times \sum_{j=1}^{n_t}\sum_{i=1}^{n_G} FC_{ij} \times Fuel\ Cost \times \Delta t_j + OE \tag{35}$$

Information about the symbols can be found in the nomenclature. The fuel cost, component cost and other expenses (OE) are calculated using the values given in Chapter 2 for the cost model. The total pure battery architecture cost is obtained as the sum of the total energy consumed by the battery per day multiplied by the electricity cost so that

$$TC_{Battery\ powered} = n \times\ Electricity\ Cost \times \sum_{d=1}^{365} \mathrm{BESS}_{kWh-consumed_d} + OE \qquad (36)$$

4.4.4 Thermal Efficiency

The thermal efficiency of a heat engine is

$$\eta = \frac{W_{out}}{Q_{in}} \qquad (37)$$

where W_{out} is the work done by the engine on its surroundings, and Q_{in} is the heat put into the engine. W_{out} is given by

$$W_{out} = \sum_{i=1}^{n} P_i\, \Delta t_i \qquad (38)$$

and Q_{in} is

$$Q_{in} = q_{\mathrm{comb}} \sum_{i=1}^{n} m_i \qquad (39)$$

where P_i is the engine power output during time step i, m_i is the mass of fuel consumed during time step i, and q_{comb} is the specific heat of combustion for a particular fuel which for marine diesel oil is 41003.2 kJ/kg [122].

4.4.5 Equivalent CO_2 Emission

GHG emissions can be calculated directly from the mass of fuel consumed by each engine. However, GHGs have different radiative forcing, which means that they have a different ability to absorb heat in the atmosphere; therefore, a different metric is required to take this effect into account. As explained in Chapter 2, the GWP measures the ability of these gases and is expressed as the ratio of each gas heat trapping capacity relative to that for CO_2. The

GWP values given in the emission model is used for emission estimation. In the case of a battery electric architecture, the emission factor is calculated as follows. Since more than 90% of the electricity generated in BC is produced by hydroelectric generation, the emission factor for a battery electric architecture is considerably lower than for series hybrid architecture. Based on the information provided in [123], the emission factor for BC Hydro and North American power plants is, on average, about 15 g/kWh and 0.3794 Kg/kWh [31], respectively.

4.5 Results and Analysis

4.5.1 Component Interactions

One of the reasons for conducting a study on the MV Klitsa was to create a forward-facing powertrain model to explore the component interactions and interdependencies. Then, the behaviour of each component can be cross-checked against real system results. The forward-facing model also gives more information about the system limitation and drivability of the powertrain. Figure 63 gives the simulation results and power profiles for different powertrain components where the demand power consists of the two propulsion loads and the hotel load. Moreover, a 10% electrical loss is introduced into the model to represent the losses associated with the electric propulsion system. The sum of the BESS power, total losses, and diesel generator power is equal to the total demand power. Figure 65 gives the battery usage during a transit as determined by a rule based energy management strategy shown in Figure 64. Initially, the battery is charged at 100% of its capacity and then when the diesel generator reaches its maximum output power, it gradually discharges and provides the rest of the power required by the vessel. At about 1200 seconds the vessel power drops and the generated power exceeds the demand power,

so the excess power flows back into the BESS and charges the battery. This follows from the formulation of the objective function that tries to minimize the SFC of the diesel engine during its operation by running the diesel generator at its rating power. Figure 66 illustrates the MV Klitsa velocity during steady state condition calculated by (28). The accuracy of the ship velocity depends on the calculated resistance coefficient (C_{TS}) value of the ship. For the MV Klitsa, this coefficient was calculated using the CFD software.

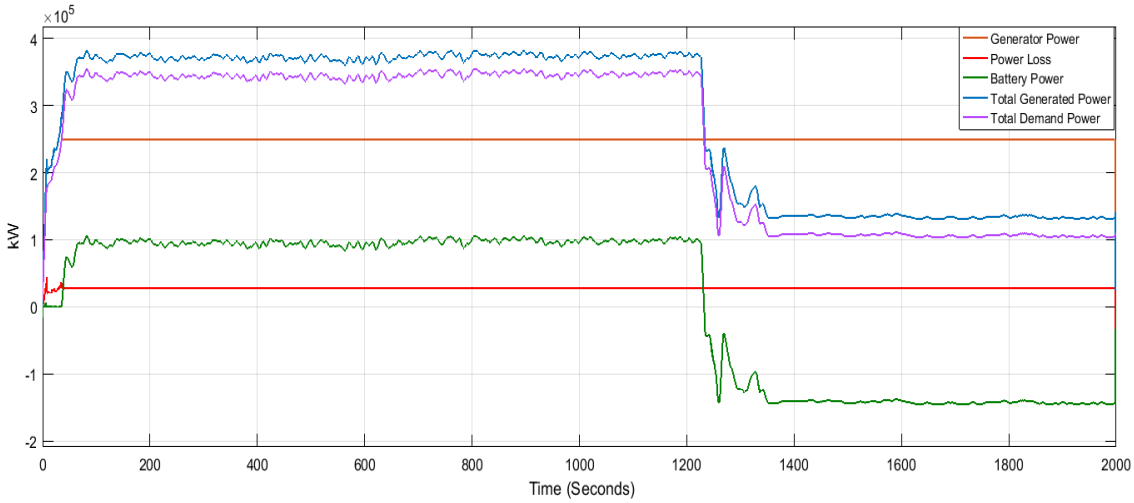

Figure 63: The output power of different components during a transit.

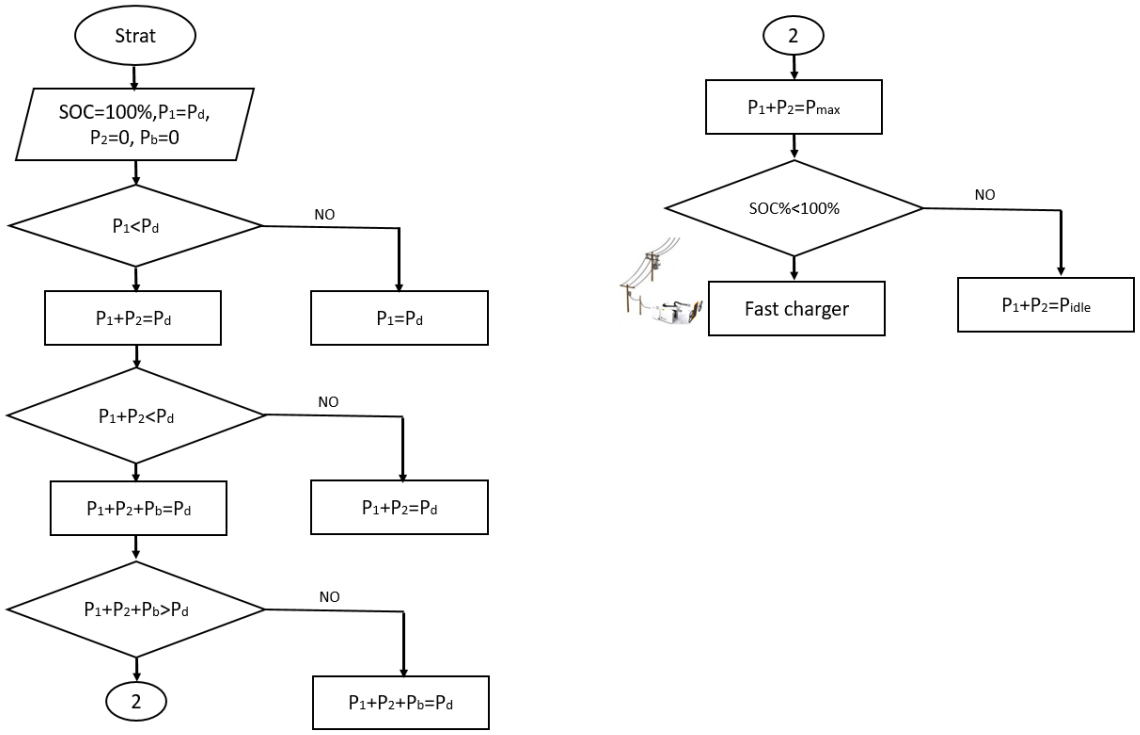

Figure 64: Rule based energy management strategy.

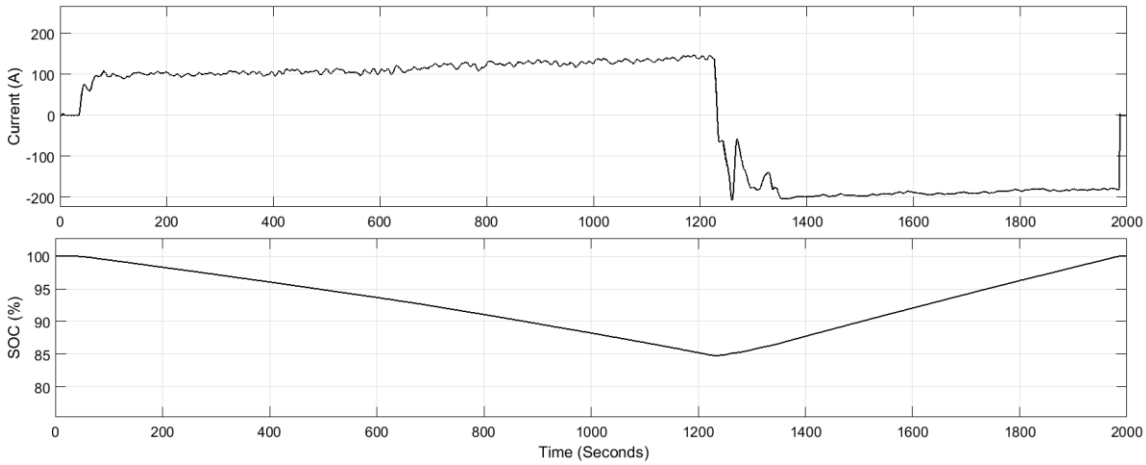

Figure 65: BESS SOC and current during a voyage.

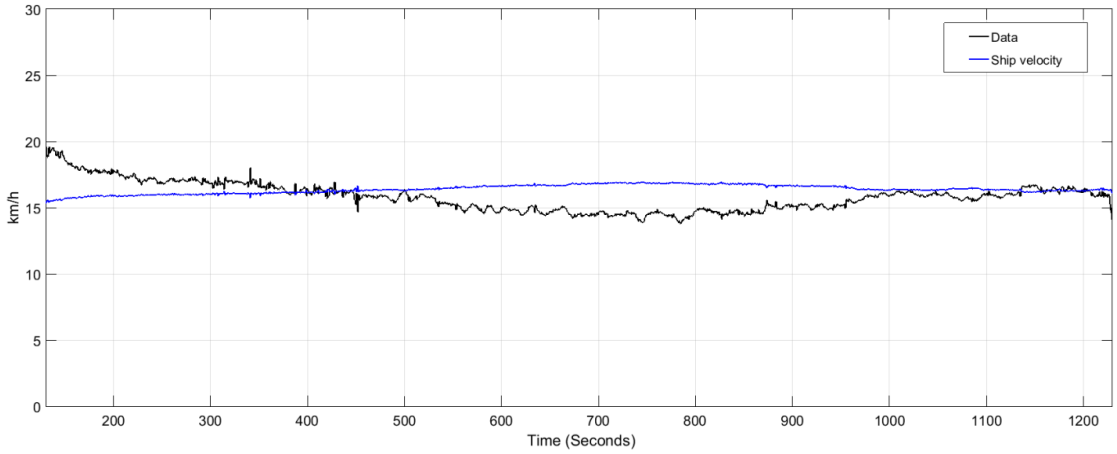

Figure 66: Simulated ship velocity during a transit

4.5.2 Cost and Emission Analysis

The emission analysis results for all three architectures are presented in Table 18. The conventional mechanical architecture has the highest CO_{2e} emissions compared to the other architectures. The series hybrid architecture with one genset installed at 370 kW produces 14% lower emissions than the conventional architecture. Interestingly, the emission analysis indicates that the pure battery system has emissions similar to a series hybrid architecture when using the North American electricity emission factor. However, emission in this architecture can be reduced significantly if the electricity is generated by renewable energy systems like hydro energy. For the MV Klitsa, emissions can be further reduced to 140 tonnes when the BC Hydro emission factor is used in the analysis. This is about a 98% reduction in emission compared to a conventional architecture.

Table 18: CO_{2e} emission per crossing for different architectures

Various Powertrain architectures	Various Fuels	CO_{2e} Emissions (Tonnes)	CO_{2e} Reduction

		Gen1+Gen2	BESS	Total	
Mechanical system	Diesel	11,195	0	11,195	0
Series hybrid system	Diesel	9,604	0	9,604	-14%
Pure-Battery system	Varies	0.0	7,516	7,516	-33%

Figure 67 shows the cost and emission analysis results for all architectures. It is clear that the series hybrid electric architecture has the lowest cost over the ten years period because one genset provides all the required power for the vessel at full power. The conventional architecture cost is 13% higher than the hybrid electric architecture and 28% lower than the pure battery system. The higher cost of the pure battery architecture is mainly due to battery degradation and the BESS replacement cost.

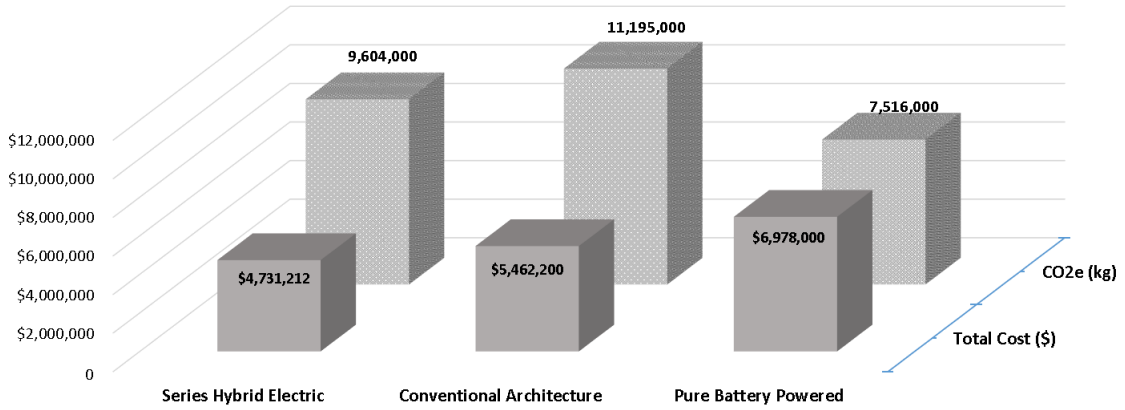

Figure 67: Cost analysis for various architectures over ten years period

Selecting a proper powertrain architecture for the MV Klitsa is a Multi-Objective Problem (MOP) since more than one objective function, such as cost and CO_{2e}, are of interest. In these problems, the objectives are in conflict with each other. Therefore, reaching a solution that optimizes each objective function without deteriorating the other is impossible. The answer to such problems is a set of solutions referred to as the Pareto

optimum or frontier [111]. The Pareto frontier points for the series hybrid architecture are shown in Figure 68. It is clear that neither of the Pareto frontier points is superior to the other points.

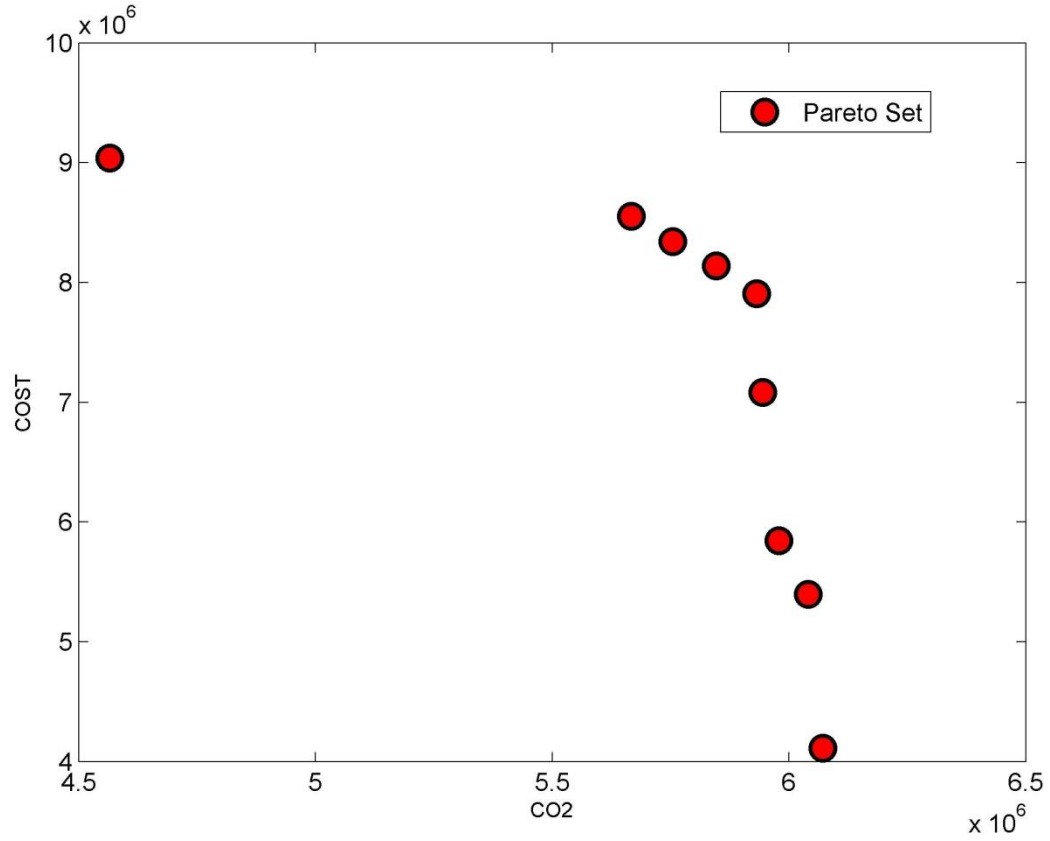

Figure 68: Pareto frontier points for a series hybrid architecture

Figure 68 shows that the lowest cost corresponds to the series hybrid architecture with one generator rated at 370 kW. However, this point is associated with the highest CO_{2e} emissions. On the other hand, as the BESS size increases, the CO_{2e} decreases but the cost increase. In the series hybrid architecture, one diesel generator normally works at its maximum rating power and extra power is provided by the BESS instead of another diesel generator. This combination of diesel generator and BESS is also able to provide enough

power for power pulses required to maneuver the ship into alignment with the jetty. These pulses often require oversizing the engines to accommodate for this transient load.

4.6 Conclusion

This chapter presented various propulsion architectures for a car-deck ferry. BC Ferries MV Klitsa was selected for this case study and real vessel performance data was collected for comparison purposes. Hybrid series and pure battery electric architecture models were developed and the results were compared with current mechanical systems. The optimization algorithm considered different sizes and combinations of generators and BESS in the series hybrid architecture. The results based on Pareto optimal theory indicate that the most cost effective series hybrid architecture is one generator providing all the power for the vessel. The pure battery electric architecture provides a considerable CO_{2e} reduction if the electricity is only from renewable energy sources. This architecture has a 28% higher cost compared to a mechanical system mainly due to the BESS and the need for BESS replacement.

5 Conclusions and Recommendations

The primary objective of this dissertation was to develop an accurate and time efficient model that can examine the performance of different propulsion system architectures. The architectures were assessed in terms of the system efficiency and CO_{2e} emissions. As an example, two different powertrain architectures, series hybrid and pure electric, were modeled for two classes of vessels. For fishing boats, the backward facing modeling approach was used and for the MV Klitsa ferry the forward facing approach was used. The powertrain was modeled using a blended modeling approach that utilized both a power loss model and prebuilt Simulink blocks for accuracy and ease of development.

A performance comparison and validation of the vessel models were achieved using experimental data collected from both vessels while in operation. A dedicated data acquisition system was installed onboard each vessel to record the operational load profiles including engine torque, speed, and vessel velocity. Using the collected data, representative load profiles were created for each vessel and simulation results were compared with actual data. The model error was found to be between 5% to 10% depending on the simulation time and control parameters. More accurate result can be obtained at the cost of higher simulation times.

In comparison to the collected operational data, the simulation results for both vessels were satisfactory. However, in the case of the passenger ferry, improvements in the vessels speed model, especially during transient conditions while maneuvering can increase the model accuracy. The vessel speed model depends significantly on CFD simulations to obtain the reduced-order hull resistance and propeller thrust model parameters.

The model results from the passenger ferry and fishing boats provided an excellent illustration of how this platform can be used in the design and analysis of alternative propulsion systems for a marine vessel. For fishing boats, a series hybrid electric architecture is a possible solution for future cost and emission reductions for the given load profile. For passenger ferries, considering BC Hydro electricity emissions, significant emission reductions can be achieved by deploying a pure battery architecture.

Another important objective of this dissertation was an environmental assessment of alternative fuels, especially NG, as a transportation fuel in BC. A comprehensive lifecycle environmental assessment of NG as a transportation fuel using data from NG producers and suppliers was presented. The results obtained indicate that NG is a desirable marine fuel in BC only if proper engine technologies are used. NG generates less air pollution and has a lower environmental impact than diesel fuel. If NG fuel is considered as a bridge to future all electric powered vessels, then it must be used carefully. The results given in this dissertation showed that high methane leakage during NG engine operations can offset the environmental benefits of NG as a transportation fuel.

The simulation time is also an important factor which needs to be considered. For a fishing boat with the backward facing modeling method, the simulation time was eight minutes for six hours of operation. For the MV Klitsa with the forward facing modeling method, the simulation time was about thirty minutes for thirty minutes of operation. This time can be reduced to about ten minutes at a cost of lower resolution for some components.

The models developed in this dissertation serve as an excellent starting point for further studies. Recommendations for future improvement of the model are the following.

- The performance degradation and capacity fade of the BESS under different use patterns can be modeled more accurately in order to predict the life and lifecycle costs of the BESS.
- Optimal energy management control and operation modeling using techniques such as dynamic programming and machine learning can be used to increase the accuracy of the model.
- Implementation of 3-DOF vessel motion into the model to replace the current 1-DOF model will reduce model errors during the free maneuvering of the vessel.
- Incorporation of the Marine System Simulator (MSS) toolbox into the model will provide additional functionality with its prebuilt blocks.

Bibliography

[1] "Review of Maritime Transport," in *United Nations Conference On Trade And Development*, 2015, no. October, p. 204.

[2] J.-P. Rodrigue, C. Comtois, and B. Slack, *The Geography of Transport Systems*. 2011.

[3] International Maritime Organization, "International Convention for the Prevention of Pollution from Ships (MARPOL)." [Online]. Available: http://www.imo.org/en/about/conventions/listofconventions/pages/international-convention-for-the-prevention-of-pollution-from-ships-(marpol).aspx. [Accessed: 17-Aug-2018].

[4] V. Eyring, H. W. Kohler, J. van Aardenne, and A. Lauer, "Emissions From International Shipping: 1. The Last 50 Years," *J. Geophys. Res.*, vol. 110, no. D17305, pp. 1–12, 2005.

[5] "Reducing emissions from the shipping sector." [Online]. Available: https://ec.europa.eu/clima/policies/transport/shipping_en. [Accessed: 27-Aug-2018].

[6] A. Smith et al., "Third IMO Greenhouse Gas Study 2014," London, UK, 2015.

[7] S. I. Raptotasios, N. F. Sakellaridis, R. G. Papagiannakis, and D. T. Hountalas, "Application Of A Multi-Zone Combustion Model To Investigate The No_x Reduction Potential Of Two-Stroke Marine Diesel Engines Using EGR," *Appl. Energy*, vol. 157, pp. 814–823, 2015.

[8] R. Verschaeren, W. Schaepdryver, T. Serruys, M. Bastiaen, L. Vervaeke, and S. Verhelst, "Experimental Study Of No_x Reduction On A Medium Speed Heavy

Duty Diesel Engine By The Application Of EGR (Exhaust Gas Recirculation) And Miller Timing," *Energy*, vol. 76, pp. 614–621, Nov. 2014.

[9] MAN Diesel & Turbo, "Exhaust Gas Emission Control Today And Tomorrow. Application On MAN B&W Two-Stroke Marine Diesel Engines.," Denmark.

[10] Hugo. Pestana, "Future trends of electrical propulsion and implications to ship design," 2014.

[11] J. F. Hansen and F. Wendt, "History and State of the Art in Commercial Electric Ship Propulsion, Integrated Power Systems, and Future Trends," *Proceedings of the IEEE*, vol. 103, no. 12. pp. 2229–2242, 2015.

[12] R. D. Geertsma, R. R. Negenborn, K. Visser, and J. J. Hopman, "Design And Control Of Hybrid Power And Propulsion Systems For Smart Ships: A Review Of Developments," *Appl. Energy*, vol. 194, pp. 30–54, May 2017.

[13] Siemens, "Setting a Course for Carbon-Free Shipping," 2016. [Online]. Available: https://www.siemens.com/innovation/en/home/pictures-of-the-future/mobility-and-motors/electromobility-electric-ferries.html. [Accessed: 31-Jul-2017].

[14] Siemens Drilling & Marine, "Ship – A Smarter Journey," 2015.

[15] "IEC/TS 61201 : Use of Conventional Touch Voltage Limits – Application Guide," International Electrotechnical Commission (IEC), 2007.

[16] G. Wu, X. Zhang, and Z. Dong, "Powertrain Architectures of Electrified Vehicles: Review, Classification and Comparison," *J. Franklin Inst.*, vol. 352, no. 2, pp. 425–448, Feb. 2015.

[17] S. Cui, S. Han, and C. C. Chan, "Overview of Multi-machine Drive Systems for Electric and Hybrid Electric Vehicles," in *IEEE Conference and Expo*

Transportation Electrification Asia-Pacific, 2014, pp. 1–6.

[18] C. Mahmoudi, A. Flah, and L. Sbita, "An Overview of Electric Vehicle Concept and Power Management Strategies," in *International Conference on Electrical Sciences and Technologies in Maghreb*, 2014, pp. 1–8.

[19] G. R. Chandra Mouli, P. Bauer, and M. Zeman, "Comparison of System Architecture and Converter Topology for a Solar Powered Electric Vehicle Charging Station," *Int. Conf. Power Electron. ECCE Asia*, pp. 1908–1915, Jun. 2015.

[20] E. Silvas, T. Hofman, N. Murgovski, P. Etman, and M. Steinbuch, "Review of Optimization Strategies for System-Level Design in Hybrid Electric Vehicles," *IEEE Trans. Veh. Technol.*, pp. 1–1, 2016.

[21] H. Kim and D. Kum, "Comprehensive Design Methodology of Input- and Output-Split Hybrid Electric Vehicles: In Search of Optimal Configuration," *IEEE/ASME Trans. Mechatronics*, vol. 21, no. 6, pp. 2912–2923, Dec. 2016.

[22] H. S. Ramadan, M. Becherif, and F. Claude, "Energy Management Improvement of Hybrid Electric Vehicles via Combined GPS/Rule-Based Methodology," *IEEE Trans. Autom. Sci. Eng.*, vol. 14, no. 2, pp. 586–597, Apr. 2017.

[23] B. Manouchehrinia, S. Molloy, Z. Dong, T. A. Gulliver, and C. Gough, "Emission and Lifecycle Cost Analysis of Hybrid and Pure Electric Propulsion Systems for Fishing Boats," *J. Ocean Technol.*, vol. 13, no. 2, 2018.

[24] J. Liu, H. Dong, T. Jin, L. Liu, B. Manouchehrinia, and Z. Dong, "Optimization of Hybrid Energy Storage Systems for Vehicles with Dynamic On-Off Power Loads Using a Nested Formulation," *Energies*, vol. 11, no. 10, p. 2699, Oct. 2018.

[25] N. DiOrio, A. Dobos, and J. Steven, “Economic Analysis Case Studies of Battery Energy Storage with SAM,” 2015.

[26] J. Liu, T. Jin, L. Liu, Y. Chen, and K. Yuan, “Multi-Objective Optimization of a Hybrid ESS Based on Optimal Energy Management Strategy for LHDs,” *Sustainability*, vol. 9, no. 10, p. 1874, 2017.

[27] Corvus Energy. Co, “Corvus Energy.” [Online]. Available: http://corvusenergy.com/. [Accessed: 02-Aug-2017].

[28] Siemens, “Low voltage AC Motors Selection And Pricing Guide,” 2015.

[29] “Caterpillar dealer: Fining.” Victoria, BC, 2017.

[30] “Vancouver, BC Average Retail Price for Diesel Fuel at Self Service Filling Stations (Monthly, NSA, CAD per liter).” [Online]. Available: https://ycharts.com/indicators/vancouver_bc_average_retail_price_for_diesel_fuel_at_self_service_filling_stations. [Accessed: 08-Oct-2018].

[31] Commission for Environmental Cooperation, “North American Power Plant Air Emissions,” Québec, 2011.

[32] Government of British Columbia, “British Columbia’s Carbon Tax,” 2018. [Online]. Available: https://www2.gov.bc.ca/gov/content/environment/climate-change/planning-and-action/carbon-tax. [Accessed: 08-Oct-2018].

[33] US Environmental Protection Agency (EPA), “Regulatory Impact Analysis: Control of Emissions of Air Pollution from Category 3 Marine Diesel Engines,” 2009.

[34] C. Trozzi and R. Vaccaro, “Methodologies for Estimating Air Pollutant Emissions From Ships,” in *Proceeding of 22nd CIMAC International Congress on*

Combustion Engines, 1998, pp. 775–782.

[35] U. Kesgin and N. Vardar, "A Study on Exhaust Gas Emissions From Ships in Turkish Straits," *Atmos. Environ.*, vol. 32, no. 47, 1994.

[36] US Environmental Protection Agency (EPA), "Basic Information of Air Emissions Factors and Quantification." [Online]. Available: https://www.epa.gov/air-emissions-factors-and-quantification/basic-information-air-emissions-factors-and-quantification. [Accessed: 08-Oct-2018].

[37] Ministry of Environment British Colombia, "2016/17 B.C. Best Practices Methodology For Quantifying Greenhouse Gas Emissions," Victoria, BC, 2016.

[38] "Natural gas 1998: Issues and trends," United States, 1999.

[39] A. R. Brandt *et al.*, "Methane Leaks from North American Natural Gas Systems," *Science (80-.).*, vol. 343, no. 6172, pp. 733–735, Feb. 2014.

[40] Natural Resources Canada, "Marketable Natural Gas Production in Canada." [Online]. Available: https://www.nrcan.gc.ca/energy/facts/natural-gas/20067#L6. [Accessed: 30-Jul-2018].

[41] Intercontinental Exchange (ICE), "NGX – Historical Natural Gas Price Summary Data – Nov 1, 2010 to Present." [Online]. Available: http://www.ngx.com/?page_id=646. [Accessed: 28-Sep-2018].

[42] International Maritime Organization (IMO), "Sulphur 2020 – Cutting Sulphur Oxide Emissions." [Online]. Available: http://www.imo.org/en/mediacentre/hottopics/pages/sulphur-2020.aspx. [Accessed: 21-Sep-2018].

[43] Intergovernmental Panel on Climate Change (IPCC), "Fifth Assessment Report,"

Geneva, 2014.

[44] G. Pétron *et al.*, “Hydrocarbon Emissions Characterization In The Colorado Front Range: A Pilot Study,” *J. Geophys. Res. Atmos.*, vol. 117, no. D4, pp. 170–182, Feb. 2012.

[45] A. Karion *et al.*, “Methane Emissions Estimate From Airborne Measurements Over a Western United States Natural Gas Field,” *Geophys. Res. Lett.*, vol. 40, no. 16, pp. 4393–4397, Aug. 2013.

[46] R. W. Howarth, R. Santoro, and A. Ingraffea, “Methane and The Greenhouse Gas Footprint of Natural gas From Shale Formations,” *Climatic Change*, vol. 106, no. 4. Springer Netherlands, pp. 679–690, 12-Jun-2011.

[47] E. Atherton *et al.*, “Mobile Measurement of Methane Emissions From Natural gas Developments in Northeastern British Columbia, Canada,” *Atmos. Chem. Phys.*, vol. 17, no. 20, pp. 12405–12420, Oct. 2017.

[48] R. A. Alvarez, S. W. Pacala, J. J. Winebrake, W. L. Chameides, and S. P. Hamburg, “Greater Focus Needed on Methane Leakage From Natural Gas Infrastructure.,” *Proc. Natl. Acad. Sci.*, vol. 109, no. 17, pp. 6435–6440, Apr. 2012.

[49] M. R. Johnson, D. R. Tyner, S. Conley, S. Schwietzke, and D. Zavala-Araiza, “Comparisons of Airborne Measurements and Inventory Estimates of Methane Emissions in the Alberta Upstream Oil and Gas Sector,” *Environ. Sci. Technol.*, vol. 51, no. 21, pp. 13008–13017, Nov. 2017.

[50] U.S. Environmental Protection Agency (EPA), “U.S. Greenhouse Gas Inventory Report: 1990-2014.” [Online]. Available: https://www.epa.gov/ghgemissions/us-

greenhouse-gas-inventory-report-1990-2014. [Accessed: 31-Jul-2018].

[51] H. Cai, A. Burnham, R. Chen, and M. Wang, "Wells to Wheels: Environmental Implications of Natural Gas as A Transportation Fuel," *Energy Policy*, vol. 109, pp. 565–578, Oct. 2017.

[52] R. A. Alvarez, S. W. Pacala, J. J. Winebrake, W. L. Chameides, and S. P. Hamburg, "Greater Focus Needed on Methane Leakage From Natural Gas Infrastructure.," *Proc. Natl. Acad. Sci.*, vol. 109, no. 17, pp. 6435–6440, Apr. 2012.

[53] Argonne National Laboratory, "The Greenhouse Gases Regulated Emissions and Energy Use in Transportation Model," 2017. [Online]. Available: https://greet.es.anl.gov/.

[54] "GHGenius, Lifecycle Analysis (LCA) Model," 2018. [Online]. Available: http://www.ghgenius.ca/. [Accessed: 01-Oct-2018].

[55] A. S. Kasumu, V. Li, J. W. Coleman, J. Liendo, and S. M. Jordaan, "Country-Level Life Cycle Assessment of Greenhouse Gas Emissions from Liquefied Natural Gas Trade for Electricity Generation," *Environ. Sci. Technol.*, vol. 52, no. 4, pp. 1735–1746, Feb. 2018.

[56] H. Thomson, J. J. Corbett, and J. J. Winebrake, "Natural Gas As a Marine Fuel," *Energy Policy*, vol. 87, pp. 153–167, Dec. 2015.

[57] S. M. Lajevardi, J. Axsen, and C. Crawford, "Examining the role of Natural Gas And Advanced Vehicle Technologies in Mitigating CO_2 Emissions of Heavy-duty Trucks: Modeling Prototypical British Columbia Routes With Road Grades," *Transp. Res. Part D Transp. Environ.*, vol. 62, pp. 186–211, Jul. 2018.

[58] BC Oil and Gas Commission, “British Columbia’s Oil and Gas Reserves and Production Report, BC Oil and Gas Commission,” Victoria, BC, 2016.

[59] N. Hultman, D. Rebois, M. Scholten, and C. Ramig, “The Greenhouse Impact of Unconventional Gas for Electricity Generation,” *Environ. Res. Lett.*, vol. 6, no. 4, p. 044008, Oct. 2011.

[60] T. Stephenson, J. E. Valle, and X. Riera-Palou, “Modeling the Relative GHG Emissions of Conventional and Shale Gas Production,” *Environ. Sci. Technol.*, vol. 45, no. 24, pp. 10757–10764, Dec. 2011.

[61] M. Jiang, W. Michael Griffin, C. Hendrickson, P. Jaramillo, J. VanBriesen, and A. Venkatesh, “Life Cycle Greenhouse Gas Emissions of Marcellus Shale Gas,” *Environ. Res. Lett.*, vol. 6, no. 3, p. 034014, Jul. 2011.

[62] Goverment of British Columbia, “Natural Gas and Oil Statistics - Province of British Columbia,” 2015. [Online]. Available: https://www2.gov.bc.ca/gov/content/industry/natural-gas-oil/statistics. [Accessed: 01-Oct-2018].

[63] “Personal Communication.” Victoria , BC, 2018.

[64] M. N. Usama, A. Sherine, and M. Shuhaimi, “Technology Review of Natural Gas Liquefaction Processes,” *Journal of Applied Sciences*, vol. 11, no. 21. pp. 3541–3546, 01-Dec-2011.

[65] N. N. Clark *et al.*, “Pump-to-Wheels Methane Emissions from the Heavy-Duty Transportation Sector,” *Environ. Sci. Technol.*, vol. 51, no. 2, pp. 968–976, Jan. 2017.

[66] Canadian Natural Gas Vehicle Alliance, “Liquefied Natural Gas: A Marine Fuel

for Canada's Great Lakes and East Coast," Ottawa, 2017.

[67] A. Manivannan, P. T. Porai, S. Chandrasekaran, R. Ramprabhu, P. Tamil, and S. Chandrasekaran, "Lean Burn Natural Gas Spark Ignition Engine - An Overview," *SAE Int.*, no. 724, Mar. 2003.

[68] Y. Iwamoto, K. Noma, O. Nakayama, T. Yamauchi, and H. Ando, "Development of Gasoline Direct Injection Engine," *J. Engines*, p. 19, Feb. 1997.

[69] J. Žaglinskis, P. Rapalis, and N. Lazareva, "An Overview of Natural Gas Use in Ships: Necessity and Engine Supply," *Period. Polytech. Transp. Eng.*, vol. 46, no. 4, pp. 185–193, Feb. 2018.

[70] "The Total Energy and Emissions Analysis in Marine Systems (TEAMS) Model." [Online]. Available: http://www.rit.edu/~w-teams/overview.htm. [Accessed: 02-Oct-2018].

[71] H. Thomson, J. J. Corbett, and J. J. Winebrake, "Natural Gas As a Marine Fuel," *Energy Policy*, vol. 87, pp. 153–167, 2015.

[72] Rolls-Royce Marine, "Overcoming Methane Slip, Rolls Royce Marine Builds Spark-Ignited LNG-Powered Engines – gCaptain," 2012. [Online]. Available: http://gcaptain.com/overcoming-methane-slip-rolls/. [Accessed: 27-Jul-2018].

[73] U.S. Energy Information Administration, "U.S. Energy Facts," 2016. [Online]. Available: https://www.neb-one.gc.ca/nrg/sttstc/ntrlgs/stt/mrktblntrlgsprdctn-eng.html.

[74] Environment Canada, "Canada's Emissions Trends," Quebec, 2014.

[75] European Maritime Safety Agency (EMSA), "European Maritime Safety Agency (EMSA)." [Online]. Available: http://emsa.europa.eu/main/air-

pollution/greenhouse-gases.html. [Accessed: 05-Feb-2018].

[76] C. Capasso, O. Veneri, E. Notti, A. Sala, M. Figari, and M. Martelli, "Preliminary Design of the Hybrid Propulsion Architecture for the Research Vessel 'G. Dallaporta,'" in *International Conference on Electrical Systems for Aircraft, Railway, Ship Propulsion and Road Vehicles and International Transportation Electrification Conference*, 2016, pp. 1–6.

[77] M. Martelli, G. Vernengo, D. Bruzzone, and E. Notti, "Holistic Modeling of the Global Propulsion Energy Index in Waves for Small Craft," *Int. J. Offshore Polar Eng.*, vol. 27, no. 04, p. 6, Dec. 2017.

[78] "Stock Photography Images Royalty Free at Can Stock Photo," 2013. [Online]. Available: https://www.canstockphoto.ca/. [Accessed: 19-Mar-2018].

[79] C. Energy, "World's First All-Electric Car Ferry." [Online]. Available: http://corvusenergy.com/marine-project/mf-ampere-ferry/. [Accessed: 18-Mar-2018].

[80] J. M. Apsley *et al.*, "Propulsion Drive Models for Full Electric Marine Propulsion Systems," *IEEE Transactions on Industry Applications*, vol. 45, no. 2. pp. 676–684, 2009.

[81] National Renewable Energy Laboratory (NREL), "Advisor Documentation and Help Files." [Online]. Available: http://adv-vehicle-sim.sourceforge.net/. [Accessed: 22-Mar-2018].

[82] G. S. Stavrakakis and G. N. Kariniotakis, "A General Simulation Algorithm For the Accurate Assessment of ISOLATED Diesel - Wind Turbines Systems Interaction. Part I: A General Multimachine Power System Model.," *IEEE Trans.*

Energy Convers., vol. 10, no. 3, pp. 577–583, 1995.

[83] S. Roy, O. P. Malik, and G. S. Hope, "An Adaptive Control Scheme for Speed Control of Diesel Driven Power-Plants," *IEEE Trans. Energy Convers.*, vol. 6, no. 4, pp. 605–611, 1991.

[84] T. Theubou, R. Wamkeue, and I. Kamwa, "Dynamic Model of Diesel Generator Set for Hybrid Wind-Diesel Small Grids Applications," in *IEEE Canadian Conference on Electrical and Computer Engineering*, 2012, pp. 1–4.

[85] T. Senjyu, T. Nakaji, K. Uezato, and T. Funabashi, "A Hybrid Power System Using Alternative Energy Facilities in Isolated Island," *IEEE Trans. Energy Convers.*, vol. 20, no. 2, pp. 406–414, Jun. 2005.

[86] C. D. Rakopoulos and E. G. Giakoumis, *Diesel Engine Transient Operation: Principles Of Operation And Simulation Analysis*. Springer, 2009.

[87] International IOR Rectifier, "IRF100B202 Product Datasheet," 2014. [Online]. Available: www.irf.com. [Accessed: 22-Feb-2018].

[88] C. C. D. Rahn and C.-Y. C. Wang, *Battery Systems Engineering*, 1st Ed. Oxford, UK: John Wiley & Sons Ltd, 2012.

[89] M. Chen and G. A. Rincon-Mora, "Accurate Electrical Battery Model Capable of Predicting Runtime and I–V Performance," *IEEE Trans. Energy Convers.*, vol. 21, no. 2, pp. 504–511, Jun. 2006.

[90] T. Huria, M. Ceraolo, J. Gazzarri, and R. Jackey, "High Fidelity Electrical Model With Thermal Dependence for Characterization and Simulation of High Power Lithium Battery Cells," in *IEEE International Electric Vehicle Conference*, 2012, pp. 1–8.

[91] B. Yann Liaw, R. G. Jungst, A. Urbina, and T. L. Paez, “Modeling of Battery Life I. The Equivalent Circuit Model (ECM) Approach.”

[92] M. W. Verbrugge and R. S. Conell, “Electrochemical and Thermal Characterization of Battery Modules Commensurate with Electric Vehicle Integration,” *J. Electrochem. Soc.*, vol. 149, no. 1, pp. A45–A53, Jan. 2002.

[93] E. Barsoukov, J. H. Kim, D. H. Kim, and K. S. Hwang, “Parametric Analysis Using Impedance Spectroscopy: Relationship Between Material Properties and Battery Performance,” *J. New Mater. Electrochem. Syst. 3*, vol. 310, pp. 303–310, 2000.

[94] B. Nykvist and M. Nilsson, “Rapidly Falling Costs of Battery Packs for Electric Vehicles,” *Nat. Clim. Chang.*, vol. 5, no. 4, pp. 329–332, Apr. 2015.

[95] John Goreham, “Can A Toyota Prius Battery Last 250,000 miles?” [Online]. Available: https://www.torquenews.com/1083/can-toyota-prius-battery-last-250000-miles. [Accessed: 16-Jul-2018].

[96] S. G. Chalk and J. F. Miller, “Key Challenges and Recent Progress in Batteries, Fuel cells, and Hydrogen Storage for Clean Energy Systems,” *J. Power Sources*, vol. 159, no. 1 SPEC. ISS., pp. 73–80, Sep. 2006.

[97] J. Wang *et al.*, “Cycle-Life Model For Graphite-Lifepo4cells,” *J. Power Sources*, vol. 196, no. 8, pp. 3942–3948, Apr. 2011.

[98] T. F. Fuller, “Simulation and Optimization of the Dual Lithium Ion Insertion Cell,” *J. Electrochem. Soc.*, vol. 141, no. 1, p. 1, Jan. 1994.

[99] R. Spotnitz, “Simulation of Capacity Fade in Lithium-ion Batteries,” *J. Power Sources*, vol. 113, no. 1, pp. 72–80, Jan. 2003.

[100] P. Ramadass, B. Haran, P. M. Gomadam, R. White, and B. N. Popov, "Development of First Principles Capacity Fade Model for Li-Ion Cells," *J. Electrochem. Soc.*, vol. 151, no. 2, p. A196, Feb. 2004.

[101] M. Safari, M. Morcrette, A. Teyssot, and C. Delacourt, "Life-Prediction Methods for Lithium-Ion Batteries Derived from a Fatigue Approach: I. Introduction: Capacity-Loss Prediction Based on Damage Accumulation," *J. Electrochem. Soc.*, vol. 157, no. 6, pp. A713–A720, Jun. 2010.

[102] Z. Song, X. Zhang, J. Li, H. Hofmann, M. Ouyang, and J. Du, "Component Sizing Optimization of Plug-in Hybrid Electric Vehicles With the Hybrid Energy Storage System," *Energy*, vol. 144, pp. 393–403, Feb. 2018.

[103] L. Zhang, Z. Wang, X. Hu, F. Sun, and D. G. Dorrell, "A Comparative Study of Equivalent Circuit Models of Ultracapacitors for Electric Vehicles," *J. Power Sources*, vol. 274, pp. 899–906, Jan. 2015.

[104] A. González, E. Goikolea, J. A. Barrena, and R. Mysyk, "Review on Supercapacitors: Technologies and Materials," *Renew. Sustain. Energy Rev.*, vol. 58, pp. 1189–1206, May 2016.

[105] H. Chen, T. N. Cong, W. Yang, C. Tan, Y. Li, and Y. Ding, "Progress in Electrical Energy Storage System: A Critical Review," *Prog. Nat. Sci.*, vol. 19, no. 3, pp. 291–312, Mar. 2009.

[106] L. P. Lima, F. A. Farret, J. G. Trapp, F. Z. Ferrigolo, D. B. Ramos, and F. T. Fernandes, "Integration of Alternative Sources of Energy as Current Sources," in *Brazilian Power Electronics Conference*, 2011, pp. 589–594.

[107] S. M. Schoenung and W. V Hassenzahl, "Long-vs. Short-Term Energy Storage

Technologies Analysis A Life-Cycle Cost Study A Study for the DOE Energy Storage Systems Program," New Mexico, 2003.

[108] C. J. Kaiser, *The capacitor handbook*, First. Springer, 1995.

[109] P. M. M. and R. G. Kanojiya, "Tuning of PID controller using Ziegler-Nichols method for speed control of DC motor," in *IEEE-International Conference On Advances In Engineering, Science And Management (ICAESM -2012)*, 2012.

[110] M. T. and H. L. M. Solomon, S., D. Qin, M. Manning, Z. Chen, M. Marquis, K.B. Averyt, "Contribution of Working Group I to the Fourth Assessment Report of the Intergovernmental Panel on Climate Change," 2007.

[111] K. Deb, *Multi-objective optimization using evolutionary algorithms*. John Wiley & Sons, 2001.

[112] J. Brander, M. S, Aman, Wylie, C, Haughton, A, Lovell, "Electricity-Specific Emission Factors for Grid Electricity," UK, 2011.

[113] U.S. Environmental Protection Agency (EPA), "Emission Factors for Greenhouse Gas Inventories," 2015.

[114] BC Ferries, "BC Ferries, Klitsa." [Online]. Available: http://www.bcferries.com/onboard-experiences/fleet/profile-klitsa.html. [Accessed: 26-Jul-2017].

[115] K. Andersen, "Development Of A Time-Domain Modeling Platform for Hybrid Marine Propulsion Systems," Master Thesis, University of Victoria, 2016.

[116] J. V. A. J. Timothy J. McCoy, "McCoy_Amy," *IEEE*, vol. 978-1–4244, 2009.

[117] S. Kim, S. Choe, S. Ko, and S. Sul, "Power System with a Battery Energy Storage System," *IEEE Electrif. Mag.*, no. May, pp. 22–33, 2015.

[118] R. D. Geertsma, R. R. Negenborn, K. Visser, and J. J. Hopman, "Design And Control of Hybrid Power And Propulsion Systems for Smart Ships: A Review of Developments," *Appl. Energy*, vol. 194, pp. 30–54, 2017.

[119] J. Chiasson and B. Vairamohan, "Estimating the state of charge of a battery," *IEEE Trans. Control Syst. Technol.*, vol. 13, no. 3, pp. 465–470, May 2005.

[120] L. Larsson, H. C. Raven, and J. R. Paulling, *Ship Resistance and Flow*. Society of Naval Architects and Marine Engineers, 2010.

[121] ANSYS, "Computational fluid dynamics software." [Online]. Available: http://www.ansys.com/products/fluids. [Accessed: 12-Sep-2017].

[122] T. R. Romana, "Marine Fuel Oil type DMB Commercial Denomination: Marine Diesel Oil – MDO." [Online]. Available: http://www.omnimpex.ro/texte/petroliere/engleza_07/MARINE DIESEL OIL (MDO).pdf.

[123] Bchydro.com, "British Columbia Hydro and Power Authority, Annual Service Plan Report 16/17," Vancouver, BC, 2017.

Appendix

Table Appendix A - 1: Units and Conversion Factors.

Unit	Equivalent to
1.0 Cubic metres (m^3)	6.2898 Barrels (bbl)
1.0 Cubic metres (m^3)	1,000 Litres (l)
1.0 Cubic metres (m^3)	35.3147 Cubic feet (cf) natural gas
1.0 Cubic feet (cf) natural gas	0.028317 Cubic metres (m^3)
1.0 US Gallons	3.7854 Litres (l)
1.0 US Gallons	3.7854 x 10-3 Cubic metres (m^3)
1.0 Litres (l)	1 x 10-3 Cubic metres (m^3)
1.0 Gigajoules (GJ)	0.9478 Million British thermal units (MMBtu)
1.0 Gigajoules (GJ)	947.8171 Cubic feet (cf) natural gas
1.0 Gigajoules (GJ)	26.853 Cubic metres (m^3) natural gas
1.0 Million British thermal units (MMBtu)	1.0551 x 109 Joules (J)
1.0 Million British thermal units (MMBtu)	1.0551 Gigajoules (GJ)
1.0 Million British thermal units (MMBtu)	1,000 Cubic feet (cf) natural gas
1.0 Gigawatt-hours (GW.h)	3.6 x 1012 Joules (J)
1.0 Cubic feet (cf) natural gas	0.0388 Gigajoules (GJ)
1.0 Cubic feet (cf) natural gas	1 x 10-3 Million British thermal units (MMBtu)
Diesel fuel energy	0.0358745 Gigajoules per liter (GJ/L)
FortisBC natural gas energy	0.055058 Gigajoules per kilogram (GJ/Kg)
1.0 Cubic metres (m^3) LNG	0.4049 Tonnes (t) LNG
1.0 Tonnes (t) LNG	1,379.549 Cubic metres (m^3) natural gas
1.0 Billion cubic feet (Bcf) natural gas	4.8471 x 104 Cubic metres (m^3) LNG